Vehicle Powertrain Model to Predict Energy Consumption for Ecorouting Purposes

Courtney Alex Tamaro

Thesis submitted to the faculty of the Virginia Polytechnic Institute and State University in partial fulfillment of the requirements for the degree of

Master of Science
In
Mechanical Engineering

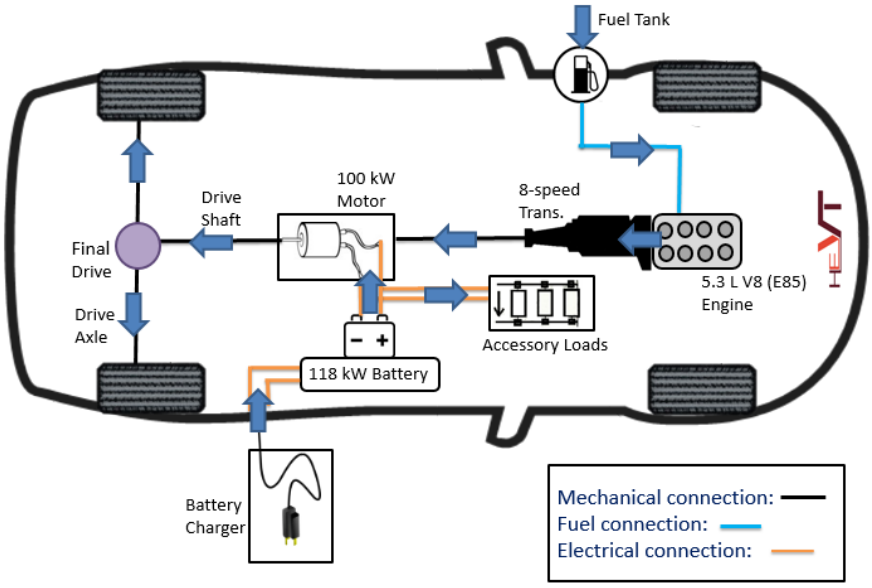

Chair: Douglas J. Nelson
John B. Ferris
Michael W. Ellis

May 3, 2016
Blacksburg, VA

Keywords: powertrain modeling, ecorouting, scalable powertrain components, fuel economy, energy consumption, hybrid electric vehicle, plug-in, battery electric vehicle, environment, greenhouse gases, petroleum

Vehicle Powertrain Model to Predict Energy Consumption for Ecorouting Purposes

Courtney Alex Tamaro

Academic Abstract

The automotive industry is facing some of the most difficult design challenges in industry history. Developing innovative methods to reduce fossil fuel dependence is imperative for maintaining compliance with government regulations and consumer demand. In addition to powertrain design, route selection contributes to vehicle environmental impact.

The objective of this thesis is to develop a methodology for evaluating the energy consumption of each route option for a specific vehicle. A “backwards” energy tracking method determines tractive demand at the wheels from route requirements and vehicle characteristics. Next, this method tracks energy quantities at each powertrain component. Each component model is scalable such that different vehicle powertrains may be approximated. Using an “ecorouting” process, the most ideal route is selected by weighting relative total energy consumption and travel time.

Only limited powertrain characteristics are publicly available. As the future goal of this project is to apply the model to many vehicle powertrain types, the powertrain model must be reasonably accurate with minimal vehicle powertrain characteristics. Future work expands this model to constantly re-evaluate energy consumption with real-time traffic and terrain information.

While ecorouting has been applied to conventional vehicles in many publications, electrified vehicles are less studied. Hybrid vehicles are particularly complicated to model due to additional components, systems, and operation modes. This methodology has been validated to represent conventional, battery electric, and parallel hybrid electric vehicles. A sensitivity study demonstrates that the model is capable of differentiating powertrains with different parameters and routes with different characteristics.

Vehicle Powertrain Model to Predict Energy Consumption for Ecorouting Purposes

Courtney Alex Tamaro

General Audience Abstract

In response to unsustainable petroleum consumption, governments are increasing environmental regulations for automotive manufacturers. Consumers are also demanding more efficient vehicles due to both monetary and environmental concerns. One method for reducing vehicle environmental impact is to select the most energy efficient route.

The objective of this research is to develop a methodology to evaluate the energy consumption of each route for a specific vehicle. Using a process called “ecorouting”, the most ideal route is selected by weighting relative total energy consumption and travel time. While ecorouting has been applied to conventional vehicles, electrified vehicles are less studied due to the complication of additional components. This thesis methodology has been validated to represent a conventional vehicle, battery electric vehicle, and hybrid electric vehicles (HEVs) including plug-in HEVs.

This model is designed to approximate the energy consumption of a wide variety of vehicles and routes. To find the total energy consumption of each route, this model first calculates the energy into, out of, and lost from each powertrain component. As many component characteristics are manufacturer proprietary, an objective of this research is to approximate component energy losses using only the minimal amount of publically-available characteristics. In a sensitivity study, the model predicts energy consumption specific to vehicles of different vehicle parameters. The model also predicts energy consumption specific to different routes demonstrating that the model is capable of differentiating routes as is necessary for ecorouting.

Acknowledgements

I would like to thank the Hybrid Electric Vehicle Team (HEVT) of Virginia Tech for years of support and encouragement. I would also like to thank General Motors, the United States Department of Energy, and Argonne National Lab for organizing and sponsoring EcoCAR 3. This program has allowed HEVT unparalleled resources and opened my eyes to the automotive industry. I would like to thank Dr. Hesham Rakha for allowing HEVT to join in his ecorouting ventures.

Next I would like to thank the American Association of University Women (AAUW) for the Selected Professionals Fellowship, the Society of Manufacturing Engineers for the E. Wayne Kay Graduate Scholarship, the Society of Automotive Engineering (SAE) for the Yanmar Scholarship, and Virginia Tech for the Mary Jones Fellowship. I would like to thank my friends and family for supporting me throughout my academic career: the stresses and the successes. Lastly, and most importantly, I would like to thank my adviser Dr. Doug Nelson for being an exceptional mentor and friend. Without his patience for teaching and passion for this field, this research would not have been possible.

Image Copyright Information

Many images in this thesis are specified as either Public Domain or Fair Use. Public Domain images used in this thesis are created public domain by U.S. Government Agencies. Some images are considered to be Fair Use as this thesis is not for profit or entertainment, is based upon facts not creativity, and uses only small pieces of the published works. All remaining unspecified images are the creation of this author.

Table of Contents

List of Multimedia Objects

List of Tables

List of Figures

List of Terms and Abbreviations

ANL	Argonne National Lab
AFM	Active Fuel Management
AVTC	Advanced Vehicle Technology Competition
BEV	Battery Electric Vehicle
BMEP	Brake Mean Effective Pressure
BSFC	Brake Specific Fuel Consumption
CAFE	Corporate Average Fuel Economy
CD	Charge Depleting
CO	Carbon Monoxide
CS	Charge Sustaining
CVT	Continuously Variable Transmission
D3	Downloadable Dynamometer Database
DOE	Department of Energy
DOT	Department of Transportation
EPA	Environmental Protection Agency
EV	Electric Vehicle
FC	Fuel Consumption
FE	Fuel Economy
FTP	Federal Test Procedure
FWD	Front Wheel Drive
GHG	Greenhouse Gas
GM	General Motors
HEV	Hybrid Electric Vehicle
HEVT	Hybrid Electric Vehicle Team
HWFET	Highway Fuel Economy Test
HV	High Voltage
INL	Idaho National Lab
LHV	Lower Heating Value
MEP	Mean Effective Pressure
NASI	Naturally Aspirated Spark Ignition
NOx	Nitrogen Oxides
PE	Power Enrichment
PEU	Petroleum Energy Use
PHEV	Plug-In Hybrid Electric Vehicle
RWD	Rear Wheel Drive
SOC	State of Charge
THC	Total Hydrocarbon
UDDS	Urban Dynamometer Drive Schedule
US06	An aggressive, high speed drive cycle
VTTI	Virginia Tech Transportation Institute
WTW	Well-To-Wheels

1 Introduction

1.1 Introduction to Automotive Environmental Impact

The US consumes 21 million barrels of oil each day, 9 million of which are used in light-duty vehicles *(NAS, 2009)*. Federal environmental regulations are increasing such that the automotive industry is facing some of the most difficult design challenges in the history of the industry. To continue compliance, companies must fund research to improve the energy efficiency of vehicles, implement alternative fuels, and reduce emissions. The Federal Corporate Average Fuel Economy (CAFE) standard, for example, is set to reduce gasoline consumption by 170 gallons throughout the lives of light-duty vehicles of 2017-2021 model years *(EPA & DOT, 2012)*. Further, initiatives for cleaner energy have continued to gain momentum in recent years. Not only is the government demanding more efficient vehicles, but many consumers are demanding vehicles with a reduced reliance on Petroleum Energy Use (PEU). Advanced vehicle technologies have proven a promising avenue for decreasing vehicle emissions and fuel consumption. Research into vehicle electrification has become a recent automotive trend as Battery Elective Vehicles (BEVs) and Hybrid Electric Vehicles (HEVs) offer a potential for abundant energy savings.

1.1.1 American Driving Habits

The U.S. Department of Transportation (DOT) periodically collects surveys to assess trends in American transportation. American geography and culture lend a large role in the American tendency to drive as the primary mode of transportation. For the last four decades, roughly 87% of workers drive to work instead of using public transportation, walking, or biking as shown in Figure 1-1 *(FHA, 2011)*. During the average daily commute, 76% drive alone as opposed to public or shared transportation *(BTS, 2014)*. The average American spends around 32 miles and 62 minutes in a vehicle with more yet in rural areas, as shown in Figure 1-2 *(FHA, 2011)*. Not only do Americans want to reduce their time spent driving, but 17% of household expenses are transportation-related with an average of $2,756 per year per household spent on gasoline and motor oil alone *(BTS, 2014)*. A breakdown of household expenses is displayed in Figure 1-3. A decrease in fuel consumption due to improvements in vehicle efficiency or route selection has the potential for great financial savings for the average American household and a significantly lower environmental impact for the U.S.

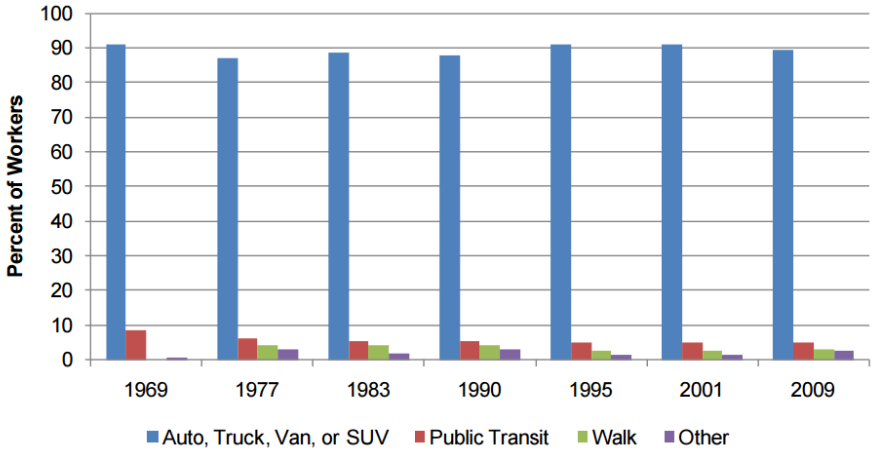

Figure 1-1: Trends in American Usual Commute Mode *(FHA, 2011, Public Domain)*

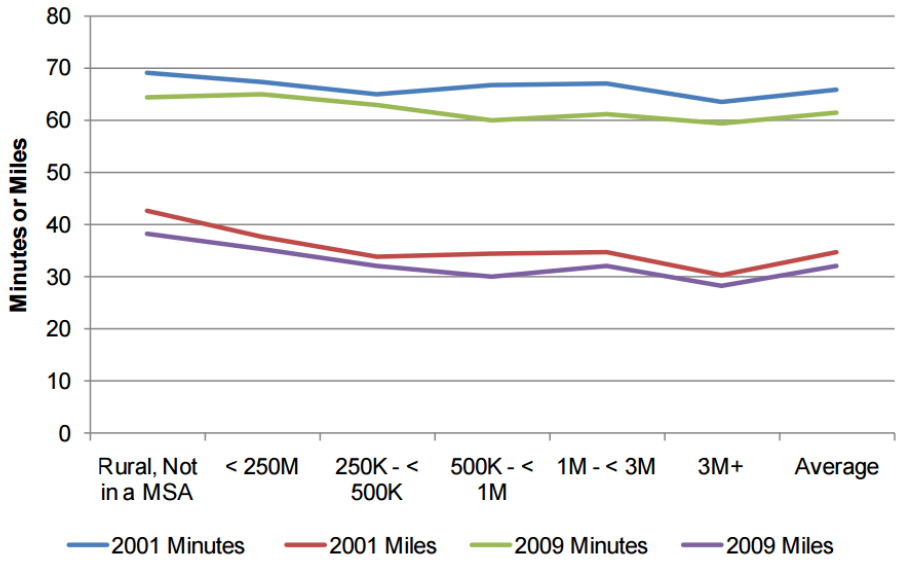

Figure 1-2: American Daily Time and Miles Spent in Vehicle *(FHA, 2011, Public Domain)*

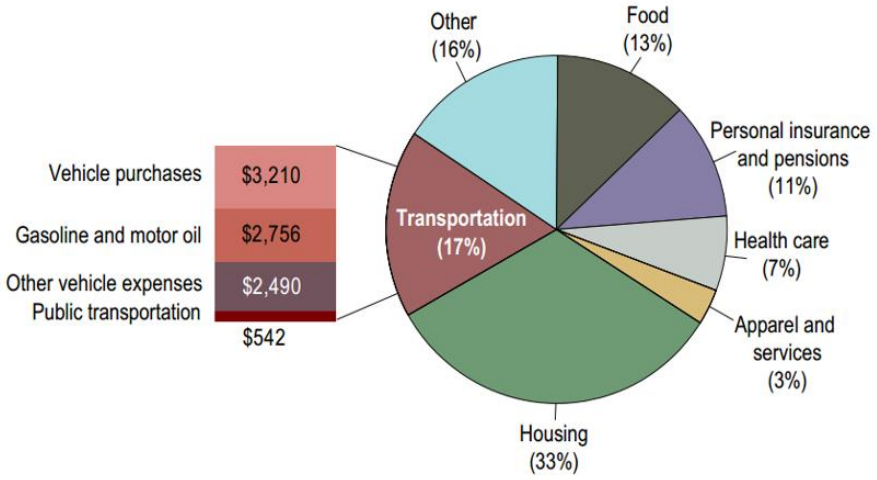

Figure 1-3: 2012 Average American Household Expenses *(BTS, 2014, Public Domain)*

Looking further into Americans driving habits, traffic congestion is a major factor. The average driving commuter spends 38 hours in delay each year, but average drivers in particular metropolitan regions may spend significantly more. *(BTS, 2014)*. For example, driving commuters in the Washington DC metropolitan region spend an average of 67 hours in delays each year *(BTS, 2014)*. As conventional vehicles are particularly inefficient during idle, ecorouting to less congested routes will likely reduce fuel consumption and may also reduce travel time for drivers who are otherwise unaware of traffic conditions.

1.1.2 Range of Vehicle Electrification

To electrify a vehicle is to power the vehicle either partially or fully by electric energy. Electrification ranges from a mild-HEV to a full BEV. Electrifying a vehicle does not in itself increase efficiency. Energy management must be carefully calibrated within a simulation model to form the basis for powertrain and control strategy selection to prevent costly failed prototype vehicles.

A mild-HEV is the lowest level of electrification and cannot obtain energy directly from the electric grid. Instead, the battery receives all energy from excess engine energy and the vehicle is therefore known as “Charge Sustaining” (CS). Many of these HEVs have a small battery and motor that are capable of powering vehicle accessory loads allowing the engine to be off during idle. With this small improvement, modern mild-HEV technology has the potential to contribute 48% of the improvements required to meet the European and US fuel efficiency standards of 2025 *(Lux Research, 2015)*. A full hybrid is generally more electrified and has electric launch capabilities and a limited electric-only driving mode.

A Plug-in Hybrid Electric Vehicle (PHEV) is a HEV that can store grid electric energy. The battery can be charged from the electric grid using an on-board charger. The battery may also be charged with excess engine energy. A PHEV offers a balance to consumers: the ability to charge deplete the battery like a BEV for increased efficiency on short trips and the ability to consume fuel for longer trips. PHEVs offer fuel saving potential compared to equivalent conventional vehicles. A PHEV capable of a 5 mile all-electric range is found to reduce petroleum consumption by 6% while a PHEV capable of a 30 mile all-electric range is found to reduce petroleum consumption by 35% *(Gonder & Simpson, 2006)*.

This thesis presents a methodology for modeling both Charge Depleting (CD) and CS modes for a PHEV. In CD mode, only the battery powers the vehicle by depleting grid electric energy until battery State of Charge (SOC) reaches a minimum threshold. At this point, the engine and battery work in conjunction for the most efficient engine operation and to charge the battery to a useable state. One type of PHEV is an Extended Range Electric Vehicle (EREV). An EREV has an additional mode where the vehicle attains nearly-full performance that is powered solely by the battery. Blended PHEVs have a complex energy consumption mixed strategy and do not have a distinct electric-only mode. Blended PHEVs will not be considered in the scope of this thesis but may be approximated with CS and an electric-only CD strategy.

The most electrified form of vehicle is a BEV. A BEV does not have an engine and the only energy source is the battery. The Tesla Model S, for example, can attain over 300 miles of electric range with an 85 kWh battery driving the 2-cycle Environmental Protection Agency (EPA) test procedure *(Musk & Straubel, 2012)*. As most Americans only drive around 32 miles per day, even the 80-100 mile electric range attainable by most BEVs is sufficient for daily activities *(FHA, 2011)*.

1.2 Motivation of Ecorouting

Drivers almost always select a route that will reach their destination in the shortest amount of time. Between 1982 and 2003, hours of traffic delay in the U.S. increased 528% *(Ahn & Rakha, 2008).* With such an increase in traffic congestion, drivers can no longer rely on prior experience to select a route with a reliable travel time. Drivers are turning to navigation systems to better understand live-updating traffic. Some routes, fast or slow, are more energy efficient than others. Similarly, certain routes produce less emissions than others. Ecorouting is a process by which the travel time, energy consumption, and emissions of each potential route are compared prior to selecting a route. Reducing the petroleum energy consumption of personal vehicles not only reduces the environmental impact of the transportation sector, but may also reduce the financial cost of transportation.

Ecorouting involves approximating the energy consumption and emissions for different route options for a specific vehicle prior to advancing onto any route option. Many ecorouting programs use polynomial approximations based upon velocity and acceleration to find energy consumption

and emissions; however, a small portion of a trip involving high engine loading may produce a significant increase in the vehicle emissions for that trip *(Ahn & Rakha, 2008)*. A highly accurate model that is capable of approximating most transient behavior is important.

All ecorouting processes look ahead in time but the time horizon varies depending on the distance to the requested destination and which routes are available to reach the requested destination. Once a routing decision is made, the system continuously recalculates at a set rate to ensure any new traffic data will not cause another potential route to be more efficient. Each ecorouting process weights travel time, energy consumption, and emission differently, but the goal is the same: find the route with the least environmental impact that does not overly inconvenience the driver due to the increased travel time.

1.2.1 Differences between Ecorouting and Ecodriving

For the purposes of this thesis, ecorouting and ecodriving are distinct. Ecorouting is a term referring to the process by which a route with the minimal environmental impact is chosen. Ecodriving is the process by which a vehicle control strategy or driver behavior is carefully calibrated to reduce the environmental impact of any route. This thesis is purely dedicated to ecorouting. The research develops a methodology by which environmentally friendly routes may be selected for any vehicle. As the methodology may be applied to any vehicle on the road today, the methodology must be accurate for stock vehicle control strategies as most drivers are unlikely to modify their vehicle control strategy. Ecodriving is another area of study may be incorporated into the design and modification of a vehicle or taught to the driver.

1.2.2 Route Differentiation

For a powertrain model to be applicable to ecorouting, the model must be able to differentiate the energy consumption and emissions between route options. Unfortunately, there are not usually "hard rules" such as "slower acceleration is always more energy efficiency". In fact, there are times where the system is more efficient if the vehicle accelerates heavily. Although there may not be "hard rules," factors such as hills, cruise speed, idle time, acceleration, and traffic congestions are all route characteristics that often have a large influence on vehicle energy consumption and emissions. The extent of influence of these characteristics is also likely to vary between vehicles which is why the ecorouting powertrain model must approximate each specific vehicle powertrain rather than assume one route is always best for all vehicle types. Once an ecorouting powertrain model predicts route behavior, routing is weighted by time and environmental cost. Users can select a preference in weighting based upon individual needs.

1.2.3 Future of Ecorouting

Some ecorouting systems are stand-alone and only route based on data collected onboard that specific vehicle. Other ecorouting systems are cooperative and vehicles share traffic and energy consumption data with vehicles of the same class. The more vehicles using a given ecorouting system, the more accurate that system becomes as more vehicles are inputting traffic information. If the entire United States road network were to utilize a central route selecting software, the overall time and environmental efficiencies of all vehicles would improve because vehicles would be aware of one another's actions before they occur, allowing for better yet traffic prediction. Further, roadway infrastructure such as traffic lights could be programmed to further increase network vehicle efficiency.

Another use for ecorouting is to input route data to vehicle controllers. Control strategies for vehicles could become further intelligent with knowledge of upcoming traffic or terrain. As HEVs have multiple modes of operation, HEVs would most benefit from future route knowledge. *(Vajedi et al., 2014)* analyzes how a Toyota Prius controller may utilize previous route data to improve fuel economy up to 11%. *(Zhang et al., 2010)* develops a parallel PHEV model and compared energy consumption outcome for two control strategies: one with future route data and one strategy without future route data. Zhang et al. focused primarily on terrain data and how a HEV may strategically store battery energy prior to a hill to be depleted ascending the hill and then recharge the battery descending with regenerative braking. Zhang et al. found a 1-4% increase in fuel economy for a parallel PHEV driving in hilly terrain.

1.3 Research Objectives

The key objective of this research is to develop and present a methodology for approximating the energy consumption of a specific vehicle such that a comparison in energy consumption between potential routes may be made. This methodology has been implemented into an excel spreadsheet for both validation and demonstration. While most ecorouting programs include emission data, this research focuses on energy consumption with only brief mention to Greenhouse Gas (GHG) emissions due to the complicated nature of other emission types. This model is designed to be simple and user-friendly such that future members of the Hybrid Electric Vehicle Team (HEVT) may use this methodology to further develop ecorouting as the EcoCAR 3 innovation topic.

Many highly accurate energy consumption modeling tools exist today and require Original Equipment Manufacturer (OEM) proprietary vehicle characteristics. The purpose of this research is to evaluate energy consumption of a vehicle using only publically available vehicle characteristics. Collecting field data for the entire operating envelope for every vehicle to supplement publically available characteristics is not realistic for modeling many different vehicles. To enable a reduction in inputs, this model scales data of known components to approximate the components of similar vehicles. Component models rely on closed form equations instead of vehicle-specific lookup tables. This model is capable of predicting the energy consumption of BEV's, HEV's, PHEV's, and conventional vehicles. Not only is a reduction of vehicle inputs easier for the user, a reduction in vehicle inputs allows for faster computation. This model is expected to operate such that preferred route may be selected in real-time with constantly updating inputs.

This model traces energy flow through each powertrain from the wheels to the energy source or sources. This approach is known as a "backwards" model as the requirements at the wheel are known and then the demand from each energy source is found. As this research consists of developing a methodology for predicting energy consumption for a variety of powertrain types, validation is of utmost importance. The energy consumption from each major powertrain type must be validated. Unlike most models, this model does not need to yield particularly high-accuracy energy consumption values; instead, this model must consistently and accurately rank routes based upon their relative energy consumption values. The application of this model is to provide insight into the difference in energy consumption between route options.

1.4 Application for EcoCAR 3 Innovation

1.4.1 Overview

This research is motivated by the addition of the "Innovation" category in the EcoCAR 3 competition. HEVT is participating in EcoCAR 3, a four-year collegiate automotive engineering competition and the latest installment of the Advanced Vehicle Technology Competition (AVTC) series. "EcoCAR 3 is challenging 16 North American university teams to redesign a Chevrolet Camaro to reduce its environmental impact, while maintaining the muscle and performance expected from this iconic American car" *(ANL, 2016a)*.

The competition represents a unique coalition of government, industry, and academia partnering to develop solutions for sustainable vehicles. The headline sponsors are the U.S. Department of Energy (DOE) and General Motors (GM). The DOE's motivation in sponsoring the competition is to accelerate the development of advanced vehicle technologies. Argonne National Laboratory (ANL), a research and development facility of the DOE, provides management for the competition with logistical and technical support. GM provides the Camaro, vehicle components, operational support, and technical mentoring. EcoCAR 3 intends to educate the next generation of automotive engineers to support the industry's need for engineers knowledgeable of advanced vehicle propulsion.

The technical goals of EcoCAR 3 are to reduce energy consumption, well-to-wheel GHG emissions, and criteria tailpipe emissions while maintaining the safety, performance and consumer acceptability of the stock vehicle *(ANL, 2016a)*. An added technical goal to the EcoCAR 3 competition is to meet the other goals while considering cost and innovation *(ANL, 2016a).* "Innovation is given added emphasis in this competition to allow for the inclusion of new or innovative technologies, reward teams for taking unconventional approaches or risks, emphasize new technologies to the public" *(ANL, 2015)*.

Teams may select a new topic every year or they may continue with one large topic for the entirety of the four-year competition. HEVT selected ecorouting on-board the vehicle as the topic for all four years. In future years, the powertrain methodology described in this thesis will be implemented on-board the vehicle to be used in real-time using live-updating map and terrain data. Other students on HEVT are working to develop the methodology by which map data can be extracted to be used as an input into this model. This research topic is inspired by the current research into conventional vehicle ecorouting at the Virginia Tech Transportation Institute (VTTI), specifically the research by Dr. Hesham Rakha who has agreed to assist HEVT in the topic.

1.4.2 Year 1

Year 1 of the competition included Fall 2014 and Spring 2015. During this year, innovation accounted for 10% of the total 1000 competition points. HEVT designated this year for researching the current state of the art in ecorouting, determining if the innovation topic was feasible with the time and resources available, and developing a plan for the next three years. HEVT received 82% compared to a competition average of 68% for the "Winter Workshop Innovation Topic Review Presentation." The objective of this deliverable was for the competition organizers to approve and provide feedback on the innovation topic *(ANL, 2015)*. The topic of Ecorouting was approved by the competition. Pramit Baul and Lucas Shoults gave this presentation on behalf of HEVT. They discussed that the current state-of-the-art is applied to conventional vehicles and not PHEVs. In exemplifying conventional vehicle ecorouting data, they

demonstrated that ecorouting has been proven to make a significant impact on fuel economy and acknowledged that hybrid vehicles could benefit even more.

For the year-end Innovation Presentation, HEVT received a 74.8% compared to a competition average of 57.4%. This presentation was given by Pramit Baul and William Dvorkin on behalf of HEVT. They refined the innovation topic by detailing that HEVT would research powertrain modeling so as to expand ecorouting to PHEVs and include all other vehicles on the road today. The scalable powertrain components they proposed are the foundation for this thesis.

1.4.3 Year 2

This year, Fall 2015 to Spring 2016, is Year 2 of the competition. Along with concurrent research by Pramit Baul in the field of extracting live traffic map data, this thesis provides the ecorouting developments made in creating a powertrain model that predicts energy consumption for a wide range of vehicles using minimal inputs. During the Year 2 Winter Innovation Review, HEVT received at score of 76 while the mean score for all teams was 66.

1.4.4 Year 3

During Year 3, HEVT will begin to apply the methodology described in this thesis to a platform that will run in an embedded processor on-board the vehicle. HEVT will also begin to integrate the ecorouting software with the vehicle controller to allow for ecodriving. HEVT will also use the model described in this thesis to plan an in-depth study of how different routes navigated in different hybrid modes affect total energy consumption to determine ideal ecodriving patterns.

1.4.5 Year 4

During the last year, Fall 2017 to Spring 2018, the ecorouting software will be fully integrated into the on-board embedded processor and will allow the driver to interface with the software. The vehicle controllers will send and receive data with the ecorouting program to increase vehicle efficiency. HEVT will demonstrate ecorouting abilities at the final competition.

1.4.6 *HEVT Selected Powertrain*

The research in this thesis develops a methodology to predict the energy consumption of a wide range of vehicles and serves as a proof-of-concept that all vehicles on the network could be modeled similarly and share traffic information with one another. For the purpose of EcoCAR 3, HEVT must demonstrate the ecorouting concept on-board the HEVT Camaro. Many examples in this research use the HEVT Camaro. The vehicle powertrain was selected during Year 1 of the competition. As the vehicle began as a 2016 Chevrolet Camaro and the team has no intention to alter the exterior, the HEVT's vehicle retains the original road load coefficients. The mass is significantly increased to 2120 kg.

The powertrain of the HEVT Camaro is discussed in an SAE publication by HEVT that may be referenced for further details *(Marquez et al., 2016)*. The vehicle is a parallel PHEV with a post-transmission motor. Torque from both the engine after the transmission gearing is mechanically combined with the motor. The power flow through the selected powertrain is demonstrated in both propel and brake cases in Figure 1-4 and Figure 1-5 respectively. Engine torque may be transmitted through the driveshaft while the motor is off and likewise the motor may operate while the engine is off. An 8-speed transmission was selected as well as a GM L83 5.3 L V8 engine capable of 265 kW. The team plans to run 85% Ethynol-15% Gasoline (E85) for fuel. The motor is custom-made with InMotion to have a max torque of 500 Nm and max power of 100 kW. The

motor also acts as a generator when capturing regenerative braking or when the battery is charged by loading the engine. The battery is A123 15s2P pack capable of 118 kW and an energy capacity of 12.6 kWh. These vehicle parameters are used for all simulations based on the HEVT Camaro.

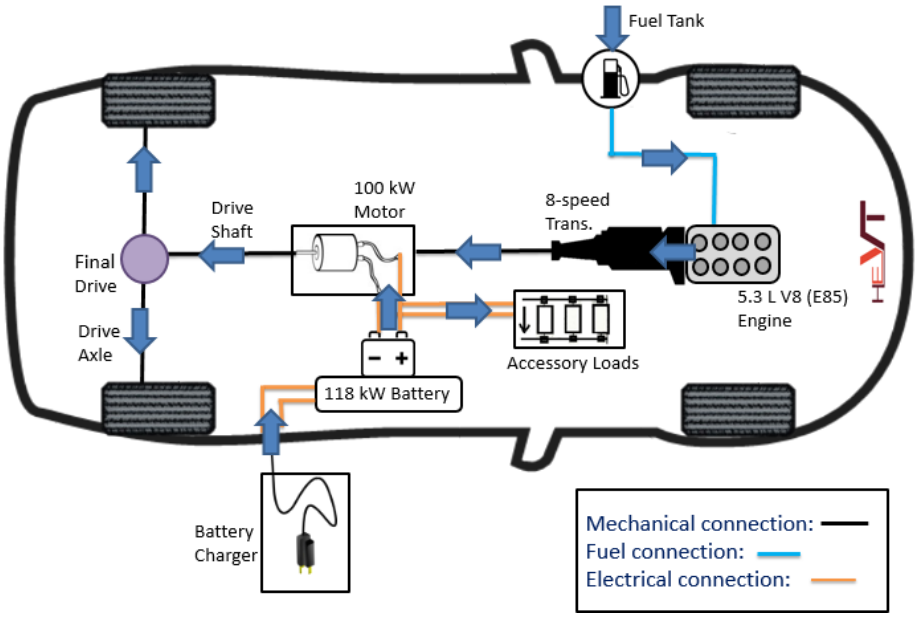

Figure 1-4: HEVT's Selected Powertrain Example Propel Case

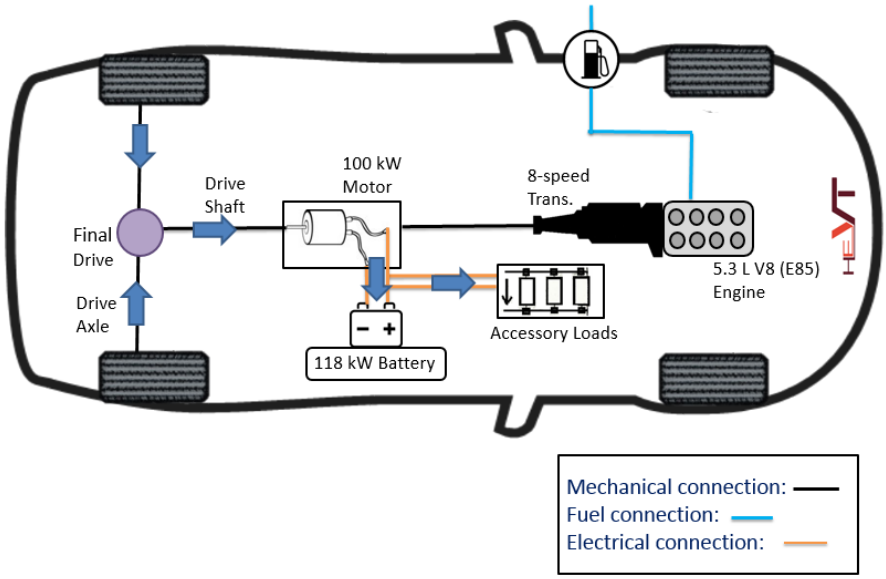

Figure 1-5: HEVT's Selected Powertrain Example Brake Case

1.5 Thesis Progression

This thesis will proceed as follows. First, a literature review is presented that overviews the benefits of ecorouting, the basis for powertrain modeling, and methods for hybrid control strategies. Next, the methodology for approximating energy consumption is presented beginning with the required route inputs as each route is determined external to this model. Similarly, all vehicle inputs are also described. As an objective of this research is to only utilize publically available vehicle parameters, there are very few vehicle inputs. Next, the description of the

powertrain methodology begins with the tractive energy required, both for propel and brake cases, at the wheels to meet the route. The tractive energy is backtracked through each component relevant to that powertrain and as such a discussion of the inputs, outputs, and losses of each component follows that of tractive energy.

After describing the methodology of how each component works and relates to one another, several component models and several powertrain models are validated with test data. The assumptions and limitations of each component and each powertrain are also discussed. Next, the model is applied to various routes to demonstrate an ability to serve in an ecorouting application. The thesis concludes with topics of future work and overall conclusions from the research.

2 Literature Review

2.1 Ecorouting Benefits

The research of this thesis is inspired by accounts of successful ecorouting by other authors, particularly the Virginia Tech researchers Ahn and Rahka.

2.1.1 Network-Wide Impacts of Ecorouting

Researchers at Virginia Tech, *(Ahn & Rakha, 2013),* published a paper summarizing a large-scale case study of the impact of ecorouting strategies for conventional vehicles. This section summarizes and analyses their publication. They developed an ecorouting system using real-world traffic conditions and map data for both Cleveland and Columbus, Ohio. The network contained a range of road types from local connectors to interstates and also included traffic features such as stop signs and traffic lights. Within the simulation model, each vehicle is given a different one-hour demand, the model runs until all vehicles cleared the network, then results are analyzed for trends.

The ecorouting strategy divides the network into links, which are potential route segments that may be strung together into a full route. The model looks ahead in time but the time horizon varies depending on the distance to the requested destination and which routes are available to reach the requested destination. Once a routing decision is made, the system continuously recalculates at a set rate to ensure any new traffic data will not cause another route to be more efficient.

Their ecorouting system is cooperative. Vehicles share traffic and energy consumption data with other vehicles of the same class. Upon completing a link, each vehicle uploads emission and energy consumption results. Other data collected and shared between vehicles includes travel time, travel distance, average speed, time for delay, and acceleration or deceleration operation. The vehicle connects all available links into potential routes and uses data from previous vehicles to estimate the emissions and fuel consumption of each link. The connection of links that yield the lowest environmental impact is selected for the route. All vehicles are divided into five classes such that the route of a given vehicle is determined by results from that vehicle class. The model is dynamic in using the results of the most recent vehicles in calculations. The model is also stochastic in that white noise may be added to prevent too many vehicles from selecting the same route at the same time thus creating unpredicted traffic. Additionally, driver variability can be imposed as a normal distribution to capture the effects of an increase or decrease in driver aggressiveness.

In general, the ecorouting program chose the shortest route but not necessarily quickest route in terms of travel time. Travel distance decreased by 5.11% and 5.46% in Cleveland and Columbus respectively. Conversely, travel time increased by 4.54% and 3.21%, respectively. Emissions are reduced 3.3% to 13.6% in Cleveland depending on the type of emission while emissions are reduced 5.2% to 17.7% in Columbus. The fuel savings between the two networks ranges from 3.3% to 9.3% in comparison with traditional minimum travel time routing systems. A three-minute increase in an hour commute leads to an average savings of 18% in fuel economy. Both fuel consumption and emission savings are found to be statistically significant between ecorouting and traditional travel time routing.

Rakha and Ahn find that the fuel savings of ecorouting are sensitive to the level of market penetration, the network configuration, the traffic congestion, and vehicle type. Market penetration relates to how many vehicles are utilizing ecorouting. All other vehicles are assumed to use traditional minimum travel time routing systems. As more vehicles use ecorouting, the greater environmental savings are for those vehicles already using ecorouting. Network configuration relates primarily to the number of route options available to reach a given destination. The Cleveland network has more connectors and therefore has more potential routes. As such, ecorouting has greater successes in Cleveland where the model has more options to consider. Another factor tested in the study is traffic congestion. They find that ecorouting consistently reduces the environmental impact of the vehicle in all traffic conditions but that an increase in congestion lead to a greater increase in environmental savings over traditional time routing. The last factor is vehicle type. Though the findings are inconclusive, the paper hypothesizes that less fuel efficient vehicles experience more of an impact using ecorouting than more fuel efficient vehicles which are better calibrated to consistently reduce environmental impact. This study concerns conventional vehicles and did not include electrified vehicles as is proposed in this thesis.

2.1.2 User Influence of Energy Efficiency in HEV Ecodriving

While the exact distinction between ecorouting and ecodriving varies in each publication, there consistently remains a significant relationship between the two. While the topic of this research is to apply a powertrain model for ecorouting purposes, ecodriving characteristics must be considered. Franke and Arend from the Technishe Universität Chemnitz and Mcllroy, and Stanton from the University of Southampton published an article this year exploring the user-energy interaction of HEVs. This section summarizes and analyses their publication *(Franke et al., 2016).* As their research is still in an infantile stage, their efforts, along with that of other researchers, exemplify the current need and demand for further research into decreasing vehicle energy consumption, particularly that of HEVs.

Franke et al. selected 39 Prius drivers who had consistently logged an average fuel efficiency above the fleet-average for the vehicle model over the previous three months. Acknowledging that driving behavior is always motivated by competing driver goals such as time, safety, and efficiency, the motivation for energy efficiency is a considerable predictor for each individual driver's attained energy efficiency. Also, the second major predictor for attained efficiency is a driver's technical knowledge of his vehicle. Franke et al. recognizes that HEVs prove especially challenging to understand due to bidirectional energy flow and the dynamic interplay between powertrain components. Within the context of this thesis, driver motivation is equivalent to the relative weighting of time versus efficiency in the route selection and technical knowledge is equivalent to the powertrain model accuracy.

Franke et al. segregated routes into four categories and assigned a complexity to each: highway (low), city (high), rural flat (medium), and rural mountainous (medium). They found that driver motivation had the strongest correlation with increased efficiency during low complexity situations. Conversely, technical knowledge had the strongest correlation with increased efficiency during high complexity situations.

Of the many ecodriving strategies suggested by the interviewees, Franke et al. identified several reoccurring themes. Acceleration rate must be carefully selected, or imposed by the route or powertrain control system. Many drivers incorrectly assume that either a very slow or an excessively quick acceleration is most efficient. Instead, there is an optimal efficiency acceleration that the work suggests could be relayed to the driver via displays or feedback in the pedal. Similarly, when on rural flat roads where there is a greater range of speed options, the driver could be alerted of the impact of each speed increment on efficiency.

Regenerative braking cannot capture all brake force and therefore encompasses a loss. In general, braking should be avoided as much as possible. The study found that drivers with future knowledge, like viewing distance traffic lights, attained greater efficiency as they could coast sooner. In general, predictive software, such as the ecorouting application of this research, could allow both the vehicle and the driver to better prepare for what is to come. Another suggestion of the publication to improve the user-energy interaction is to alert drivers of the impact of their current behavior on efficiency with either colors or symbols. Such an alert would train new drivers and reassure experienced drivers. Within the realm of this research, storing the results of prior situations may allow the powertrain model to better predict the outcome of similar future routes.

2.2 Powertrain Modeling

Within ecorouting, the research presented in this thesis pertains only to the powertrain model used to predict energy consumption for each route for a specific vehicle.

2.2.1 Energy Consumption Model for Ecorouting

Rakha et al. published details of a program called INTEGRATION which is designed for ecorouting purposes. This section summarizes and analyses their publication *(Rakha et al., 2012).* INTEGRATION is a microscopic traffic assignment and vehicle simulation software that tracks vehicles in the model at 10 Hz. The model is sufficiently detailed to account for vehicle lane changes and crashes. Vehicles are assigned to pursue certain route links based upon the expected fuel consumption. Fuel consumption predictions on a link are continuously refined based on the experiences of other vehicles of the same class. Upon completing each link, each vehicle uploads its fuel consumption data for that link.

When fuel consumption and emissions data is not available from previous vehicles, Rakha and Ahn use a function of instantaneous acceleration and velocity as sudden changes in vehicle acceleration may account for a large percentage of total emissions and fuel consumption. They selected the VT Micro model as the model had previously proven consistent with field data collection and could easily be integrated into microscopic traffic simulation models. VT Micro statistically predicts emissions and fuel consumption on a second-by-second vehicle trajectories using polynomial combinations of vehicle velocity and acceleration *(Rakha et al., 2004)*. Both fuel consumption and emission equations are derived using data collected by Oak Ridge National Lab and the EPA.

This thesis also proposes a methodology to predict fuel consumption for each route option. Rather than using statistical data and approximating fuel consumption only using instantaneous velocity and acceleration, this thesis proposes stepping through every powertrain component specific to that vehicle and analyzing the individual losses to ultimately approximate fuel consumption. Further, Rakha et al. only devised methods for predicting energy consumption for conventional vehicles. This research expands this work to include electrified vehicles.

2.2.2 Modeling Modern Engines

Nam and Sorab analyzed both full and partial spark-ignition engine maps from multiple manufacturers. This section summarizes their publication and discusses the application to this thesis *(Nam & Sorab, 2004).*They found a 25% reduction in engine friction between 1973 and 2003. Over the same time period, the found that thermal efficiency remained constant. They define the engine thermal efficiency as the slope of fuel Mean Effective Pressure (MEP) and Brake Mean Effective Pressure (BMEP). In the paper, an example engine thermal efficiency is given as 43.4% which sets a ballpark by which a thermal efficiency can be approximated in this thesis.

Friction losses are due to components rubbing, pumping fluid, or auxiliary components. Measuring engine friction directly is difficult during normal operation. A popular method for indirect measurement of these losses is to use a motor to operate an engine at a given speed. This method is called “motoring an engine” and is used by Nam and Sorab. Extrapolating the data, a Willan’s line relates fuel input to engine brake output. Fuel power is the product of fuel rate and the lower heating value (LHV) of the fuel. For convenience, Nam expresses both fuel and brake power per unit engine displacement and engine speed:

$$fuel\ MEP = \frac{P_{fuel}}{VN} \qquad \textbf{Equation 2-1}$$

where V is the engine displacement volume and N is the engine speed. Mean Effective Pressure (MEP) is a variation of engine torque that is scaled by engine displacement volume. As such, different sized engines share the same MEP values which allows for the simplification of assigning the same relationships to multiple engines of different displacements. The engine methodology in this thesis also uses a MEP approach as an objective of this work is to scale an engine loss model to match other size engines.

On the plot of BMEP vs fuel MEP, the value of BMEP at which fuel MEP is zero is considered to be the Friction Mean Effective Pressure (FMEP):

$$fuel\ MEP = \frac{BMEP}{\eta_{thermo}} + FMEP \qquad \textbf{Equation 2-2}$$

where η_{thermo} is the thermodynamic efficiency of the engine. Many engines fall on the same Willan’s line. Nam and Sorab obtained fuel engine maps for 10 vehicles ranging from model year 1997 to 2003 all of which had very similar Willan’s lines as shown in Figure 2-1.

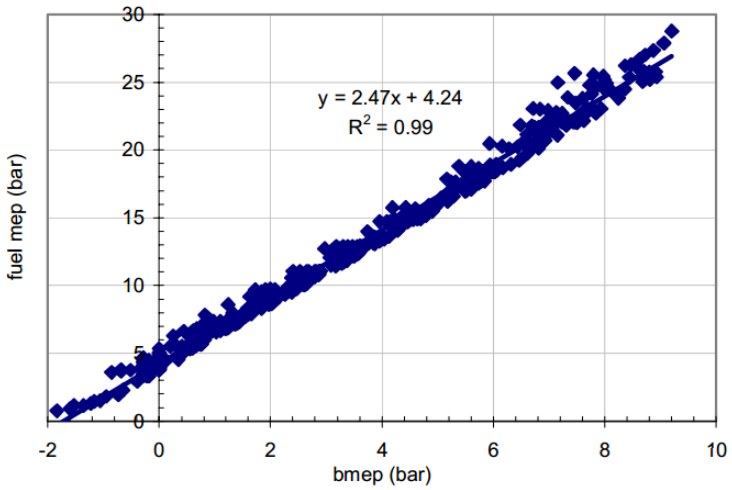

Figure 2-1: Fuel MEP versus BMEP for 10 Modern Engines *(Nam & Sorab, 2004, Fair Use)*

Nam and Sorab also explore limitations in a linear approach to engine modeling. As a start, the line is derived from motoring the engine but the engine can be expected to behave differently during firing operation due to lower gas loading and lower temperatures that increase component clearance. Nam and Sorab suggest that including Wide Open Throttle (WOT) and Fuel Enrichment operating points would result in a more non-linear relationship and are therefore omitted from the study. Likewise, the methodology in this thesis is known to be less accurate above the fuel enrichment (also known as power enrichment) limit.

Further, Nam and Sorab mention that other studies have found that engine friction is dependent upon the square of engine speed. In their study, Nam found a linear fit between FMEP and engine speed, but suggest that a second order term of engine speed would improve the fit. The methodology in this thesis expands their work to include the second order speed term in finding FMEP. Despite limitations, the Willan's line is a very simple model that can be used to estimate both thermal efficiency and mechanical friction when little data is available, as demonstrated in this publication.

2.2.3 Composing Component Models into a Powertrain

In an effort to better understand the potential of HEV powertrain design, Rizzoni et al. published an article in 1999 that describes a framework by which users may conduct an energy flow analysis of HEVs. This section summarizes their publication and discusses the application to this thesis *(Rizzoni et al., 1999).* Their modeling approach is to create component models which can be assembled to create any vehicle powertrain. While Rizzoni et al. provide specific attention to the engine and the electric motor, they hope that this framework will form a foundation for an even better equipped "toolbox" for HEV analysis. For each component model, Rizzoni et al. strive for both scalability and composability. Scalability requires the component model to be independent of size such that defining a scalar component parameter allows the model to represent all components within that class. Composability is the ability to easily compose the components so as to create any arbitrary powertrain.

The objectives of this thesis are similar to that of Rizzoni et al.: to create component models that may be scaled to capture a variety of sizes for that component and that can be arranged to capture a variety of powertrains. Rather than approaches like that of Rakha et al. in Section 2.2.1 that

require a new curve fit for each type of vehicle, Rizzoni et al.'s methodology allows a single model to be arranged in a way to capture the energy consumption of many vehicles.

Rizzoni et al. identify two types of variables that are most important in energy conversion: flow variables and effort variables, the product of which is power. They exemplify flow variables as current, translational and rotational velocity, and fuel flow rate. They exemplify effort variables as voltage, torque, force, and LHV of the fuel. Each component has an "efficiency-versus-effort-and-flow characterization" where the component efficiency is variable.

Further, Rizzoni et al. identify three types of components. Interdomain is when energy remains of the same form such as mechanical energy in a transmission. Intradomain is when energy is converted from one form to another such as electrical to mechanical energy in a motor. The last category is energy storage devices like a battery or fuel tank. Beginning with an engine model, Rizzoni et al.'s model is scalable with only two size parameters: BMEP and mean piston speed. The model works using the same principle as Nam and Sorab's Equation 2-2. Rizzoni et al. select mean piston speed because flow friction is affected by local speed, not engine speed. The thermal efficiency of the engine is found using polynomial approximations based upon piston speed, unlike a constant value used by Nam and Sorab.

Rizzoni et al. develop the electric motor model of the same form as the engine model in an attempt to match components of a similar energy conversion category. An affine relationship between output torque and input energy is assumed to determine motor efficiency. The BMEP is also defined as the mean force acting on the rotor divided by rotor surface. The two expressions for BMEP are equated to find an expression for motor power necessary in for a given output torque. Although the efficiency coefficients will vary between a motor and an engine, the models are constructed in a similar manner.

2.3 Hybrid Control Strategies

The methodology presented in this thesis combines a variant of a thermostatic and power-demand PHEV control strategies. A future goal of the powertrain methodology presented is to analyze the ecorouting program such that the hybrid control strategy of the HEVT Camaro can be adapted for improved ecodriving.

2.3.1 Parallel HEV Control Strategies

Researchers from Texas A&M published a study comparing the fuel consumption and emissions resulting from two control strategies for parallel HEVs. This section summarizes their publication and discusses the application to this thesis *(Rahman et al., 2000).* They chose to focus on parallel PHEVs for many of the same reasons as HEVT's performance hybrid: in comparison to series PHEVs, parallel PHEVs are "more suitable satisfying high road power demands" such as high speeds or accelerations. Rahman et al. concede that parallel PHEVs are far more complicated to model since parallel PHEVs are more challenging to define a good power strategy and also because parallel PHEVs may exist with a variety of component configuration, particularly that of the transmission. In this study, they evaluated a pre-transmission motor, a post-transmission motor, and motor following a Continuously Variable Transmission (CVT).

The first proposed control strategy is a variant of a thermostatic or "on/off" approach. An upper and lower battery SOC threshold is defined using battery parameters. They defined the range as 60%-80%. Many drivers charge their PHEV during the night and often begin a route with a high SOC. When SOC is greater than the upper threshold, the vehicle is fully propelled by the motor.

When SOC drops below the lower threshold, the engine turns on and operates at Wide Open Throttle (WOT), or maximum available torque. The required torque is sent to the wheels and all remaining torque is used to charge the battery via the motor which then acts as a generator. In case of high power demand, the motor will assist the engine regardless of SOC.

The second proposed control strategy is an electrically assisted "power-split" approach, which will subsequently be referred as a "power-demand" approach in this thesis. The engine is the main power source and the motor only operates when the engine would run inefficiently or the engine needs more power. They defined the engine to be "inefficient" when the torque demand is less than 60% engine max torque or the engine speed would be less than 2000 rpm. If SOC drops below a lower threshold, the engine will produce excess power that is a function of SOC. Both strategies incorporate regenerative braking.

For the purposes of this thesis, the results attained for which powertrain achieved the lowest energy consumption and emissions are not relevant. This thesis is not to be used to guide the design of vehicles, but rather, find flexible approaches to modeling actual HEV vehicles on the road today. A combination of variants of both the thermostatic and power-demand parallel HEV control strategies presented in their paper are implemented into the methodology of this thesis. Likewise, the ability to account for pre- and post-transmission motors is also incorporated into this thesis.

2.3.2 PHEV Control with Knowledge of Future Route

At the International Battery, Hybrid and Fuel Cell Electric Vehicle Symposium in 2012, Lee et al. presented a methodology for determining how to control an HEV such that the battery continuously depletes throughout the route. Their paper makes the assumption that the entire route is known from the start, as would be the case for a vehicle with ecorouting software pulling live-updating map data. This thesis section summarizes their publication and discusses the application to this thesis *(Lee et al., 2012).* For each location on the route their algorithm weights the speed limit, average speed of current vehicles, and length of the segment to create a speed profile. Idle time, acceleration, and deceleration rates are also determined using these weighted factors. Similar to this thesis, Lee et al. uses a distance-based system. This thesis, however, assumes a constant acceleration between nodes and that the speed profile has been pre-processed externally as part of the route determination.

Lee et al. pursued Pontryagin's Minimum Principle (PMP) as a simple yet promising power management theory that operates the vehicle in blended mode. The method is assumed to be simple enough to complete in real-time. The only cost function to be minimized is a function of fuel consumption and rate of change in SOC. The cost function is constrained by vehicle component limitations such as maximum engine torque and speed. As the model is designed to run real-time but must iterate many times until finding the optimum power split between the engine and motor, the model must first make an approximate guess. Lee et al. has related battery energy and required average SOC drop rate into a function that provides an initial guess of high accuracy.

The model used for this publication approximates a 2004 Toyota Prius which is a power-split hybrid that uses a single planetary gear set. The end SOC did not always end at the expected value because the predicted speed profile is used to formulate the end SOC but the vehicle did not always follow the predicted path, as expected. The control strategy did, however, prove useful in reducing fuel consumption in comparison to methods that charge deplete the battery and then turn on the engine to charge balance the battery. A comparison is shown in Figure 2-2 where the

left image demonstrates the SOC versus time. The right image demonstrates how the PMP method initially has higher fuel consumption but has less total fuel consumption by the end of the route.

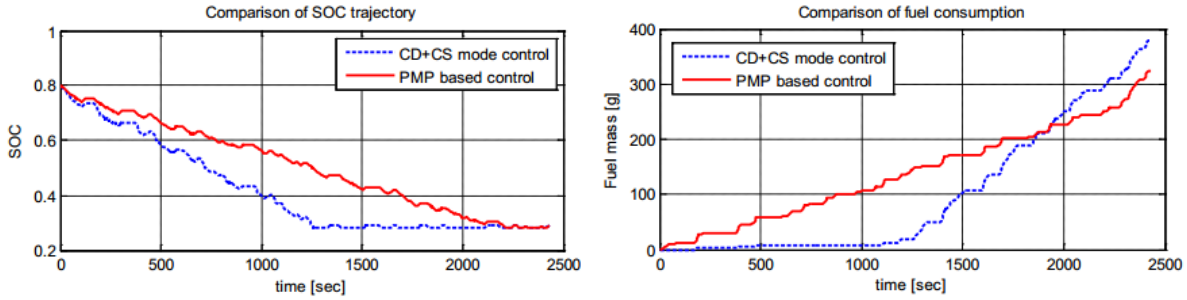

Figure 2-2: Comparison of PMP and CD+CS Control Strategies *(Lee et al., 2012, Fair Use)*

The application of this thesis could be used to improve HEV control strategies, as done in this publication. Instead of a single vehicle, like the Prius, the methodology in this thesis could be used to represent the energy consumption of many different vehicles. Though the details of the model by Lee et al. are not provided, rather than a single cost function, this thesis presents a methodology by which the energy consumption of each component of the powertrain can be approximated individually and then combined into the total energy consumption of a given route.

2.4 Literature Review Summary

This literature review includes a variety of topics forming the foundation of this research with work on modeling the fuel consumption of engines from as far back as 1999 to work applying a vehicle consumption model to PHEV ecodriving as recent as this year. This thesis is inspired by research at VTTI by Dr. Hesham Rakha. As discussed in Section 2.1.1, Rakha and Ahn have had great success in demonstrating the environmental benefits attainable by ecorouting conventional vehicles. They found a 3.3-17.7% reduction in emissions and 3.3-9.3% reduction in fuel consumption for vehicles that used ecorouting instead of traditional time routing software. The range in environmental savings varied with driving conditions and vehicle type. Rakha and Ahn found that ecorouting is most successful in networks with many connectors allowing more route options. Further, ecorouting is most successful when a greater percentage of vehicles on the road use cooperative ecorouting to share experiences. This thesis intends to expand into ecorouting electrified vehicles to allow for all vehicles on the network to utilize the same model.

Electrified vehicles, particularly HEVs, are much more complicated to predict energy consumption, as is described by Franke et al. in research published just this year. Through interviews with HEV drivers, they determined that driver motivation and technical knowledge of their vehicle greatly impacted vehicle efficiency. Within the context of this thesis, driver motivation is equivalent to the relative weighting of time versus efficiency in the route selection and technical knowledge is equivalent to the powertrain model accuracy. Areas of interest for ecodriving included acceleration rates, cruise speeds, and thinking ahead, which are all areas that are also critical in ecorouting.

Looking toward the powertrain model, Rahka et al. provides setup for how ecorouting works and where the powertrain model fits into ecorouting as a whole. When the experiences of prior vehicles are unknown, the energy consumption of the powertrain for each specific route is determined by statistical correlations of speed and acceleration in the model of Rahka et al. The resulting energy

consumptions are used to select the most fuel efficient route. Rather than using statistical correlations to approximate the entire powertrain, this thesis attempts to model every component and then assemble the components into each required powertrain. This method is proposed by Rizzoni et al. as a way to obtain both scalable component models and a composable powertrain model. One component model that is easy to make scalable is the engine. Working with BMEP instead of torque approximates engine efficiency regardless of engine size, as is demonstrated by Nam and Sorab.

Rahman et al. discussed two parallel PHEV control strategies: thermostatic and power-demand. The values of critical points for both strategies have been modified, but the premise of both strategies have been combined into the research in this thesis. Looking towards future research, once this powertrain model is proven accurate in predicting the energy consumption of the HEVT Camaro, HEVT can utilize this model to improve the ecodriving nature of the vehicle control strategy. Lee et al. provided a framework by which different control strategies can be iterated for the same route to find the strategy that most consistently depletes the battery throughout the entire route. This model does not incorporate a blended hybrid strategy, but as future work the HEVT Camaro could input ecorouting data to component controllers so the controllers may use future route data to may make decisions for increased overall powertrain efficiency.

3 Component and Vehicle Model

This chapter details each equation and component interaction that forms the basis for energy consumption approximation. The principles of a route are first presented and then a description of how the vehicle glider model finds the tractive effort required at the wheels to meet a route. Backtracking through the powertrain, the energy inputs, outputs, and losses for each individual powertrain component are discussed as well as which powertrain characteristics are required inputs for the model to adequately approximate the behavior of that component. A discussion of how certain components may be assembled to form different powertrains follows. This section concludes with overall model outputs.

3.1 Route Properties

A route is any potential combination of roads between the current location and destination. Map data for each potential route must be pre-processed prior to entering this model. As the routes are pre-processed, the uncertainty of how the vehicle will actually encounter the route is not considered but has potential to be significant in the event of sudden traffic changes. This model accepts inputs on a node-by-node basis where each node is a physical location in space with associated distance, velocity, grade, and idle time data. The model is distance-based to emulate collecting traffic data at specified geographic locations rather than discrete locations in time. From these four inputs, this model can analyze the route to find the tractive effort required at the wheels of the vehicle to complete such a route.

The distance between the two nodes is referred to as a segment. The relationship between nodes and segments is exemplified in Figure 3-1. For a segment between Nodes 1 to 2, the segment-start velocity is the velocity of the average traffic velocity of Node 1. Likewise, the mode-end velocity is the average traffic velocity of Node 2.

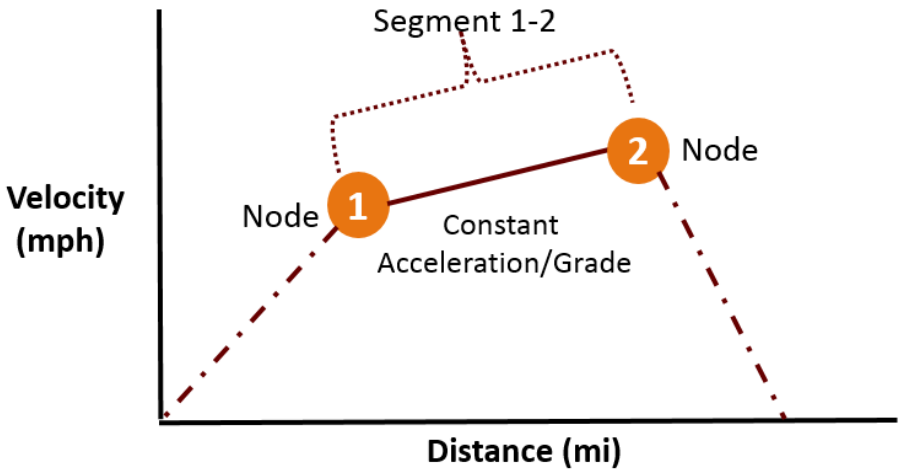

Figure 3-1: Arbitrary nodes with segment between of constant acceleration

3.1.1 Distance from Origin

In the next two years as HEVT implements this methodology onto a processor on-board the vehicle, the model will receive live traffic map updates. Each grouping of node inputs are associated with a point in space in which those conditions are occurring. The distance input for each route is an absolute distance from origin. This is to say, as the vehicle moves forward, the distance input should continuously increase similar to a mile marker.

3.1.2 Target Velocity

Each node begins a new segment which will end when the next node is reached. Target velocity for each node is the velocity which the vehicle should obtain by the next node. Target velocity is the desired segment-end velocity. The target velocity is used with the current vehicle velocity to find an average acceleration that the vehicle must maintain during that segment. At each distance node, the velocity of the following node is the associated velocity input. Using the segment-start velocity would cause error when the vehicle may previously have a different speed when reaching the start of a new segment. Looking forward allows the vehicle to correct for any prior changes. As such, at each node, the segment-end velocity is the associated velocity input.

Target velocity encapsulates traffic data. The target velocities received by the vehicle are average velocities of recent vehicles at the same location. In moments of high traffic, vehicles will travel at a slow velocity between distance nodes. When the vehicle is anticipated to stop, each nearby node leading up to the stop has a progressively slower target velocity. The purpose of this research is to model the vehicle as the vehicle is expected to drive, not determine a methodology to approximate how the vehicle should be driven.

3.1.3 Average Grade

Average grade is the average slope during the entire segment to come. If a hill rises and falls completely back to the original height during one segment, the average grade is zero. Ideally, nodes are sufficiently discretized to capture variations in grade.

3.1.4 Idle Time

A vehicle is idle when both the velocity and acceleration are zero. As the nodes in this model are based on distance, there is no way to know how long a vehicle may idle at a particular node other than to specifically input idle time at that node.

3.1.5 Route Kinematics

A route describes how the vehicle is expected to drive and is a compilation of segments created by a string of nodes. From the route inputs of distance from origin, target velocity, grade, and idle time, other route kinematics may be derived. As this methodology assumes that the nodes are sufficient in frequency, a constant acceleration is assumed between nodes:

$$a = \frac{v_b^2 - v_a^2}{2(x_b - x_a)} \quad \textbf{Equation 3-1}$$

where $v_b$is the velocity at the end of the segment and v_a is the velocity at the start. Likewise, x_b is the end position of the segment, $x_a$is the start, and $x_b - x_a$ is the length of the segment. As a verification that the model is correctly coded, the velocity attained approaching node b should be equal to the input velocity at node b:

$$v_{\mathrm{b}} = v_{\mathrm{a}} + a(\Delta t) \quad \textbf{Equation 3-2}$$

Knowing the distance traveled during a segment, the start velocity, end velocity, and assuming a constant acceleration, the elapsed time is fully constrained. When acceleration is zero, which is true under cruise conditions, the time duration between the first and second node can be determined using:

$$\Delta t = \frac{x_{\mathrm{b}} - x_{\mathrm{a}}}{v} \quad \textbf{Equation 3-3}$$

where v is the constant velocity between the nodes. Alternatively, if acceleration is not zero, the commonly used kinematic equation for a constant acceleration, Equation 3-4, may be solved for time as shown in Equation 3-5.

$$x_{\mathrm{b}} = x_{\mathrm{a}} + v_a \Delta t + \frac{1}{2} a(\Delta t)^2 \quad \textbf{Equation 3-4}$$

$$t_{\mathrm{b}} = t_{\mathrm{a}} + \frac{v_1^2 + \sqrt{v_{\mathrm{a}} + 2a(x_{\mathrm{b}} - x_{\mathrm{a}})}}{a} \quad \textbf{Equation 3-5}$$

Creating a route that is equivalent to a standard drive cycle is often of interest. As standard drive cycles are provided in terms of time and velocity, idle time may be extracted. Similarly, assuming a constant acceleration between velocity values, Equation 3-4 may be used to find the distance from the origin at each time step. When solving for time, Δt is the elapsed time between velocity inputs, which is normally one second in a standard drive cycle. Distance-based and time-based "routing" are equivalent when assuming a constant acceleration rate between velocity values. See Appendix F for example routes plotted as a function of distance and as time.

3.2 Tractive Energy Requirements at the Wheels

3.2.1 Glider Model

A glider model inputs vehicle velocity, acceleration, road grade, and vehicle glider properties to calculate the effort required at the wheels of the vehicle to attain the required velocity. A glider model does not consider the powertrain required to produce the effort at the wheels. The powertrain model will be described in Section 3.4 of this thesis. Figure 3-2 isolates the major forces on the vehicle in a Free Body Diagram. Equation 3-6 sums the forces in the direction of velocity and Equation 3-7 forms the base equation for a Glider Model in solving for tractive force

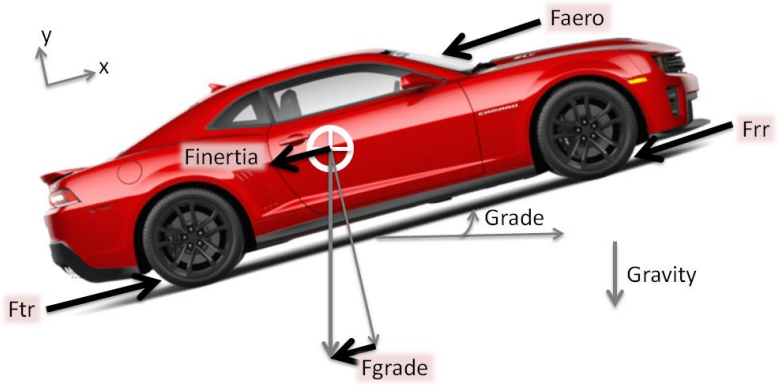

Figure 3-2: Free Body Diagram of the Chevrolet Camaro *(Adpt. From GM, 2016, Fair Use)*

$$\sum F_x = m_i a \qquad \textbf{Equation 3-6}$$

$$F_{tr} = F_{inertia} + F_{rr} + F_{aero} + F_{grade} \qquad \textbf{Equation 3-7}$$

where a is the acceleration of the vehicle, m_i is the inertial mass of the vehicle, F_{tr} is the tractive force at the wheels, $F_{inertia}$ is the inertial force, F_{rr} is the rolling resistance force, F_{aero} is the aerodynamic drag force, and F_{grade} is the grade force.

A glider model is backwards-facing as the desired velocity is known and used to find the required powertrain output. The glider model finds the tractive force and similarly the tractive power:

$$P_{tr} = F_{tr}\bar{v} \qquad \textbf{Equation 3-8}$$

where $\bar{v}$ is the average velocity during that mode. Tractive power is the power that must be exerted from the wheels to obtain the desired velocity. A negative tractive power signifies braking. Tractive energy may be found as the integral of power with respect to time or the integral of force with respect to distance.

$$E_{tr} = \int P_{tr} dt = \int F_{tr} dx \qquad \textbf{Equation 3-9}$$

3.2.1.1 Inertia Force

One important vehicle characteristics in determining energy consumption is mass. A separate inertial mass is used for calculations requiring rotational inertia. The mass and size of most rotating parts typically require OEM proprietary data or a coast down test of each vehicle to find the rotational inertia. The EPA approximates equivalent inertial mass in increments of 10 kg based upon groupings of loaded vehicle mass *(Cornell, 1998)*. As a constant approximation, the inertial mass is slightly larger than the actual mass of the vehicle by about 4% as shown in Equation 3-10,

$$m_i = mk_{inertia}$$ **Equation 3-10**

where kinertia is assumed to be 1.04 to capture the rotational inertia of components, primarily axles, wheels, and tires.

Inertial force, found using Equation 3-11, is the often most significant force acting on the vehicle:

$$F_i = m_i a$$ **Equation 3-11**

where mi is the inertial mass of the vehicle. The acceleration, a, is the vehicle acceleration, which is a known value based upon the route velocity inputs. This model assumes a constant acceleration. Given a start and end velocity for each mode, the constant acceleration may be found using Equation 3-1.

3.2.1.2 Grade Force

Grade force accounts for the resistance of a grade when the vehicle ascends a hill, or conversely, the assistance of a grade when the vehicle descends a hill. This model assumed a constant grade during each segment. Grade force is caused by the component of vehicle weight, mg, acting in the direction of travel. Grade force may be found using:

$$F_{grade} = mgsin(\alpha)$$ **Equation 3-12**

where m is the mass of the vehicle, g is the acceleration of gravity, and α is the grade angle. Maps do not often offer the grade angle and model input is the percent grade. The percent grade can be converted to grade angle, α, with:

$$\alpha = tan^{-1}\left(\frac{\%\ Grade}{100}\right)$$ **Equation 3-13**

3.2.1.3 Road Load

Road load is the combination of rolling resistance and aerodynamic drag. The vehicle rolling resistance can be modeled using two coefficients: crr0 and crr1. Likewise, aerodynamic drag can be approximated with the product of the drag coefficient and the vehicle frontal area: CDAF. These resistance coefficients are not commonly publically available in this form. Instead, they are often published in the form of A, B, and C coefficients with units lbf, lbf/mph, and lbf/mph2 respectively. The EPA publishes these coefficients for all production vehicles. After converting the lbf to N and the mph to m/s, the conversions to the desired resistance coefficients are shown below:

$$c_{rr0} = \frac{A}{ETW * g}$$ **Equation 3-14**

$$c_{rr1} = \frac{B}{ETW * g}$$ **Equation 3-15**

$$C_D A_F = \frac{C}{\frac{1}{2}\rho_{air}}$$ **Equation 3-16**

where g is the acceleration of gravity and ρair is air density. ETW stands for Equivalent Test Weight.

The EPA rounds the actual vehicle test weight to form ETW to calculate A, B, and C *(Cornell, 2000)*. To capture this rounding, ETW is also a separate input from mass to allow EPA A, B, and

C factors to be used to model a more exact vehicle mass or a vehicle that has changed in mass since the original testing, as is the case for the HEVT Camaro.

As a tire rotates, the weight of the vehicle causes a cyclic deformation and recovery of the rubber. The majority of rolling resistance can be accounted for by the energy dissipated as heat in the resulting tire hysteresis *(Ehsani et al., 2010)*. While the rolling resistance coefficient depends on factors such as tire material, tire tread geometry, tire pressure, and road material, both rolling resistance coefficients are assumed constant for this model *(Ehsani et al., 2010).* Finding rolling resistance as a linear function of speed has been found sufficient by *(Ehsani et al., 2010).* The rolling resistance can be approximated using Equation 3-17:

$$F_{rr} = mg(c_{rr0} + c_{rr1}\bar{v}) \quad \textbf{Equation 3-17}$$

where c_{rr0} and c_{rr1} are rolling resistance coefficients for that vehicle.

Aerodynamic drag is the result of air resistance on the vehicle and can be found using Equation 3-18:

$$F_{aero} = \frac{1}{2}\rho_{air} c_d A_f v_{rms}^2 \quad \textbf{Equation 3-18}$$

where ρ_{air} is the density of air, $c_d A_f$ may be found with Equation 3-16, and v_{rms} is the root mean square velocity. Aerodynamic drag is heavily dependent upon velocity as noted by the velocity squared term. Root mean square velocity can be found using Equation 3-19:

$$v_{rms} = \sqrt{\frac{v_b^2 + v_a^2}{2}} \quad \textbf{Equation 3-19}$$

where v_b is the velocity at the end of the segment and v_a is the velocity at the start. As nodes become more frequent, root mean square velocity becomes closer in value to average speed. This model may input nodes as frequently or as infrequently as data is available.

3.2.1.4 Glider Model Parameters

Table 3-1 lists all of the values necessary to create a glider model for a particular vehicle. The HEVT Camaro parameters are listed as an example. There are two physical parameter inputs: the acceleration of gravity and the density of air. Both parameters change with altitude and overall geographic location. When implemented onboard the vehicle, these parameters may live update. For now, constant values are assumed. All other glider model inputs are discussed in the previous subsections.

Table 3-1: Vehicle Glider Parameters for HEVT Camaro

*Parameter	Value	Unit
Gravity	9.81	[m/s2]
ρair	1.2	[kg/m3]
Mass	2120	[kg]
kinertia	1.04	[---]
ETW	3750	[lb]
EPA A	30.1	[lbf]
EPA B	0.4825	[lbf/mph]
EPA C	0.01823	[lbf/mph2]

*Green cells signify required inputs

3.2.2 Tractive Cases

A node is a physical location in map data with corresponding information regarding target velocity, grade, and idle time. The distance between two nodes forms a segment, as shown in Figure 3-1. During a segment, the vehicle has a constant acceleration and also a constant tractive power. Major tractive cases are propel, brake, and idle which typically correlate with accelerate, decelerate, and remain still. Cruising, or driving at constant velocity, is not a major case as vehicles rarely maintain exactly the same speed. Instead, vehicles that are cruising have a slight acceleration or deceleration.

3.2.2.1 Propel Case: PTR≥0 when V≠0 while PTR=0

The propel case includes all segments where the vehicle powertrain must provide a positive or zero tractive power. A positive tractive power accelerates the vehicle if the power overcomes all resistive power. In some cases, such as ascending a very large hill, the vehicle may be providing positive tractive power and still decelerate. A tractive power of zero may occur as a transient passing between positive to negative tractive power. The propel case excludes idle time, as is denoted by excluding the conditions of idle when both tractive power and average velocity are zero.

3.2.2.2 Brake Case: PTR<0

The brake case includes all segments where the vehicle powertrain must provide a negative tractive power. A negative tractive power typically decelerates the vehicle. In some cases, a vehicle may descending a steep hill and accelerating despite braking. BEVs and HEVs may often capture a portion of the negative tractive power for regenerative braking that can be used to charge the battery. For all vehicle types, the negative tractive power that cannot be captured in regenerative braking is lost to friction.

3.2.2.3 Idle Case: PTR=0 and V=0

During idle, there is no tractive power at the wheels and the vehicle velocity is zero. The vehicle remains in the same location. The model requires idle time as an input for each node because a distance-based input cannot otherwise capture the amount of time spent in idle at that node. During idle, energy is still required to power accessory loads. For a BEV, the battery SOC is depleted. For a conventional vehicle, the engine experiences an idle load and consequent fuel use. A hybrid vehicle experiences a combination of BEV and conventional idle loads.

3.2.2.3.1 Charging: PTR=0, V=0, Pbatt,out<0

Charging is the act of using external grid electric energy to increase the charge in the battery. Charging occurs during the idle case. This model does not capture charging. Instead, the input of initial battery SOC is increased prior to running the next simulation.

3.2.2.3.2 Fueling: PTR=0, V=0, Peng,out<0

Fueling is the act of adding fuel to the fuel tank. Fueling occurs during the idle case. This model does not capture fueling. Instead, the input of initial fuel in gallons is increased prior to running the next simulation.

3.3 Component Models

This section details each individual component model. The energy into, out of, and lost from each component is discussed as well as the methodology for how each value is found. For each component, a table will exemplify the component parameter values necessary to model the HEVT

Camaro as this is the prototype vehicle of primary interest. Listing component inputs serves as a showcase for how few vehicle parameters are necessary to utilize this methodology. As a major objective of this research is to predict energy consumption using only publically available powertrain characteristics, there are very few input characteristics required. The required input parameters for each component are shaded in light green in that table corresponding with that specific component. The model does not require any characteristics that are commonly considered to be OEM-proprietary. Not all model inputs are vehicle-specific characteristics. Non-input parameter values in Section 3 designate values that are model-calibrated as either constants for all vehicles or functions of known vehicle characteristic inputs. If extra information for a specific vehicle is known, such values may be overwritten. Appendix H consolidates all required inputs and computed parameters for the entire vehicle.

3.3.1 Energy Loss Modeling

Energy Loss Modeling takes an external perspective of each component and classifies all energy transfers of the component as energy in, energy out, and energy loss. Energy loss modeling captures the overall energy balance:

$$E_{in} = E_{out} + E_{loss} \qquad \textbf{Equation 3-20}$$

Figure 3-3 show a generic component energy balance. Component characteristics are needed to calculate each energy value for that component. Torque and speed characteristics are used in this model to approximate motor and engine contributions. Likewise, voltage and current characteristics are used in this model to approximate battery contributions. The method and characteristics needed for each component model are discussed in the following sections. *(White et al., 2015)* develops a time-based backwards-facing model for a BEV and series PHEV that also uses an energy loss modeling approach.

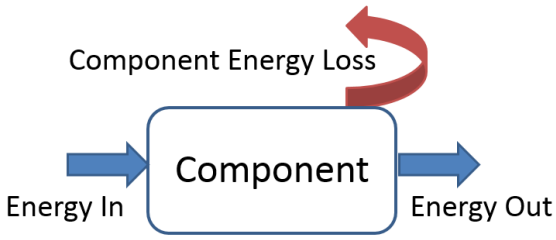

Figure 3-3: Energy Loss Diagram

Energy is the time integral of power. Like energy, the power into, out of and lost from a component must be balanced. Energy cumulatively accounts for all power interactions over a given time period. As power is an instantaneous value, energy is used for validation purposes with complete drive cycles.

3.3.2 Driveline Model

The driveline model includes the drive axles, final drive, and driveshaft. Figure 3-4 provides a driveline diagram for a Rear Wheel Drive (RWD) vehicle. One important characteristic of the driveline is the driven axle. The HEVT Camaro is RWD while many other vehicles are Front Wheel Drive (FWD). In this model, the only distinction comes from regenerative braking, as discussed in Section 3.4.2. For non-electrified vehicles, the driven axle does not make a distinction within this model.

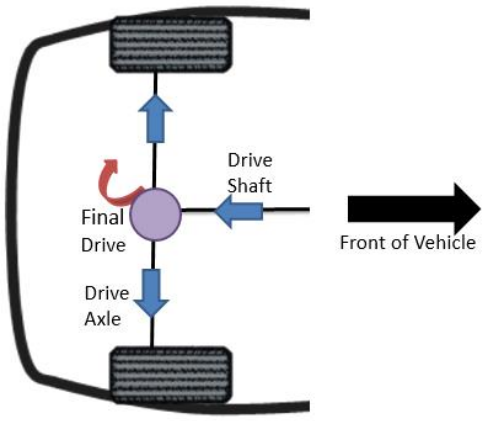

Figure 3-4: Diagram of Propel Case RWD Driveline Components

The glider model yields the tractive effort and speed at the wheels. Tractive effort comes immediately from the driveline. Tractive power out of the wheels is equal to the power out of the driveline. The only exception is tractive brake power. Only the tractive brake power that has been captured by regenerative braking is transmitted to the driveline. The rest of the tractive brake power is lost to friction. The amount of tractive power transmitted by the driveline is given by:

$$P_{DL,out} = {P_{tr}}^{+} + {P_{tr,regen}}^{-} \quad \textbf{Equation 3-21}$$

where ${P_{tr}}^{+}$ is the propel tractive power and ${P_{tr,regen}}^{-}$ is the brake tractive power captured with regenerative braking. ${P_{tr,regen}}^{-}$ is a negative quantity because power is traveling back towards the battery.

To relate the tractive effort at the wheels to the rest of the powertrain, the wheel radius and final drive are driveline inputs for this model. The component of the driveline adjacent to the wheels is the drive axle or axles. The speed of the drive axle is related to vehicle speed such that:

$$\omega_{axle} = \frac{v}{r_w} \quad \textbf{Equation 3-22}$$

where rw is the radius of the wheels and v is the vehicle speed. Using axle speed, axle torque may be found:

$$T_{axle} = \frac{P_{DL,out}}{\omega_{axle}} \quad \textbf{Equation 3-23}$$

Another important value is the speed of the drive shaft. The drive shaft speed serves the transmission output speed and the output speed of a post-transmission motor. The drive shaft is related to the drive axle by a factor of the final drive, FD:

$$\omega_{shaft} = FD * \omega_{axle} \quad \textbf{Equation 3-24}$$

The drive shaft speed is directly related to vehicle speed. The factor that relates vehicle and drive shaft speed is commonly referred to as the “N/V ratio”. For many vehicles, this ratio may be easily accessible from the EPA and can be used to derive either final drive or wheel radius:

$$\frac{N}{V} = \frac{60FD}{2\pi(r_w)} \quad \textbf{Equation 3-25}$$

where FD is the final drive ratio and rw is the wheel radius. The “N/V” ratio has units of rpm/mph. The final drive ratio is a constant gear that multiplies the torque and speed of the engine, motor, or both. For some vehicles, the final drive and wheel radius may be easily accessible and the “N/V ratio” must be evaluated. The model is setup such that the user may input the two knowns and find the one unknown.

For the purposes of this model, the driveline loss is assumed to occur while power is passed through the final drive. For the simplicity of this model, a constant spin loss in the form of a constant torque loss is assumed as 1.2% maximum motor torque in electrified vehicles. For conventional vehicles, the driveline torque loss is assumed to be 7% of maximum engine torque. The torque percentages are calibrated with experimental data.

$$T_{DL,loss} = (0.012)T_{mot,max} \text{ or } = (0.07)T_{eng,max} \quad \textbf{Equation 3-26}$$

Driveline loss only occurs when torque is transmitted through the driveline and therefore does not occur during idle time or non-regenerative braking. Driveline loss does not include transmission loss. The torque loss can be equated to a power loss:

$$P_{DL,loss} = T_{DL,loss}\omega_{shaft} \quad \textbf{Equation 3-27}$$

Once the driveline power loss is found, the power into the driveline can be determined with a power balance.

$$P_{DL,in} = P_{DL,out} + P_{DL,loss} \quad \textbf{Equation 3-28}$$

To demonstrate the impact of a constant torque loss, Table 3-2 shows driveline loss and efficiency data for three values of tractive power: a heavy load of 80 kW, a light load of 10 kW, and a regenerative braking case of -10 kW. Each load case shows results for four vehicle speeds. These vehicle speeds are translated to driveshaft speeds. The torque loss is constant for all cases, but the power loss varies since power is the product of torque and speed shown in Equation 3-27. The magnitude of the power loss is greater at higher speeds. Similarly, the driveline efficiency decreases with speed for the same load. At the same speed, the driveline is more efficient at high loads and least efficient during regenerative braking.

Table 3-2: Example Driveline Efficiency Table

	P_{tr}	Vehicle Speed	Shaft Speed	Torque DLloss	Power DLloss	Mot P_{In}	η_{DL}
	(kW)	(mph)	(rpm)	(Nm)	(kW)	(kW)	(---)
Heavy Load	80	25	2296	6	1.4	81	98.2
	80	40	3674	6	2.3	82	97.2
	80	55	5051	6	3.2	83	96.2
	80	70	6429	6	4.0	84	95.2
Light Load	10	25	2296	6	1.4	11	87.4
	10	40	3674	6	2.3	12	81.2
	10	55	5051	6	3.2	13	75.9
	10	70	6429	6	4.0	14	71.2
Regen	-10	25	2296	6	1.4	-9	85.6
	-10	40	3674	6	2.3	-8	76.9
	-10	55	5051	6	3.2	-7	68.3
	-10	70	6429	6	4.0	-6	59.6

Table 3-3 lists all of the values necessary to create a glider model for a particular vehicle. The HEVT Camaro parameters are listed as an example.

Table 3-3: Driveline Parameters for HEVT Camaro

*Parameter	Value	Unit
Driven Axle	RWD	[---]
rwheel	0.34	[m]
Final Drive	3.27	[---]
Tdl,loss	6	[Nm]

*Green cells signify required inputs

3.3.3 Accessory Model

Accessory loads on the vehicle include power draws from components such as controllers, pumps, fans, etc. For the purposes of this model, accessory loads are considered to be a constant power draw throughout all routes during all modes of operation. Accessory loads act during idle and both propel and brake. For a BEV or HEV, electric accessory power comes directly from the battery. For a conventional vehicle, an alternator supplies the load and the engine provides power to the alternator. As an alternator is not modeled in this thesis, the accessory load is a portion of the engine output power.

Vehicles with more electrification typically have less accessory loads. HEVs typically have higher accessory loads than BEVs in order to power all of the additional powertrain components and controllers. Conventional vehicle alternators are inefficient requiring a significant fuel use for a small electrical power draw. While there is variation for each vehicle, the default accessory load for production BEV is 200 W. HEVs and conventional vehicles are assumed to have a 600 W accessory load. The accessory load value may be overwritten if additional information is known. The accessory load on the vehicle is listed in

Table 3-15, the control strategy inputs. To incorporate the effects of cabin heating or air conditioning, increase the accessory load value as heating and air conditioning may require significant energy draw during certain seasons.

3.3.4 Motor Model

A motor converts electrical energy from the battery into mechanical energy in the form of torque that is transmitted to the driveline. Power is the product of torque and speed:

$$P_{mot} = T_{mot}\omega_{mot} \quad \textbf{Equation 3-29}$$

where Pmot is the power out of the motor, Tmot is the torque out of the motor, and ω_{mot} is the motor speed in rad/s. Motor speed is dependent upon the motor placement before or after gearing. Motor speed is discussed in Sections 3.4.4.1 and 3.4.4.1. When the motor propels the vehicle, the power into the motor is electrical power and the power out of the motor is the mechanical power as shown in Equation 3-30 and Figure 3-5.

$$P_{mot,elect} = P_{mot,mech} + P_{mot,loss} \quad \textbf{Equation 3-30}$$

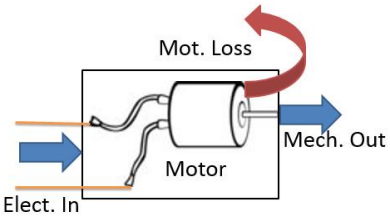

Figure 3-5: Motor Energy Diagram

3.3.4.1 Creating a Motor Loss Model

There is no direct equation for computing motor losses due to the complexity of the machines. Motor system losses may be approximated using a simplified model in terms of motor torque and speed. Equation 3-31 is taken from *Electric Vehicle Technology Explained (Larminie & Lowry, 2003).*

$$P_{loss} = k_c T^2 + k_i \omega + k_w \omega^3 + C \quad \textbf{Equation 3-31}$$

where kc, ki, kw, and C are each motor loss constants. The motor system loss includes inverter loss. While this equation is developed for brushed DC motors, the principles also apply to modern motors.

Each term in Equation 3-31 represents a different kind of loss within the motor. The first loss term is copper loss which is a result of electrical resistance of the windings of the motor. This loss is due to resistance and the square of current. In a DC motor, the rotor current is directly proportional to the torque produced as shown in Equation 3-32. In most motors, the copper loss tends to be the largest source of loss.

$$P_{loss,,C} = I^2 R \; where \; I^2 \propto T^2 \quad \textbf{Equation 3-32}$$

$$P_{loss,C} = k_c T^2 \quad \textbf{Equation 3-33}$$

The next loss term is iron loss which is a result of magnetic effects in the iron of the motor. As the metal in the rotor rotates the magnetic field, the rotor experiences changes, a "hysteresis loss" occurs from the constant magnetization and demagnetization of the iron. Additional loss occurs because the changing magnetic field generates a current in the iron via electromagnetic induction. The current creates heat loss. Iron losses are proportional to the frequency at which the metal experiences a change in magnetic field such a remagnetization.

$$P_{loss,I} = k_i \omega \quad \textbf{Equation 3-34}$$

The third loss term is a loss to windage, also known as wind resistance. Windage torque resistance increases with square of speed as other aerodynamic forces. As power is torque multiplied by speed, the windage power loss is:

$$P_{loss,W} = k_w \omega^3 \quad \textbf{Equation 3-35}$$

The last loss term is independent of torque and speed and considered constant. Power is needed to operate all of the electronic control circuits and other parasitic losses.

$$P_{loss,constant} = C \quad \textbf{Equation 3-36}$$

3.3.4.2 Scaling a Motor Loss Model

Unless motor efficiency or loss data is available, the motor loss coefficients cannot be found. The motor loss coefficients used in Equation 3-31 are only used to create an approximation of motor losses and therefore the coefficients are not published. (Eli Hampton White, 2014) proposes expanding the motor loss equation by Larminie and Lowry to allow a motor of known loss coefficients to be scaled such that the motor model approximates the losses for another size but similar motor of unknown motor loss coefficients. White et al. scaled using maximum motor torque and maximum motor speed:

$$P_{loss,scaled} = \left[\frac{T_{max}\omega_{max}}{T_{ref}\omega_{ref}}\right]\left[k_c T^2\left(\frac{T_{ref}}{T_{max}}\right)^2 + k_i\omega\left(\frac{\omega_{ref}}{\omega_{max}}\right) + k_w\omega^3\left(\frac{\omega_{ref}}{\omega_{max}}\right)^3 + C\right] \quad \textbf{Equation 3-37}$$

where Tmax is the maximum torque for the motor to be approximated, ωmax is the max speed of the motor to be approximated, Tref is the maximum torque of the reference motor, and ωref is the max speed of the reference motor. Instead of maximum speed, this thesis proposes scaling with base motor speed:

$$P_{loss,scaled} = \left[\frac{T_{max}\omega_{base}}{T_{ref}\omega_{ref}}\right]\left[k_c T^2\left(\frac{T_{ref}}{T_{max}}\right)^2 + k_i\omega\left(\frac{\omega_{ref}}{\omega_{base}}\right) + k_w\omega^3\left(\frac{\omega_{ref}}{\omega_{base}}\right)^3 + C\right] \quad \textbf{Equation 3-38}$$

where Tmax is the maximum torque for the motor to be approximated, ωbase is the base speed of the motor to be approximated, Tref is the maximum torque of the reference motor, and ωref is the base speed of the reference motor, unlike Equation 3-37. Base speed is defined as the highest motor speed that is capable of attaining maximum torque as shown in Figure 3-6. Base speed is selected so that the accuracy of the scaled motor losses would be greater along the base speed which is where the motor is likely to operate. Also, unlike maximum torque and maximum speed which are not simultaneously possible motor operation, maximum torque and base speed are attainable points with the motor operating region.

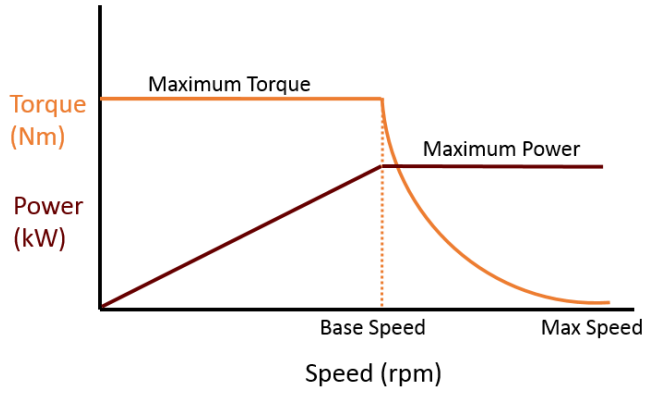

Figure 3-6: Motor Torque vs Speed and Power vs Speed

To find standard motor coefficients, two sets of coefficients are found that best matched the efficiency maps for each the UQM PP75 motor and the 2004 Prius motor. A table summarizing each set of motor loss coefficients is found in Table 3-4. Efficiency maps comparing validation data and model efficiency results for both motors can be found in Appendix B. Table 3-4 summarizes each set of loss coefficients. The motor parameters of maximum torque, base speed, maximum speed, and peak power are displayed. Also, the motor efficiency at max torque and base speed is displayed as “corner η,” for reference.

Table 3-4: Summary of Motor Coefficients

Coefficients	Tmax	Sbase	Smax	Ppeak	Corner η	Ideal			
						kc	ki	kw	C
	(Nm)	(rpm)	(rpm)	(kW)	(%)	(---)	(---)	(---)	(---)
PP75	240	2984	7500	75	90.7%	0.0870	8.00	8(10-7)	200
2004 Prius	302	1800	6000	57	87.4%	0.0780	4.30	100(10-7)	200
Standard	270	2400	6750	66	85.7%	0.0825	6.15	54(10-7)	200

The standard motor coefficients used in this model are the average of the PP75 and the Prius motor coefficients. Likewise, the reference motor is a rounded average of both sets of motor parameters. The standard motor coefficients are used for all motors unless motor efficiency information is otherwise available. Using maximum torque and base speed of the motor to be approximated, the loss equation is linearly scaled in both the direction of maximum torque and base speed as shown in Equation 3-37 where the reference motor has a maximum torque of 270 Nm and a base speed of 2400 rpm.

In this model, the power output on the mechanical side of the motor is known from previous powertrain analysis. A positive power output implies the motor is sending torque to the driveline and a negative power output implies the motor is receiving torque to send to charge the battery. Using Equation 3-30 and Equation 3-38, the motor loss and electrical input to the motor are found. To find the efficiency of a motor:

$$\eta_{motor} = \frac{P_{mech}}{P_{elect}} \qquad \textbf{Equation 3-39}$$

where Pmech is the power out of the mechanical side of the motor to the driveline and Pelect is the power into the motor from the electric bus. Figure 3-7 displays the approximate efficiency plot for the 2013 Nissan Leaf motor system.

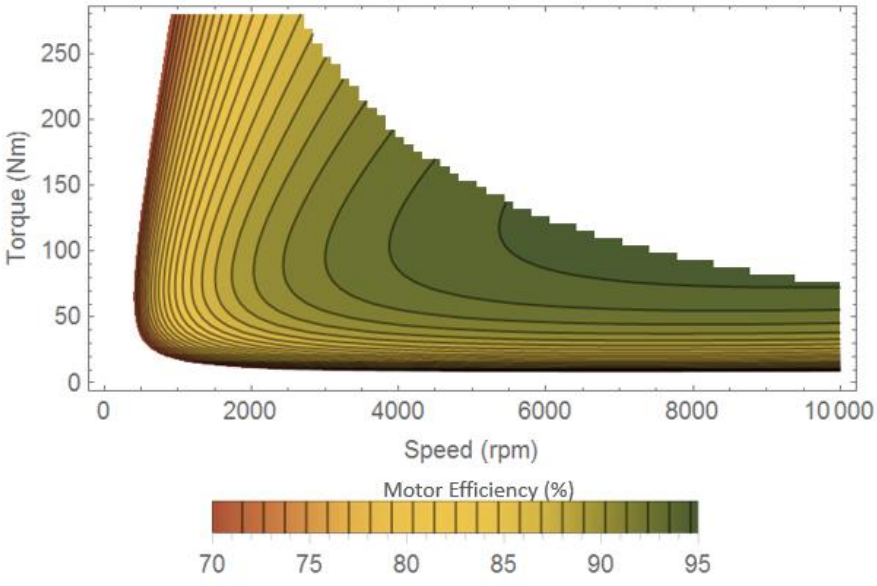

Figure 3-7: Example 2013 Leaf Motor System Efficiency Plot

To model the motor losses, only max torque and base speed are required for each motor. If known, a max speed can be input as a limitation. In many cases, the base speed may not be published and the peak power is instead available. Peak power and max torque may be used to find base speed using the relationship shown:

$$\omega_{mot,base} = \frac{P_{mot,peak}}{T_{mot,max}} \qquad \textbf{Equation 3-40}$$

The left portion of Table 3-5 lists all other motor parameters related to the motor to be modeled. The right portion of Table 3-5 displays the reference motor information that remains constant for all vehicles.

Table 3-5: Motor Parameters for HEVT Camaro

*Parameter	Value	Unit
Tmax	500	[Nm]
Sbase	1900	[rpm]
Ppeak	99.5	[kW]
Smax	4500	[rpm]

*Green cells signify required inputs

*Parameter	Value	Unit
kc	0.0825	[s/kg*m2]
ki	6.15	[J]
kw	54(10-7)	[kgm2]
C	200	[W]
Tref (Max)	270	[Nm]
Sref (Base)	2400	[rpm]

3.3.4.3 Generator Model

Most automotive motors are bidirectional and can also act as generators. A motor acts as generator when receiving mechanical energy to convert into electrical energy to charge the battery as shown in Figure 3-8. A motor may act as a generator when receiving regenerative brake power or when receiving extra power from the engine. The energy flow changes directions between a motor and a generator.

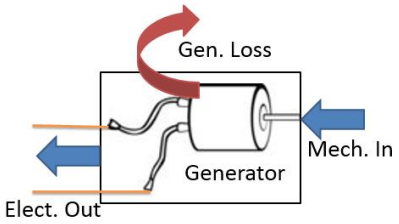

Figure 3-8: Generator Energy Diagram

With the change in direction comes a change in the sign of motor output torque. Likewise, the power into and out of the motor changes sign but Equation 3-29 and Equation 3-30 still hold true. Negative torque or power imply torque or power into the generator to be sent to the HV bus. Using data from a known reference motor, the scaled power loss is approximately the same for both motors and generators. A generator will input a negative torque in to the loss equation that is subsequently squared resulting in a positive loss. Negative speeds, as when the vehicle reverses, are not modeled. In a generator Pelect and Pmech are both negative quantities yet Ploss remains a positive quantity, as shown in Equation 3-42. All losses in this powertrain model are positive values that may be added or subtracted from other quantities. This motor or generator loss equation is Equation 3-37. The definition of efficiency flips for a generator due to the change in energy direction:

$$\eta_{generator} = \frac{P_{elect}}{P_{mech}} \qquad \textbf{Equation 3-41}$$

$$\eta_{generator} = \frac{-8\ kW}{-10\ kW} = 0.8$$ **Equation 3-42**

Figure 3-9 displays the approximate generator efficiency plot for the 2013 Nissan Leaf motor system. White regions of the map are omitted as they are less than 70% efficient. Regenerative braking is inactive at high torques and low speeds as this region is particularly inefficient. Discussion of regenerative braking limitations can be found in Section 4.4.

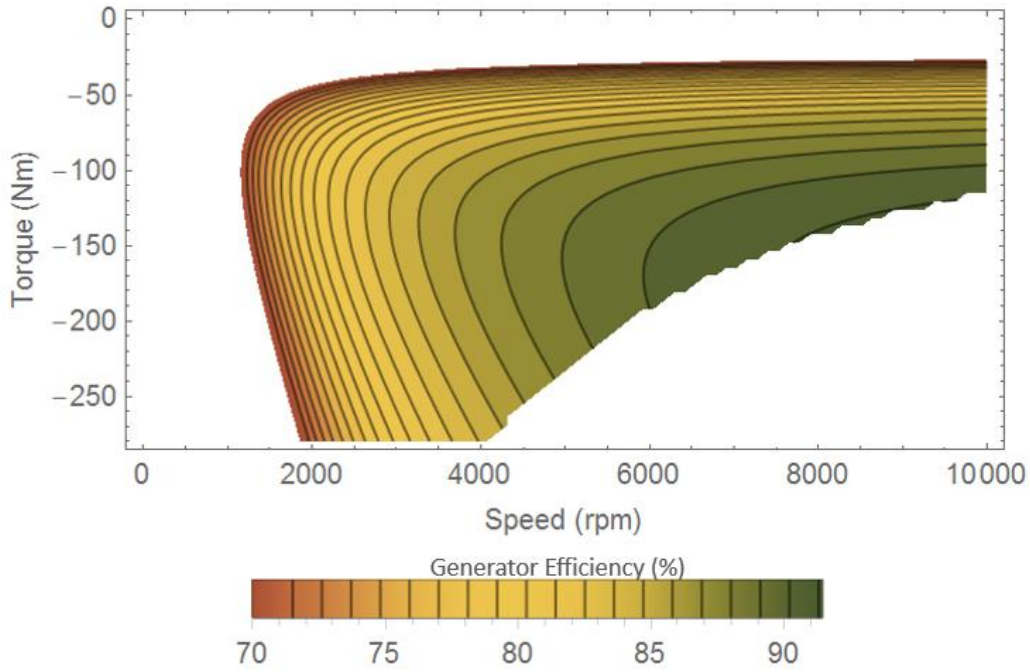

Figure 3-9: Example 2013 Leaf Generator Efficiency Plot

3.3.5 Battery Model

3.3.5.1 Battery Losses

The power out of the battery terminals is known from prior powertrain analysis. Batteries experience a loss as power leaves the internal voltage source of the battery and passes through the battery internal resistance. Figure 3-10 shows the internal circuit within a battery. VOC is the open circuit, or internal, voltage of the battery while Vterm is the voltage found at the battery terminals. There is a voltage drop between the terminal voltage and the internal voltage of the battery as a result of the internal resistance, Rint. Using Kirkoff's voltage law these Vterm can be found as a function of VOC, Rint, and the current, I as shown in Equation 3-43.

$$V_{term} = V_{oc} - IR_{int}$$ **Equation 3-43**

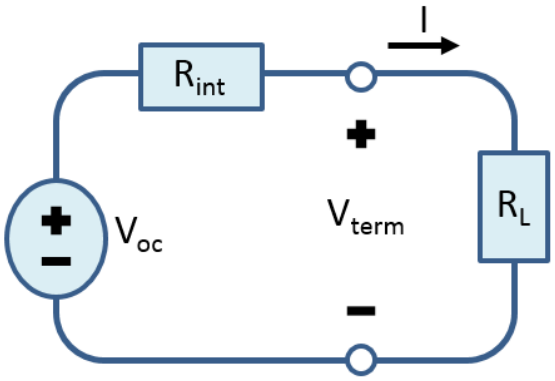

Figure 3-10: Battery Internal Circuit Diagram

Equation 3-43 can be evaluated for current as shown in Equation 3-44.

$$I = \frac{V_{oc} - \sqrt{V_{oc}^2 - 4R_{int}P_{term}}}{2R_{int}} \quad \textbf{Equation 3-44}$$

Where Pterm is the terminal power out of the battery, which is known due to prior powertrain analysis. The terminal power of the battery connects to the High Voltage (HV) bus. From the HV bus, motor electric power and accessory power is drawn.

Lithium Ion batteries have very high coulombic efficiency that is assumed to be 100%. The power lost to heat in a battery is:

$$P_{loss} = I^2 R_{int} \quad \textbf{Equation 3-45}$$

Using the power out and the power loss of the battery, the power in can be found using Equation 3-46

$$P_{int} = P_{term} + P_{loss} \quad \textbf{Equation 3-46}$$

3.3.5.2 Finding Battery Loss

Internal resistance is not always a publically available battery property and must therefore be estimated. This model presents an approximation using common publically available battery properties: open circuit voltage and energy capacity. Battery packs are formed by placing cells in series and/or parallel.

When cells are in series the current through each cell is the same but combining cell resistors in series increases the overall resistance. Adding cells in series directly increases the open circuit voltage. Same current and higher resistance requires a higher open circuit voltage. As an alternate viewpoint, increasing open circuit voltage increases internal resistance as if a higher number of cells in series.

$$R_{int} \propto V_{OC} \quad \textbf{Equation 3-47}$$

When cells are in parallel, the voltage across each cell is the same but combining cell resistors in parallel reduces the overall resistance. Amp-hour (Ah) capacity is the amount of energy change in a battery that will allow one ampere of current to flow for one hour. Adding cells in parallel directly increases Ah capacity. As Ah capacity increases, like by adding more cells in parallel, the internal resistance decreases. Internal Resistance is inversely proportional to Ah capacity which is proportional to the quotient of battery energy capacity and open circuit voltage.

$$R_{int} \propto \frac{1}{Ah} \propto \frac{1}{\frac{E_{cap}}{V_{OC}}} \propto \frac{V_{OC}}{E_{cap}} \quad \textbf{Equation 3-48}$$

Combining Equation 3-47and Equation 3-48, internal resistance is proportional to the square of open circuit voltage and inversely proportional to energy capacity. Internal resistance is not equal to this ratio, only proportional, and therefore requires a proportionality constant, R0. Combining the proportions given in Equation 3-47 and Equation 3-48:

$$R_{int} = R_0 \frac{{V_{OC}}^2}{E_{cap}} \quad \textbf{Equation 3-49}$$

The value of R0 is assigned due to battery type and size classifications that are discussed in battery validation, Section 4.6.

3.3.5.3 Battery SOC

An important measure of energy consumption within a battery is SOC. Battery SOC is the percent of charge remaining internal to the battery. When the model is on-board the vehicle, battery SOC will be known. As this model cannot receive vehicle updates at this time, initial SOC when beginning the route must be manually input. The battery energy at any time is the integral of internal power as shown in Equation 3-50. SOC can be evaluated using Equation 3-51 and Equation 3-52.

$$E_{int} = E_0 + \int P_{int}\, dt \quad \textbf{Equation 3-50}$$

$$\Delta SOC = \frac{\Delta E}{E_{cap}} * 100 \quad \textbf{Equation 3-51}$$

$$SOC_{new} = SOC_i + \Delta SOC \quad \textbf{Equation 3-52}$$

where E0 is the initial battery energy, SOC_i is the initial SOC, and ΔSOC is the change in percent SOC during a particular time step over which ΔE is the change in energy.

3.3.5.4 Charging

Every battery charger has a different charging efficiency. On the highest end of chargers, the Tesla Powerwall claims a 92% charging efficiency *(Tesla Motors, 2016)*. As Tesla does not define charging efficiency, this value is assumed optimistic. As a simplification in this model, the battery charging efficiency is assumed to be 87% for all vehicles. An 87% charging efficiency is approximately consistent with EPA data comparing Electric Vehicle (EV) range with grid electricity use. The charging efficiency is used to find the grid electric energy used to charge a battery:

$$E_{grid} = \frac{E_{batt,int}}{\eta_{charging}} \quad \textbf{Equation 3-53}$$

where Ebatt,int is the internal energy used from the battery. This charging efficiency includes all losses between the grid electric AC energy input to the vehicle and the stored internal energy inside the battery that corresponds to battery SOC. This efficiency includes the wiring, electric vehicle supply equipment, battery charger AC-DC electronics losses, and battery charging losses due to internal resistance.

3.3.5.5 Battery Parameters

To model the battery, only open circuit voltage and energy capacity are required. The composition of the battery is also required. This model is capable of simulating lithium-ion and nickel metal hydride batteries. Table 3-6 displays battery parameters with values from the HEVT Camaro.

Table 3-6: Battery Parameters for HEVT Camaro

*Parameter	Value	Unit
Type	Li-Ion	[---]
Ecap	12.6	[kWh]
Voc	340	[V]
R0	0.01129	[hr]
Rint	0.10	[Ω]
SOCi	40	[%]
SOCmin	20	[%]
SOCmax	30	[%]
ηcharger	87	[%]

*Green cells signify required inputs

3.3.6 Transmission Model

The transmission model configures the engine to operate such that the engine may attain the desired acceleration or fuel economy. Prior to determining which gear to select, the transmission power out, power loss, and power in can be determined. The transmission transmits torque directly to the drive shaft. As such, the speed of the transmission output is the same as the speed of the drive shaft. Likewise, the power into the driveline is the same as the power out of the transmission.

Similar to the driveline loss, the transmission loss is assumed to be a constant torque loss. Most automatic transmissions range from about 85-95% efficient *(Stacey, 2011)*. As the range is an overall efficiency, assigning a constant torque loss allows for the model to be more efficient at high loads and less efficient at low loads which is a better approximation than a constant efficiency. Testing three drive cycles for the 2012 Ford Fusion, 2012 Chrysler 300, the 2013 Hyundai Sonata, and the HEVT Camaro found 3.2% of maximum engine torque to yield roughly a 90% drive cycle average transmission efficiency. The drive cycle average transmission efficiency for each simulation can be referenced in Appendix Table D-1.

A constant transmission torque loss is selected for the same reasons as constant driveline torque loss: to be more efficient at high loads and less efficient at high speeds, as demonstrated in Table 3-2. Using 3% of maximum engine torque, the transmission torque loss is:

$$T_{trans,loss} = (0.032)T_{eng,max} \quad \textbf{Equation 3-54}$$

Using the drive shaft speed, which is also the transmission output speed, the torque loss can be equated to a power loss.

$$P_{trans,loss} = T_{trans,loss}\omega_{shaft} \quad \textbf{Equation 3-55}$$

Once the transmission power loss is found, the power into the transmission driveline can be determined with a power balance:

$$P_{trans,in} = P_{trans,out} + P_{trans,loss} \quad \textbf{Equation 3-56}$$

3.3.6.1 Throttle Percent

The transmission selects gears based upon the throttle percent. The throttle percent is calculated differently depending on the type of vehicle. For a conventional vehicle, the throttle percent is a ratio of the torque demand to the WOT torque limit for the engine. In a post-transmission HEV, like the HEVT Camaro, only engine torque is transmitted through the transmission. Thus, only the engine throttle is considered in transmission gear selection and the throttle equation is identical with that of a conventional vehicle For pre-transmission HEVs, the motor and engine torque are summed prior to the transmission. As such, the engine wide open throttle torque and the max motor torque may be summed directly. Throttle percent is the ratio of the torque demand prior to the transmission to the sum of maximum torque from both the motor and the engine:

Conventional/ Post-Trans HEV

$$\%\,Throttle = \frac{T_{eng,dem}}{T_{eng,WOT}} \quad \textbf{Equation 3-57}$$

Pre-Trans HEV

$$\%\,Throttle = \frac{T_{pretrans,dem}}{T_{eng,WOT} + T_{mot,max}} \quad \textbf{Equation 3-58}$$

where Teng,WOT is the engine WOT torque, Tmot,max is the maximum torque of the motor, Teng,dem is the torque demand from the engine to meet the route in a conventional vehicle, and Tpretrans,dem is the torque demand from the engine and motor before the torque enters the transmission in a pre-transmission HEV. The percent throttle is used to determine the transmission gear. In real time driving, the throttle varies with the aggressiveness of the driver. For the purposes of this model, the vehicle is assumed to demand exactly what the vehicle needs to meet the route target velocities at the target location with a constant acceleration. Real drivers will often accelerate quicker than necessary and then cruise or the opposite. Interdriver variability is not considered in this model.

3.3.6.2 Gear Selection

The method by which transmissions select gears is incredibly complicated and involves a lot of OEM-proprietary information. Most Transmission Control Units (TCUs) receive information about the vehicle speed, engine load, engine capabilities at that load, rotational speed of the torque converter, and whether a vehicle is ascending or descending a hill. Using these inputs, the TCU uses OEM-proprietary logic to determine gear selection.

For the Civic, Honda has posted very basic shift maps online. The upshift map can be referenced in Figure 3-11 and the downshift map can be referenced in Figure 3-12. The upshift and downshift shift plots have a similar shape but with different shift speed values *("I-Shift," 2008)*. When shift speeds are known for each gear at a variety of throttle positions, Mathworks suggests creating a similar basic relationship between throttle and vehicle speed within MATLAB Simulink *(Mathworks, 2016)*. Likewise, ANL proposes the same approach using Autonomie *(Namdoo et al., 2015)*. Mathworks organizes the data such that as the vehicle exceeds the designated upshift speed for the current gear and throttle position, the transmission upshifts one gear. Likewise, as the vehicle speeds drops below the downshift speed for the current gear and throttle position, the vehicle transmission downshifts one gear *(Mathworks, 2016)*. For this research, very few vehicle transmission maps will be available. In fact, very few transmission maps are publically available, if any. This research follows the Mathworks approach but involves defining the relationship between vehicle speed and throttle percent for each transmission to be modeled.

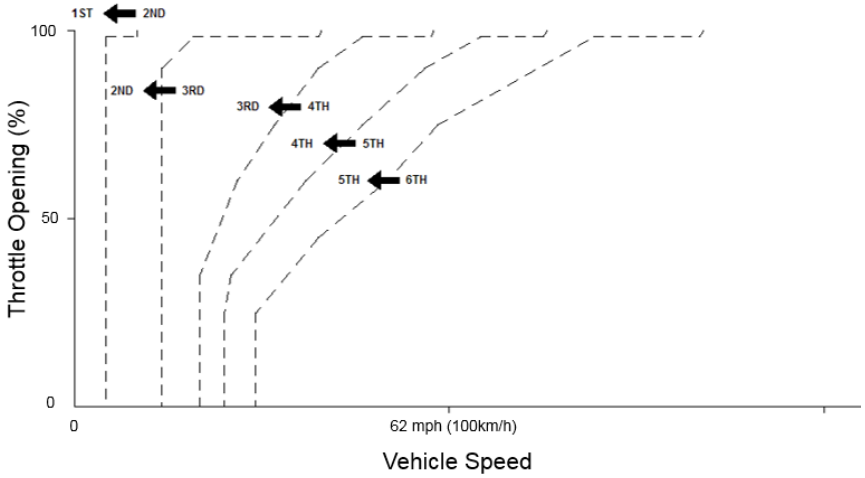

Figure 3-11: Honda Civic Upshift Strategy (Adpt. from "I-Shift," 2008, Fair Use).

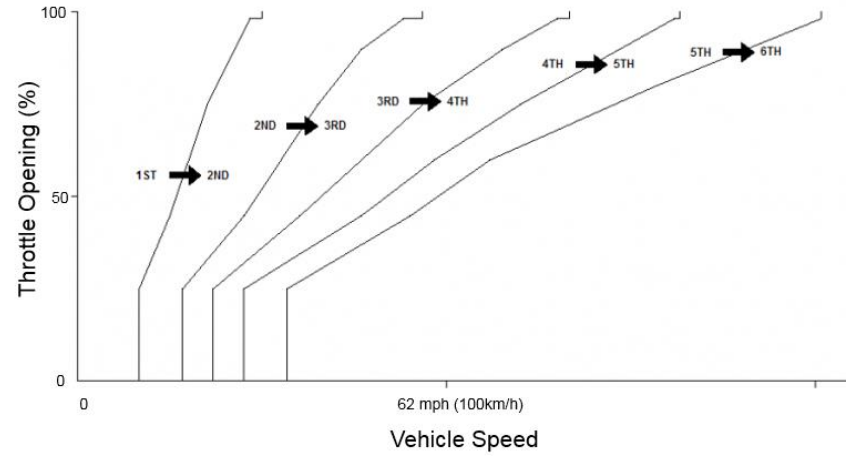

Figure 3-12: Honda Civic Downshift Strategy (Adpt. from "I-Shift," 2008, Fair Use).

A hyperbolic tangent as a function of engine throttle position is selected to best fit the shape for a collection of proprietary transmission data as well as the Honda Civic maps. Specifically, Equation 3-59 shows the hyperbolic tangent relationship that best yields the normalized shift speed:

$$normal = \frac{\tanh\left(\frac{Throttle\%}{10} - 5\right) + 1}{2} \qquad \textbf{Equation 3-59}$$

where normal is unitless normalization of speed from zero to one. Equation 3-59 is plotted in Figure 3-13. Please note that the axes are switched from the Civic plot as the methodology presented in this thesis is not based upon test data and instead finds shift speed as a function of throttle percent. Also, the excessively high speeds of 100 mph are highly unlikely to be obtained in regular driving, but are included to demonstrate the hyperbolic tangent shape.

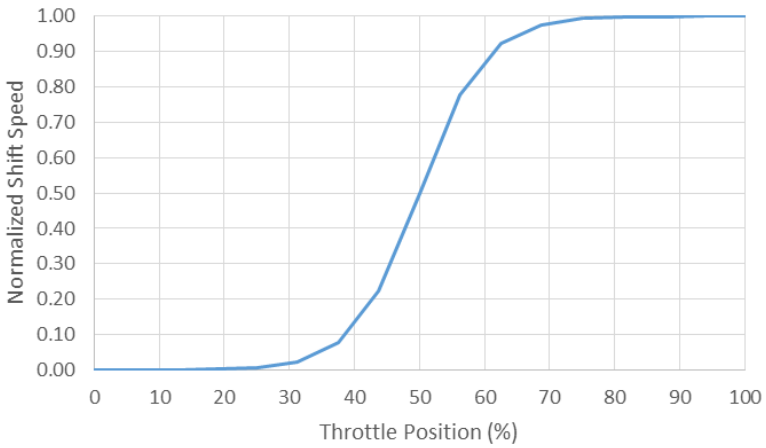

Figure 3-13: Plot of Normalized Shift Speed versus Throttle Position

Conventional vehicles operate such that the driver inputs an accelerator pedal command and the vehicle controllers interpret the pedal command using complicated pedal maps. The driver pedal demand is not always proportional to the engine demand; however, pedal map interpretation involves the drivability of the vehicle which is outside the scope of this research. Hence, engine throttle percent determines gear shifts.

As Equation 3-59 only yields the normalized shift speed as a function of throttle percent, the actual shift speed value at 100% throttle and the shift speed at 0% throttle must be determined in order to find the upper and lower bound of the hyperbolic tangent function. The shift speed as a function of throttle percent is:

$$v_{shift}(Throttle\ \%) = v_{low} + [v_{high} - v_{low}]normal(Throttle\ \%) \qquad \textbf{Equation 3-60}$$

where vlov is the shift speed at 0% throttle and vhigh is the shift speed at 100% throttle. In order to determine vehicle speeds at which the transmission would shift, the logic begins with engine speeds. To simplify this model, inputs such as engine lug limit and max speed are used to determine engine shift speeds. The basis for these engine speeds is selected with reference to a collection of proprietary transmission data as well as knowledge of the physical implication of these engine speeds.

Downshifting at 0% throttle occurs when the engine approaches a function of the engine lug speed limit as otherwise the vehicle will stall. As engines rarely operate at such very low throttle percentages, the downshift speed of the engine at 0% throttle is set to slightly lower than the lug limit. Downshifting at high throttle keeps the engine from operating at too high a torque at too low of a speed.

Likewise, upshifting at 100% throttle occurs as the engine approaches a percentage of engine max speed as otherwise the engine will exceed recommended limits. Upshifting at 0% throttle is also a function of the maximum engine speed but occurs at lower speeds than at 100% throttle. Engines are typically more efficient in higher gears but can only continue to meet demand in higher gears with a relatively low engine load. Confirming with proprietary transmission data, post-shift engine speed is generally close to the engine lug limit. As such, when at low throttle, the transmission upshifts such that the post-shift engine speed is a percentage of the engine lug limit.

A breakdown of the formulas used to find the upshift and downshift speed for each gear at both high and low throttle can be found in Appendix Table D-2. These formulas are also functions of

constant values designated as ΔH and ΔL by which the speed values could be quickly calibrated using validation data discussed in Section 4.8.2.

Upon finding the engine speeds at which the shift occurs, the vehicle speed is found via a relation with gear ratio:

Downshift b to a $$v_{preshift} = \frac{S_{eng,preshift}}{\left(\frac{N}{V}\right) GR_b}$$ **Equation 3-61**

Upshift a to b $$v_{preshift} = \frac{S_{eng,preshift}}{\left(\frac{N}{V}\right) GR_a}$$ **Equation 3-62**

Upshift a to b $$v_{preshift} = \frac{S_{eng,postshift}}{\left(\frac{N}{V}\right) GR_b}$$ **Equation 3-63**

where a and b are generic gear numbers, vpreshift is the vehicle speed upon reaching the shift should occur, Seng,preshift is the engine speed upon reaching the shift should occur, Seng,postshift is the engine speed to be obtained after the shift, GRx is the gear ratio of the xth gear, N/V is the relationship between vehicle speed in mph and driveshaft speed in rpm. An example table of predicted transmission shift points for the Hyundai Sonata at 0% and 100% throttle is shown in Table 3-7. An example for an 8-speed transmission is shown in Appendix Table D-4. The low shift speeds into 8th gear are also explained in Section 4.8.2.

Table 3-7: Example 2013 Hyundai Sonata Transmission High/Low Shift Points

Current Gear				GR1	GR2	GR3	GR4	GR5	GR6
Downshift	**Gear Pair**			**1-0**	**2-1**	**3-2**	**4-3**	**5-4**	**6-5**
	0% Throttle	Target Eng. Speed	[rpm]	--	600	600	950	950	900
		Pre-Shift Veh. Speed	[mph]	--	5.78	8.89	18.64	25.91	31.88
		Post-Shift Eng. Speed	[rpm]	--	986	923	1258	1321	1169
	100% Throttle	Target Eng. Speed	[rpm]	--	2700	2800	4140	4140	4140
		Pre-Shift Veh. Speed	[mph]	--	26.02	41.50	81.23	112.90	146.63
		Post-Shift Eng. Speed	[rpm]	--	4436	4307	5480	5755	5377
Upshift	**Gear Pair**			**1-2**	**2-3**	**3-4**	**4-5**	**5-6**	**6-7**
	0% Throttle	Target Eng. Speed	[rpm]	1624	1384	1390	1460	1234	-
		Pre-Shift Veh. Speed	[mph]	9.53	13.34	20.60	28.63	33.65	-
		Post-Shift Eng. Speed	[rpm]	900	900	1050	1050	950	-
	100% Throttle	Target Eng. Speed	[rpm]	4500	4500	6300	6300	6200	-
		Pre-Shift Veh. Speed	[mph]	26.39	43.36	93.37	123.60	169.08	-
		Post-Shift Eng. Speed	[rpm]	2739	2926	4759	4532	4774	-

Once the vehicle speed shift values for 0% and 100% throttle have been found for each gear and for each shift direction, Equation 3-59 and Equation 3-60 can be evaluated for vehicle speeds as continuous functions of throttle percent. There is one relationship for each gear pair in each shifting direction. Figure 3-14 displays the expected relationship for the six-speed 2013 Hyundai Sonata.

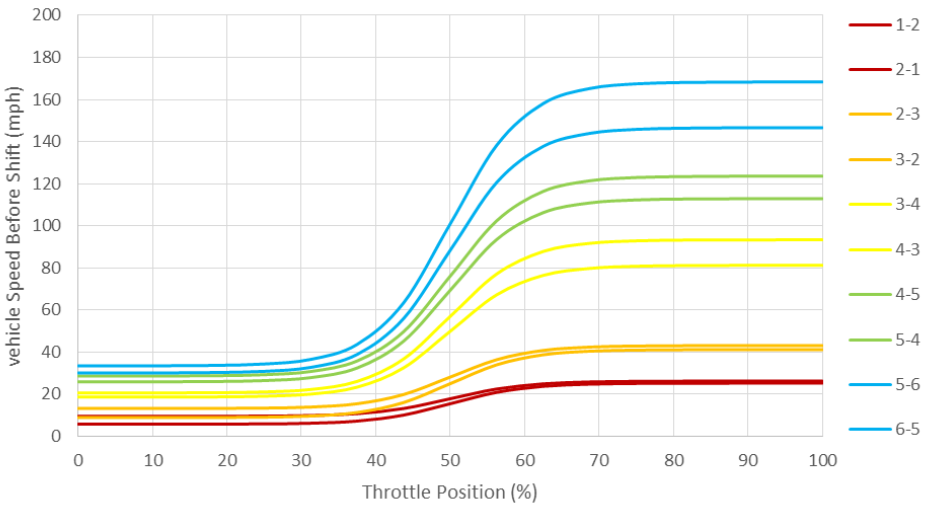

Figure 3-14: Example 2013 Hyundai Sonata Shift Points

To avoid excessive shifting with sudden increases in throttle position due to shifting to higher gears and a lower engine speed, the average of the two previous node throttle values is used in gear selection. Nodes are assumed to be sufficiently frequent that this average will not cause a large error in shift strategy.

Another note is that many HEVs use a Continuously Variable Transmission (CVT). There is a lot of literature on modeling a CVT, but this thesis does not discuss a modeling method. As the HEVT Camaro will utilize an automatic 8-speed transmission, a standard transmission is the focus.

3.3.6.3 Transmission Parameters

To model a transmission, the number of gears and the respective gear ratio for each gear are required. These values are the only required inputs to model a transmission in this model as shown in the list of transmission parameters in Table 3-8. All parameters are discussed in previous subsections. The values listed reflect those of the HEVT Camaro.

Table 3-8: Transmission Parameters for HEVT Camaro

*Parameter	Value	Unit
# Gears	8	[---]
GR1	4.56	[---]
GR2	2.97	[---]
GR3	2.08	[---]
GR4	1.69	[---]
GR5	1.27	[---]
GR6	1.00	[---]
GR7	0.85	[---]
GR8	0.65	[---]
Ttrans,loss	16.2	[Nm]
ΔH	1600	[rpm]
ΔL	100	[rpm]

*Green cells signify required inputs

3.3.7 Engine Model

From a power-loss standpoint, the engine model is very straight forward: fuel enters the engine and power out and engine losses leave as shown in Figure 3-15. The power in an engine is the product of engine torque and speed as shown in Equation 3-64.

$$P_{eng} = T_{eng}\omega_{eng} \quad \textbf{Equation 3-64}$$

where ω_{eng} is engine speed in rad/s, Teng is torque out of the engine in Nm, and Peng is power out of the engine in W.

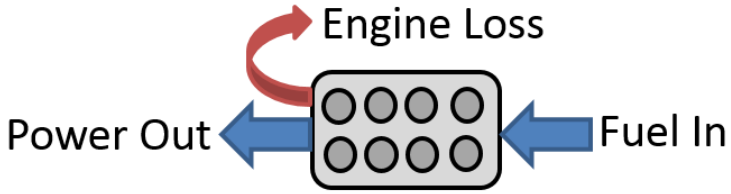

Figure 3-15: Engine Power-Flow Schematic

The power out of the engine is equal to the power into the transmission plus any power needed for the alternator to supply the accessory load. In a hybrid vehicle, the accessory load is always drawn from the HV bus instead of an engine alternator. The speed of the engine is given by:

$$\omega_{eng} = GR * \omega_{shaft} \quad \textbf{Equation 3-65}$$

where GR is the gear ratio for the current transmission gear.

The torque demand from the engine used to find BMEP is a function of the power out of the engine and the engine speed.

$$T_{eng} = \frac{P_{eng,out}}{\omega_{eng}} \quad \textbf{Equation 3-66}$$

The peak engine BMEP is assumed to be around 1200 kPa for all engines; however, as engine maximum torque is commonly available information this value may be overwritten if known. The peak engine torque provides a limitation on the engine. Similarly, maximum engine speed is often known. Maximum engine speed is assumed to be around 6000 rpm for all engines, but this value may also be overwritten to properly limit the engine. The engine lug limit provides a lower speed limit on the engine. The lug limit is assumed to be 1050 rpm but may also be overwritten.

3.3.7.1 Engine Efficiency Approximation

The engine efficiency model scales only with engine volumetric displacement. BMEP is the equivalent average pressure acting on the piston during one cycle. BMEP is engine torque normalized by volumetric displacement and is therefore used as a basis for the engine model to approximate the efficiency for engines of different displacements. “Brake” refers to actual engine output at the flywheel as measured by a dynamometer. The relation between BMEP and engine torque is given by Equation 3-67

$$BMEP = \frac{n2\pi}{V_{disp}} T_{eng} \quad \textbf{Equation 3-67}$$

where n is the number of revolutions per cycle which is two for a four-stroke engine. In Equation 3-67, BMEP is in kPa when Teng is in Nm and Vdisp is in L.

Indicated Mean Effective Pressure (IMEP) is the ideal average pressure acting on the piston during one cycle. IMEP is the theoretical thermodynamic combustion cycle pressure. Likewise, Friction Mean Effective Pressure (FMEP) represents the pressure losses such as bearing friction, windage, and crankcase pump losses. FMEP also incorporates the power loss to power devices such as oil, fuel and coolant pumps, or the ignition system. The relationship between pressure values is:

$$BMEP = IMEP - FMEP$$ **Equation 3-68**

Engine efficiency includes both thermodynamic losses and friction losses. The power input by fuel is first reduced by the thermodynamic losses. The remaining power is output as two quantities: the power that is lost to friction and the usable power that will output from the crankshaft into the transmission:

$$P_{fuel} = P_{thermo,loss} + P_{fricti,loss} + P_{eng,out}$$ **Equation 3-69**

where Pfuel is the power input to the engine via fuel. Pthermo,loss represents the thermodynamic losses of the fuel conversion, Pfricti,loss is the power lost to friction within the engine, and Peng,out is the usable power output from the engine to the rest of the powertrain. The definition for thermodynamic efficiency is given in Equation 3-70 and then rearranged to solve for the power input from fuel in Equation 3-71.

$$\eta_{thermo} = \frac{P_{totalout}}{P_{fuel}} = \frac{P_{eng,out} + P_{fricti,loss}}{P_{fuel}}$$ **Equation 3-70**

$$P_{fuel} = \frac{P_{eng,out} + P_{fricti,loss}}{\eta_{thermo}}$$ **Equation 3-71**

where Ptotalout is the remaining power after thermodynamic losses which is both the power to be output from the engine and the power to be lost to friction.

The expressions found describing thermodynamic efficiency can be used to describe the overall engine efficiency as shown in Equation 3-72. The power ratios are equivalent to pressure ratios as shown in Equation 3-73.

$$\eta_{eng} = \frac{P_{eng,out}}{P_{fuel}} = \frac{P_{eng,out}}{\frac{P_{fricti,loss} + P_{eng,out}}{\eta_{thermo}}} = \frac{\eta_{thermo}}{\frac{P_{fricti,loss}}{P_{eng,out}} + 1}$$ **Equation 3-72**

$$\eta_{eng} = \frac{\eta_{thermo}}{\frac{P_{fricti,loss}}{P_{eng,out}} + 1} \; OR \; \frac{\eta_{thermo}}{\frac{FMEP}{BMEP} + 1}$$ **Equation 3-73**

For any engine operating point, the BMEP is known because torque out of the engine is known by prior powertrain analysis. The thermodynamic efficiency is assumed to be a constant value which is consistent with the *(Nam & Sorab, 2004)* findings that most Naturally Aspirated Spark Ignition (NASI) engines have approximately the same value. The value of 43% is selected for thermodynamic efficiency from calibration discussed in Section 4.8.1. This value is comparable to the example of 43.4% provided in *(Nam & Sorab, 2004).*

FMEP is unknown and must be approximated. FMEP can be approximated as a function of a constant, engine speed, and engine speed squared with corresponding friction coefficients fmep0, fmep1, and fmep2, as shown in Equation 3-74.

$$FMEP \approx f_{mep0} + f_{mep1}\omega + f_{mep2}\omega^2$$ **Equation 3-74**

These ideal coefficients are found by fitting experimental data as discussed in Section 4.8.1. Table 3-9 provides a summary of engine constants. As fmep1 is best fit at zero, the engine friction is a pure quadratic, as assumed by *(Nam & Sorab, 2004)*. The relationship between speed and BMEP at constant engine efficiency is most apparent in Figure 3-16. This figure does not include engine torque limitations such as Wide Open Throttle (WOT) which is discussed in the next section. These coefficients are constant for all NASI engines. If the coefficients are adjusted, this model can be applied to other engine types such as a turbo-charged spark-ignited engine or a compression-ignition direction-injection engine. Each term in the FMEP equation has units that match that of BMEP, which in this model is kPa. Using this method, engine efficiency can be approximated:

$$\eta_{eng} = \frac{\eta_{thermo}}{1 + \frac{f_{mep0} + f_{mep1}\omega + f_{mep2}\omega^2}{BMEP}}$$ **Equation 3-75**

Table 3-9: Engine Constant Summary

Variable	Value	Unit
ηthermo	0.43	[---]
fmep0	127	[kPa]
fmep1	0	[kPa/(rad/s)]
fmep2	0.00024	[kPa/(rad/s)2]

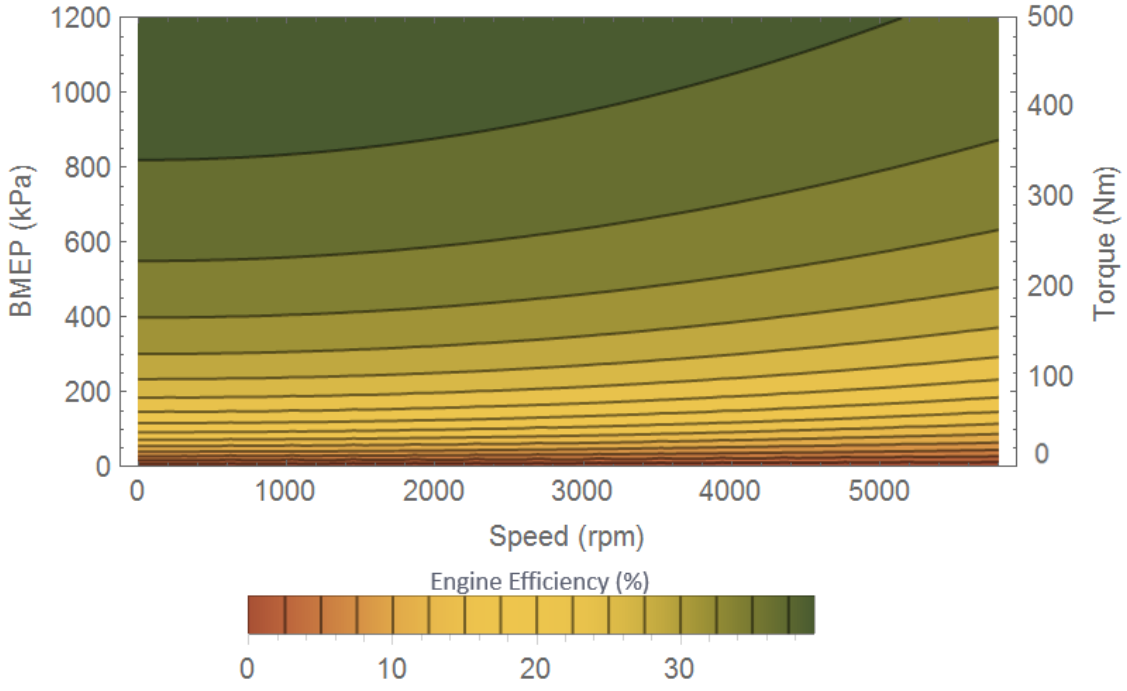

Figure 3-16: Example engine efficiency plot

3.3.7.2 Engine WOT

WOT is the maximum torque or BMEP that an engine can produce. In order to approximate the WOT limit, data from a V8 engine is curve fit into three linear sections shown in Figure 3-17. The middle orange section is a constant value and therefore has a low R2 value due to the linear fit. Each curve fit is based upon engine speed. The sections scale as a percentage of max engine speed such as the three categories are 0-22% max engine speed, 22-81% max engine speed, and 81-100% max engine speed. As these equations yield a value in BMEP, these equations can be scaled to approximate WOT torque limits for engines of different displacements.

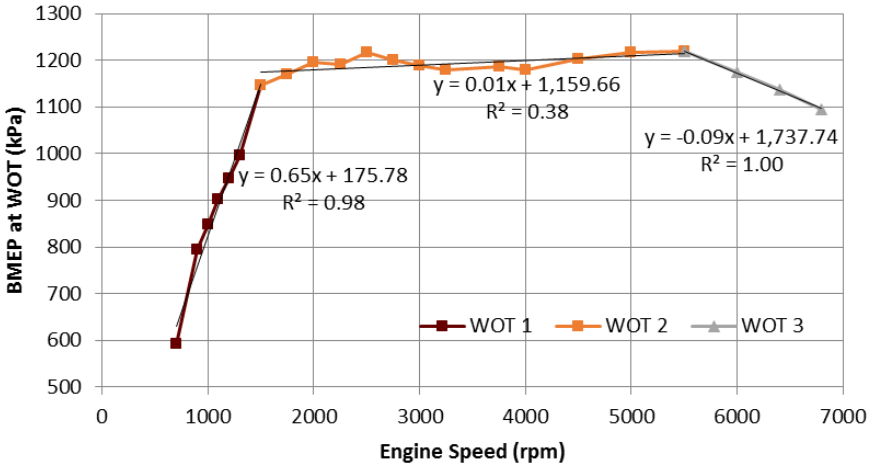

Figure 3-17: Wide Open Throttle Curve of a V8 Engine approximated into three sections

3.3.7.3 Engine Power Enrichment Limit

Before reaching the WOT limit, an engine reaches the Power Enrichment (PE) limit. In the operating region between the PE and WOT limits, engines are commonly calibrated to run rich, or use extra fuel, in order to generate more power while limiting the peak temperature of the engine. Above the PE limit engine efficiency decreases with increasing torque. Simple models, such as the methods presented in this thesis, do not capture the change in behavior of engines above the PE limit. Engines do not typically operate above the PE limit except for transient performance. As the engine will not commonly operate in this region, the model is chosen to accept the increase in inaccuracy in the region.

Similar to the WOT curve, the PE curve is found matching a V8 engine. The PE limit can be seen in Figure 3-18. The middle orange section of the PE limit is also a constant value and therefore has a low R2 value due to the linear fit. As these equations yield a value in BMEP, these equations can be scaled to approximate limits for engines of different displacements. The PE limit is useful for understanding where the efficiency model becomes less accurate.

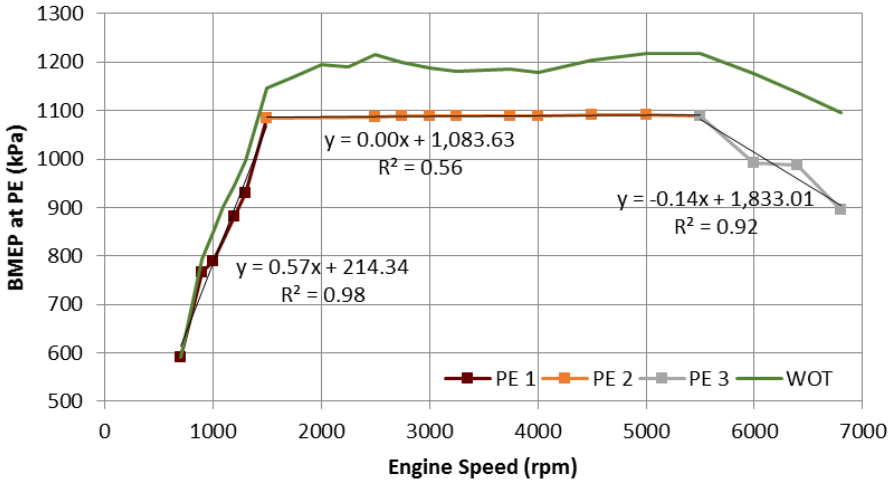

Figure 3-18: Power Enrichment Limit of a V8 Engine approximated into three linear sections

3.3.7.4 Additional Engine Losses

Engines experience losses not only during time of propelling the vehicle, but also during deceleration and idle times while the engine is on. As a simplification a constant power draw from the engine is assumed for both deceleration and idle times in addition to the constant accessory power draw. Both the deceleration and idle power are drawn from the output of the engine and thus require the engine to consume additional fuel. A draw of 1 kW from the engine during deceleration is selected for all engines. Likewise, a draw of 0.8 kW is selected as a constant for all engines during idle. A discussion of the rationale for these power draws can be found in Section 4.8.3. Engine idle power draw occurs at a constant engine idle speed of 600 rpm.

Another engine loss is the start loss. The start loss occurs when the engine is stopped and turns on once more. This loss is especially influential in hybrid control strategies to limit the number of times that the engine starts and stops. A constant energy draw of 16 kJ is added to the engine input as a fuel penalty to account for each engine start.

3.3.7.5 Engine Parameters

To model the engine losses, only the displacement volume is required. All engine parameters may be referenced in Table 3-10. The values in the table reflect those of the HEVT Camaro. This model does not have the ability to capture Active Fuel Management (AFM) behavior, also known as cylinder deactivation. The best approximation is to reduce the displacement volume when the vehicle is to operate with deactivated cylinders.

Table 3-10: Engine Parameters for HEVT Camaro

*Parameter	Value	Unit
Vdispl	5.3	[L]
Smax	5800	[rpm]
ηthermal	0.43	[---]
fmep0	127	[kPa]
fmep1	0	[kPa/(rad/s)]
fmep2	0.00024	[kPa/(rad/s)2]

*Parameter	Value	Unit
Max T	506	[Nm]
Sidle	600	[rpm]
PIdle	0.80	[kW]
Pdecel	1.00	[kW]
Smin	1050	[rpm]
Start Eeng,in	16	[kJ]

*Green cells signify required inputs

3.3.7.6 Fuel Properties

Fuel type is required to determine the quantity of fuel to be consumed on that route for a given amount of engine input energy. GHG emissions and PEU also depend on fuel type. From the fuel type, the model will pull data from the EcoCAR 3 fuel properties such as fuel density and energy content. EcoCAR 3 fuel properties are used as shown in Table 3-11 and Table 3-12. Electricity used to charge the battery of a PHEV or BEV is included as a fuel type as electricity has an upstream environmental impact. One important use of fuel properties is the fuel rate:

$$FuelRate = \frac{P_{eng,in}}{LHV} \qquad \textbf{Equation 3-76}$$

where LHV is the lower heating value of the fuel and Peng,in is the power entering the engine via fuel.

Table 3-11: General Fuel Properties *(ANL, 2016c)*

	LHV	Density		Energy Density	
	[kWh/kg]	[kg/L]	[kg/gal]	[kWh/L]	[kWh/gal]
Gasoline	11.73	0.76	2.87	8.90	33.67
E10	11.44	0.75	2.82	8.53	32.31
E85	7.96	0.79	2.98	6.27	23.72
B20	11.55	0.86	3.24	9.88	37.39

Table 3-12: Well to Wheel Fuel Properties *(ANL, 2016c)*

	Green House Gases			Petroleum Energy Content		
	GHGWTP	GHGPTW	GHGWTW	PEUWTP	PEUPTW	PEUWTW
	[g/kWh]	[g/kWh]	[g/kWh]	[kWh PE/kWh]	[kWh PE/kWh]	[kWh PE/kWh]
E10	70	264	334	0.077	0.93	1.009
E85	-15	259	244	0.063	0.21	0.274
B20	27	273	299	0.076	0.81	0.887
Electricity	489	0	489	0.033	0.00	0.033

Brake Specific Fuel Consumption (BSFC) is the rate of fuel consumption divided by the power produced. BSFC is a measure of fuel efficiency. As "brake" implies the power that actually is produced by the engine, the term literally means the fuel consumption to produce brake power.

$$BSFC = \frac{FuelRate}{P_{eng,out}} = \frac{FuelRate}{\eta_{eng} P_{eng,in}} = \frac{1}{\eta_{eng} * LHV} \qquad \textbf{Equation 3-77}$$

Another useful quantity is the amount of fuel consumed in gallons:

$$V_{fuel,consumed} = \frac{E_{total,in}}{E_{dens,fuel}} \qquad \textbf{Equation 3-78}$$

where Etotal,in is the total energy into the engine and Edens,fuel is the energy density of the fuel. This model does not distinguish the efficiency of the engine based upon fuel type. A flex fuel engine running on either E85 or E10 requires the same total input energy.

While the only required fuel input is the fuel type, Greenhouse Gas (GHG) emissions and PEU will be discussed in Section 3.5. Table 3-13 displays fuel parameters for the HEVT Camaro. The HEVT Camaro uses a combination of E85 and electricity. All GHG and PEU values reported for the HEVT Camaro were found using this fuel combination.

Table 3-13: Fuel Parameters

*Parameter	Value	Unit
Fuel Type	E85	[---]
ρfuel	2.98	[kg/gal]
LHV	8.0	[kWh/kg]
E Density	23.7	[kWh/gal]
GHGWTW	244	[g GHG/kWh]
PEUWTW	0.274	[kWh PE/kWh]

*Green cells signify required inputs

3.4 Powertrain Assembly and Energy Management Strategies

This section will describe how specific components may be assembled to form different powertrain configurations. This section will also detail the control strategies which allow each powertrain assembly.

3.4.1 Conventional Control System

The conventional control system requires all power into the powertrain to come from the engine. During all portions of the route, the engine is on. During idle, the engine experiences an idle loss in addition to providing accessory loads. Power leaves the engine, enters the transmission, and then the driveline, with losses in each respective component. Figure 3-19 is a schematic of a generic conventional powertrain.

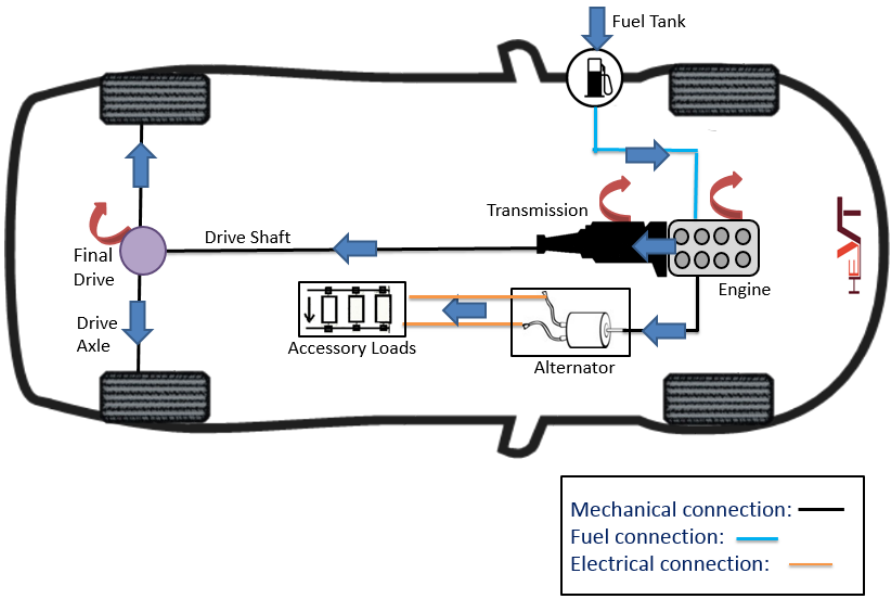

Figure 3-19: Generic Conventional Vehicle Powertrain Schematic

3.4.2 Regenerative Braking

All electrified vehicles are assumed to have regenerative braking. The regenerative braking factor depends on the driven axle. As the front axle of the vehicle experience more force during braking than the back axle, a FWD vehicle can capture a greater percentage of the total brake force than a RWD vehicle. For approximation purposes, a FWD vehicle capture 80% of the potential tractive power and a RWD vehicle captures 60% of potential tractive power.

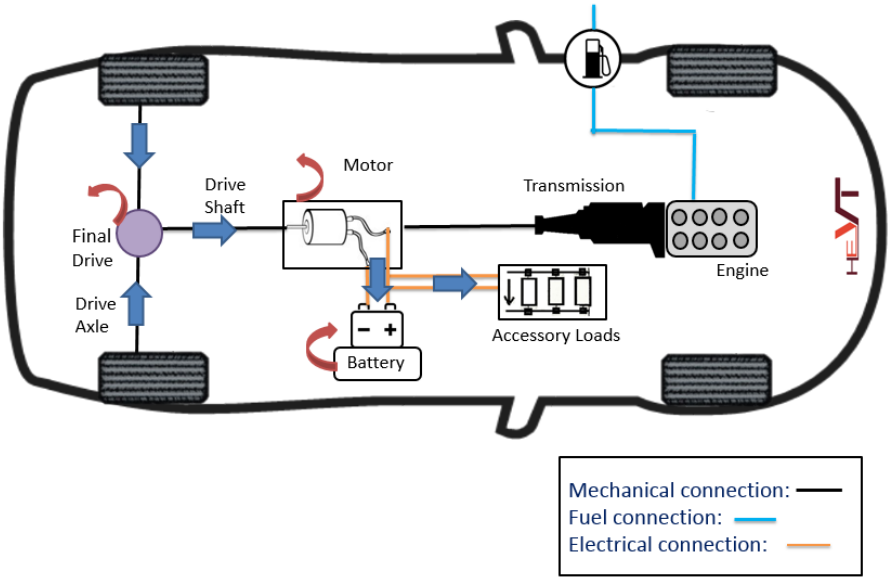

Figure 3-20: Generic Regenerative Braking Schematic

All regenerative brake parameters are considered constant for all vehicles of the same driven axle for model simplicity. The fraction of total brake energy that is captured varies with the wheel drive of the vehicle. Most HEVs are FWD. Ford claims to be able to capture 95% of brake energy, but also claims that their brake energy capture is 45-65% more than competitors *(Jaynes, 2013)*. For simplification in this model, FWD captures a constant 80% and RWD captures a constant 60%. As regenerative braking is inefficient at low speeds, no brake energy is captured below 5 mph. Similarly no power greater than 70 kW or wheel torque greater than 2000 Nm can be captured. All excess power or torque is lost to friction.

Table 3-14: Regenerative Brake Parameters for HEVT Camaro

Parameter	Value	Unit
Fraction	0.6	[---]
Speedmin	5	[mph]
Ptr,min	-70	[kW]
Tw,min	-2000	[Nm]
Ftr,min	-5.88	[kN]

3.4.3 BEV Control System

The BEV control system is the most simple. All power required into the powertrain must come from the battery. The power out of the battery enters the HV bus which supplies the accessory loads and the electrical side of the motor. The motor sends torque to the driveline, with losses associated with each respective component. During braking, a percentage of the brake power is captured in regenerative braking which is sent back through the motor and then to charge the

battery, with losses in each respective component. A single speed gear reduction is assumed; thus, a final drive provides a constant and the only gear reduction. Figure 3-21 is a schematic of a generic BEV powertrain.

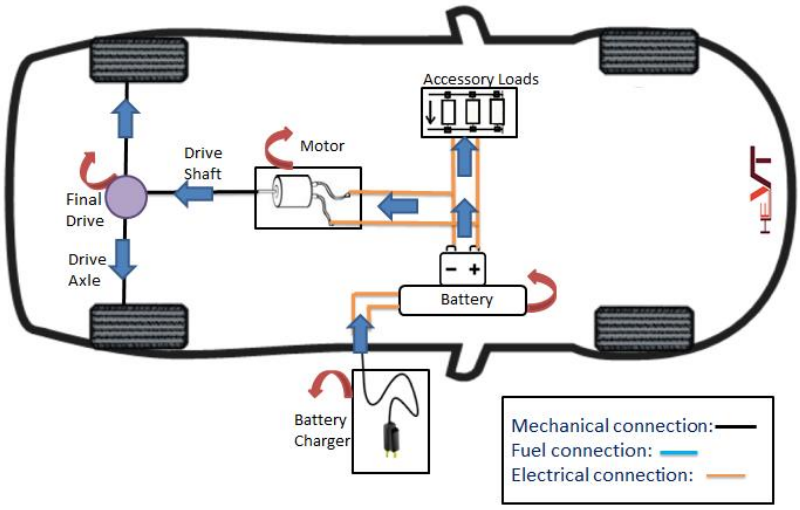

Figure 3-21: Generic BEV Powertrain Schematic

3.4.4 Hybrid Control System

3.4.4.1 Post-transmission Motor

A post-transmission motor signifies that the electric motor is mechanically coupled with engine torque after the engine torque has been multiplied by a transmission as shown in Figure 3-22. The HEVT Camaro has a post-transmission motor and so this model focuses on a post-transmission motor placement. Assuming that the motor does not have a separate gear ratio or independent transmission apart from that of the engine, the drive shaft speed is equal to the motor speed:

$$\omega_{motor} = \omega_{shaft} \qquad \textbf{Equation 3-79}$$

Transmission throttle is derived the same way for a post-transmission motor HEV as for a conventional vehicle.

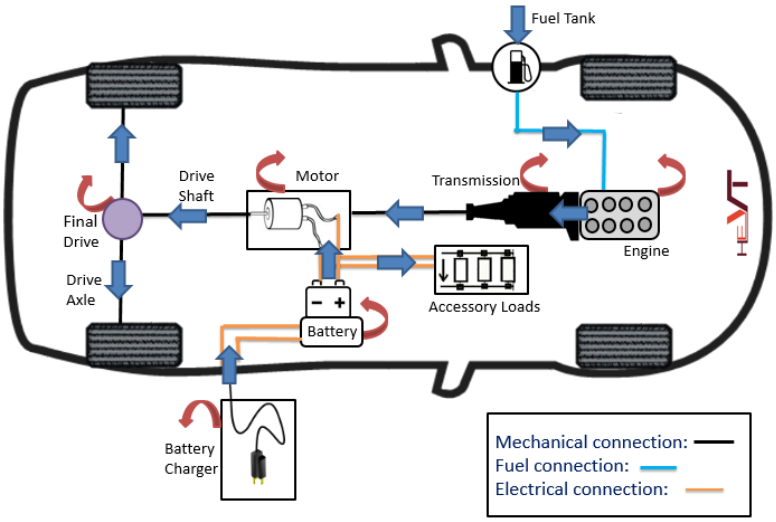

Figure 3-22: Generic Post-Transmission Parallel PHEV Powertrain Schematic

3.4.4.2 Pre-transmission Motor

A pre-transmission motor signifies that the electric motor is mechanically coupled directly with engine output torque as shown in Figure 3-23. The combined motor and engine torque is then multiplied by a transmission gear ratio. The motor speed of a pre-transmission motor is:

$$\omega_{motor} = \omega_{shaft}(GR) \quad \textbf{Equation 3-80}$$

where GR is the current transmission gear ratio. Transmission throttle requires maximum motor capabilities as discussed in Section 3.3.6.1.

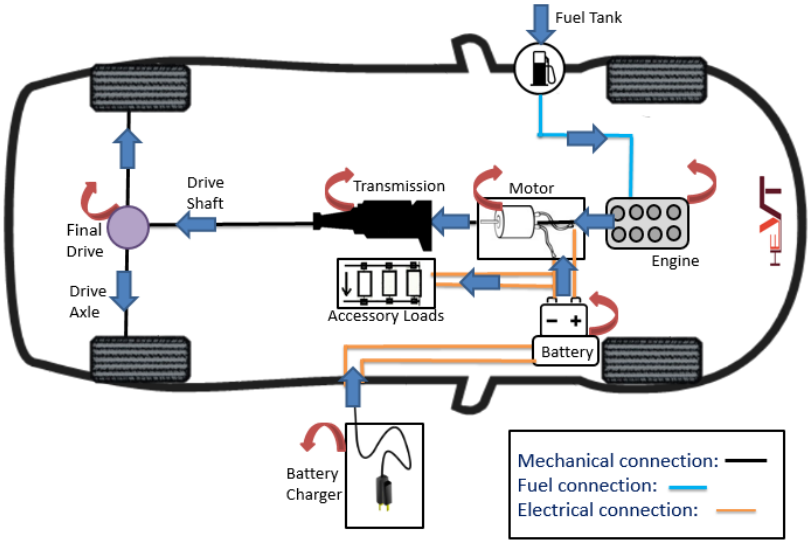

Figure 3-23: Generic Pre-transmission Parallel PHEV Powertrain Schematic

3.4.4.3 Parallel PHEV Control Strategy

The primary HEV powertrain modeled is a post-transmission parallel PHEV, like that of the HEVT Camaro. There are many control strategies available and many are highly complicated or proprietary. *(Marquez, 2016)* takes in-depth look into control strategy options for the HEVT Camaro. As this model needs to capture behavior from other vehicles, the strategy is highly simplified. There are three modes of operation: CD mode, Engine Loading Mode, and Engine Efficiency Mode. CD mode is when the vehicle is propelled solely by the battery. Engine Loading Mode is when the engine matches the demand and also includes an additional torque amount that is specified in the control strategy inputs. This extra torque amount is sent to the generator to change the battery. Engine Efficiency Mode is when the engine operates 100 kPa below the PE limit for high efficiency. Any extra torque is sent to the generator to charge the battery.

The rules for changing modes are shown in Figure 3-24. Starting with the rules leaving CD mode, the vehicle enters Engine Loading Mode when the SOC drops below SOCmin and a specified time delay has elapsed to prevent excessive engine starts and stops. The vehicle will also switch from CD to Engine Loading when the motor is incapable of supplying the demanded torque after a specified delay. The vehicle will switch from CD to Engine Efficiency when the SOC is less than a specific SOC, a specified time delay, and when the torque demand is less than a specified engine torque minimum limit. A torque minimum is established within the control strategy such that the engine does not operate in low torque low efficiency regions. Instead of operating at the low requested torque, the engine instead operates just below the PE limit for increased efficiency.

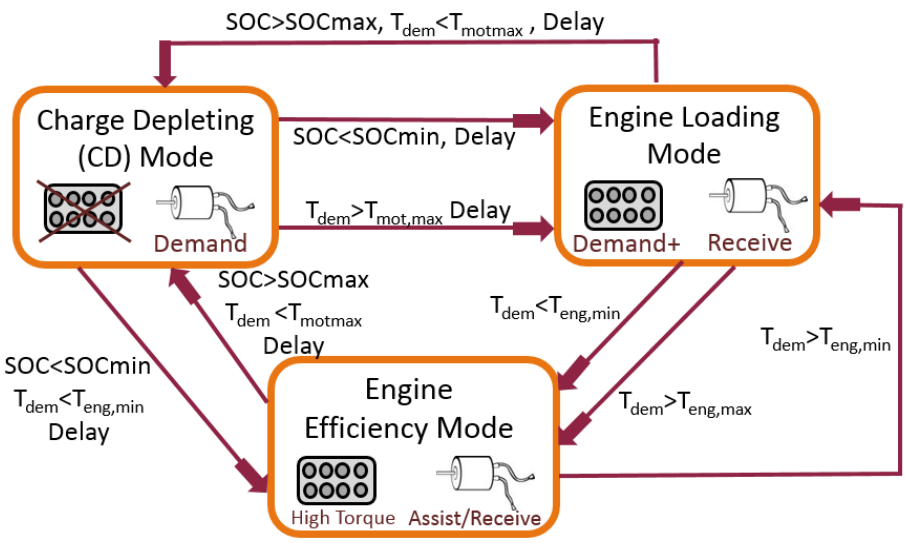

Figure 3-24: Parallel PHEV Control Strategy

When the vehicle is in Engine Loading Mode, if the SOC is greater than SOCmax, the motor is capable of meeting the torque demand, and a time delay has occurred, the vehicle switches back to CD. If the torque demand drops before the specified minimum torque limit for the engine, the vehicle will switch to Engine Efficiency. If the engine is unable to supply the required torque, then the vehicle will also switch to Engine Efficiency, which acts as a performance mode as the motor will supplement as the engine operates at the PE limit. There is no time delay between Engine Loading and Engine Efficiency because the engine is already running for both modes.

When the vehicle is in Engine Efficiency Mode, if the SOC is greater than SOCmax, the motor is capable of meeting the torque demand, and a time delay has occurred, the vehicle switches back to CD. While in Engine Efficiency, if the torque demand becomes greater than the specified engine torque minimum limit, then the vehicle will switch to Engine Loading.

In all modes of operation, the transmission is constantly reevaluating the gear. When the engine is off, the transmission constantly calculates in which gear the engine would operate if the engine were to meet the exact demand. When the engine turns on, the transmission starts in the predicted gear instead of always first gear. When the engine is on, the transmission bases the throttle off of actual engine torque out. A limitation of the model is that in this control strategy the engine often exceeds the torque demand via motor loading and so when the engine turns on the output torque is temporarily greater than anticipated by the transmission.

3.4.5 Control Strategy Inputs

To select the proper powertrain, which engages the proper components, the vehicle powertrain type is required. If parallel PHEV is selected, other inputs are required relating to the control strategy. Also, the motor position must also be specified as either pre-transmission or post-transmission for parallel PHEVs

Table 3-15: Control Strategy Parameters for HEVT Camaro

*Parameter	Value	Unit
Type	Parallel PHEV	[---]
Motor Pos.	Post-Trans	[---]
Paccy	600	[W]
tdelay	8	[s]
Tengextra	40	[Nm]
Tengmin	202	[Nm]

*Green cells signify required inputs

3.5 Model Outputs

Most ecorouting programs weight the same quantities for each route option: time duration, total energy consumption, and GHG emissions. The relative importance of each quantity varies with each ecorouting program. The outputs of this model are expected to be input into an ecorouting program for post-processing route selection.

3.5.1 Time Duration

Like a traditional GPS system, this model inputs map data in the form of a route and outputs the time required to complete each route option. As the route inputs are on a node-by-node distance basis, the time must be calculated using basic kinematics under the assumption that the vehicle will use constant acceleration between nodes. Time is evaluated using Equation 3-1, Equation 3-3, and Equation 3-5.

3.5.2 Total Energy Consumption

The primary objective of this research is the total energy required for each potential route for a specific vehicle. For conventional vehicles, the total energy consumption is the total expected fuel energy consumed during the route. Likewise for a BEV, the total energy consumption is the total expected grid electric energy to be used by the battery.

HEVs are more complicated in that they have two energy sources whose energy values cannot be directly combined. A PHEV that only operates in CD mode for all routes can be classified like a BEV in that total energy consumption is equal to the total expected grid energy to be used by the battery. If some route options allow the PHEV to operate only in CD mode while other route options fully deplete the battery, almost always the route options that operate only in CD mode are more eco-friendly due to the high efficiency of grid electric energy.

3.5.2.1 SOC Correction Factor

Comparing electric energy consumption with fuel consumption is difficult. For standard drive cycles, each test is often repeated with different initial SOC until the test ends with a similar SOC as the start. This iterating process is referred to as charge-balancing. In ecorouting, the vehicle has a set initial SOC and so the vehicle is not expected to charge-balance during every route. To compare routes when some routes allow the vehicle to entirely remain in CD while others eventually enter CS mode, an SOC correction factor can be used to adjust non-charge-balanced results. While called an SOC Correction Factor, this factor adjusts directly for net battery internal energy.

To compare routes that use different quantities of fuel and battery energy consumption, all battery consumption must be equated to a fuel consumption. One method for obtaining a relation between

battery and fuel energy is to plot the fuel energy on the y-axis and the change in battery internal energy on the x-axis as shown in Figure 3-25 for the Insight, Volt, and HEVT Camaro. A negative change in battery internal energy represents charging the battery and increasing the SOC. Likewise, a positive change in battery internal energy represents depleting the battery energy from the start of the route. The correlation between battery and fuel energy is mostly linear and the slope determines the SOC correction factor. This SOC correction factor plot is an extension of an SAE J1711 plot *(Duoba et al., 2009).*

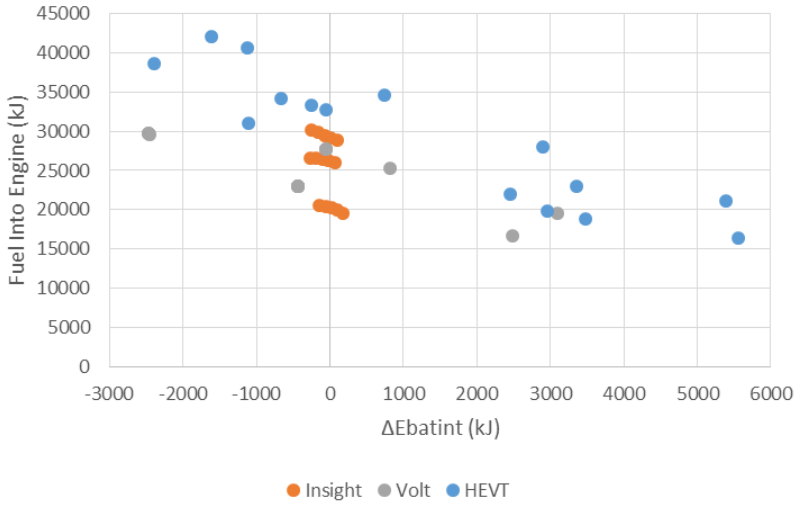

Figure 3-25: SOC Correction Factor Plot for Multiple Vehicles

As shown in Figure 3-25, each vehicle has significant variability due to variations in powertrain and control strategy. This figure shows results for all three vehicles for the UDDS, US06, and HWFET with varying initial state of charges. The US06 is an aggressive, high speed drive cycle. The HEVT Camaro has a steeper slope and higher y-intercept than the Volt, but are otherwise similar. The Insight has three tight lines, each representing a different drive cycle. The Insight is a mild-hybrid and therefore differs due to the very small motor. Mild hybrids will likely need a different SOC correction factor depending on the nature of the route. The two non-mild HEVs have results mostly on the same line for all three drive cycles and a constant value may be applied for an SOC correction on any route.

Due to variations between each vehicle, each vehicle is assigned an individual SOC correction factor. The HEVT Camaro is the focus of this research and the SOC correction factor plot for this vehicle is shown in Figure 3-26. The correlation is linear with an R2 value of 0.84. The line drops 2.991 kJ of fuel for every 1 kJ of battery internal energy. The relation is negative. For every 1 kJ that battery internal energy increases, an additional 3 kJ of fuel is consumed. For the HEVT Camaro, the SOC correction factor is 3. To equate a net change in battery internal energy to fuel energy:

$$E_{fuel} = -k_{SOC,corr}\Delta E_{bat,int} \qquad \textbf{Equation 3-81}$$

where Efuel is the additional fuel energy to be added to the fuel consumption to account for extra charging of the battery. kSOC,corr is the SOC correction factor. ΔEbat,int is the change in internal energy in the battery. A negative change in battery energy means that the battery is charged equating to a positive fuel penalty. If the battery is depleted, as with a positive change in battery energy, then the total fuel consumption will be deducted to charge balance the route.

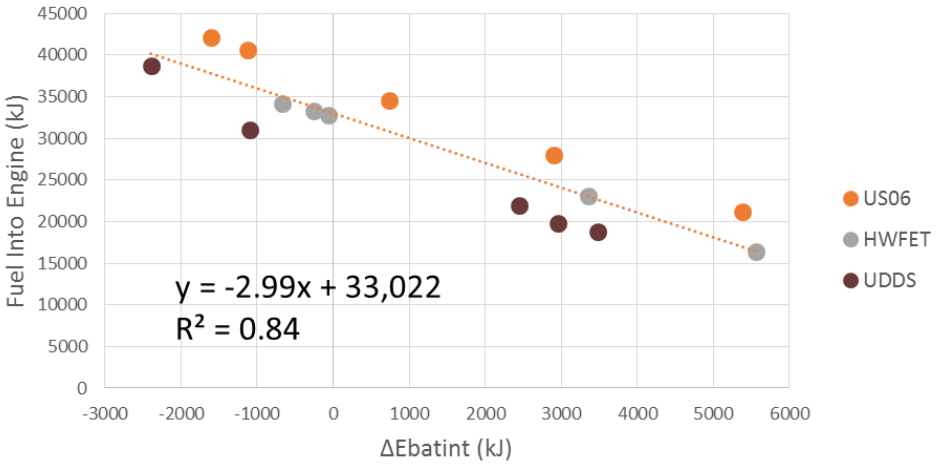

Figure 3-26: HEVT Camaro SOC Correction Factor Plot

3.5.2.2 PEU

Related to energy consumption, the PEU of a given route may also be interest for ecorouting purposes. The Well-To-Wheels (WTW) PEU values for select fuels are provided by the EcoCAR 3 competition are can be referenced in Table 3-12.

$$PEU = \left(PEU_{\text{wtw,fuel}}\right)E_{fuel} + \left(PEU_{\text{wtw,elect}}\right)E_{grid} \quad \textbf{Equation 3-82}$$

where PEU is the quantity of petroleum energy consumed, PEUwtw is the WTW factor provided by ANL in kWh PEU/kWh for each fuel type, Efuel is the energy of fuel used in kWh, and Egrid is the electric grid energy used in kWh.

3.5.3 GHG Emissions

While the objective of this research is to present a methodology for calculating the total energy consumption of each route for a specific vehicle, GHG emissions may also be approximated. For model simplification, GHG emissions are assumed to be linearly proportional with fuel energy used. The relationship between fuel energy and GHG emissions are defined in Table 3-12. These values are those specified by ANL for EcoCAR 3 by incorporating upstream processing emissions and assuming efficient fuel combustion in the vehicle engine *(ANL, 2016c)*. The mass of GHG emissions may found using:

$$m_{GHG} = \left(GHG_{\text{wtw,fuel}}\right)E_{fuel} + \left(GHG_{\text{wtw,elect}}\right)E_{grid} \quad \textbf{Equation 3-83}$$

where mGHG is the mass of GHG in g, GHGwtw is the WTW factor provided by ANL in g/kWh for each fuel type, Efuel is the energy of fuel used in kWh, and Egrid is the electric grid energy used in kWh. Well-to-wheel means that the emission factor considers both upstream and downstream emissions. While electric vehicles may have no emissions from the tailpipe, power plants produce emissions while producing electricity. In this thesis grid electric energy is loosely considered a fuel.

GHG emissions may be weighted in ecorouting, but no other emissions can be determined with only this methodology. Other emissions such as Carbon Monoxide (CO), Nitrogen Oxides (NOx), and Total Hydrocarbon (THC) depend on factors relating to the fuel combustion rate, engine pressure, the vehicle catalytic converter, or if the engine has a hot or cold start. As these emissions are highly complicated to model, they are omitted from this research.

4 Model Assumptions, Limitations, and Validation

As the principle objective of this thesis is to propose a methodology by which energy consumption for a given route for a particular vehicle can be found, the methodology must be validated both per component and inter-component. Assumptions in creating each component model are also discussed as many assumptions lead to model limitations.

4.1 Energy Balance

As this methodology is based upon tracking the energy flow through each component in a powertrain, summing the energy into, out of, and lost for each component verifies that energy is not lost due to inconsistent equations or programming. When components interact sequentially, the energy into the second component must be equal to the energy into the previous plus any energy lost from the previous. Figure 4-1 and Figure 4-2 show the net energy balance for the HEVT Camaro acting as a conventional vehicle and a BEV respectively on the Urban Dynamometer Driving Schedule (UDDS). An energy balance for a parallel PHEV is also conducted; however, due to the size and complexity of two energy sources, the data is not plotted.

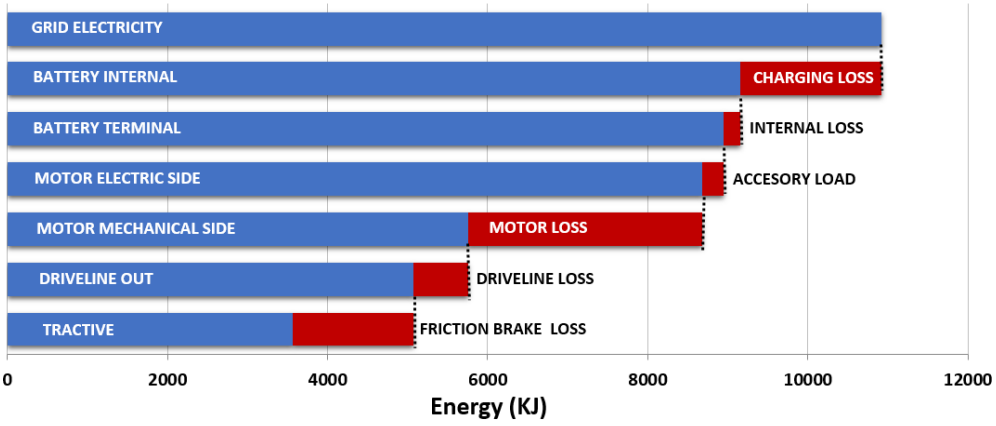

Figure 4-1: UDDS Net Energy Balance for BEV HEVT Camaro

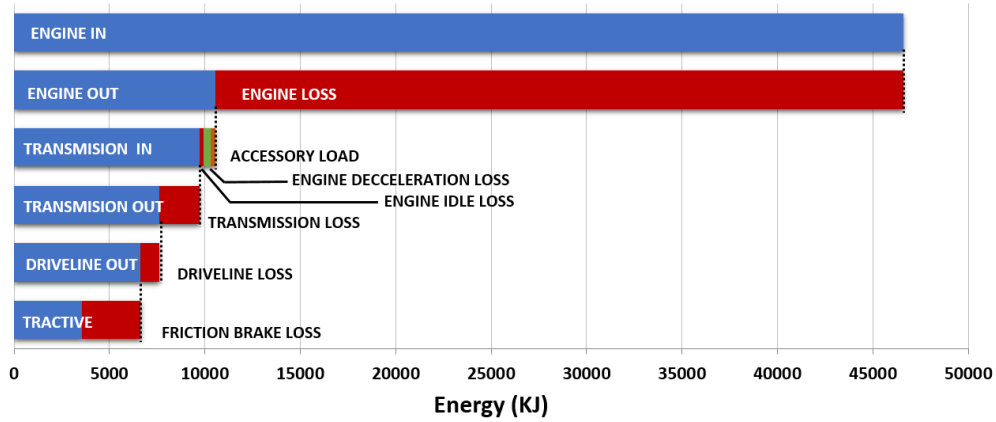

Figure 4-2: UDDS Net Energy Balance for Conventional HEVT Camaro

For complete verification, energy balances are completed separately for the propel and brake cases as well as the overall net case. All three cases balanced for all powertrain types. Data tables for each energy balance are shown in Appendix A. The parallel PHEV Camaro has three

tables: one for the electrical components, one for the conventional components, and another for the torque summing node to tractive energy. The energy transfer for all powertrains are correctly balanced such that no energy is created or left unaccounted.

4.2 Glider Model Validation

ANL published a presentation detailing the energy flow through each major component of the 2013 Nissan Leaf *(Lohse-Busch, 2012)*. This presentation provides energy values for both the UDDS and the Highway Fuel Economy Test (HWFET). The experimental data and model results used in to validate components in Section 4.2-4.5 can be referenced in Table 4-1 and Table 4-2. Three sets of motor loss coefficients are tested and will be explained in Section 4.5. Due to the usefulness of the energy breakdown, this data is used to validate the entire BEV model. Summaries of the error can be found in Appendix Table C-1 and Table C-2.

Table 4-1: UDDS 2013 Nissan Leaf Validation (*Lohse-Busch, 2012)*

UDDS		*ANL (kWh)	Standard Motor Coefficients (kWh)	Scaled Motor Coefficients (kWh)	Unscaled Motor Coefficients (kWh)
Inertia	Propel	0.928	0.925	0.925	0.925
	Brake	0.928	0.925	0.925	0.925
Road Load	Propel	0.673	0.670	0.670	0.670
	Brake	0.205	0.209	0.209	0.209
Tractive	Propel	1.601	1.595	1.595	1.595
	Brake	0.723	0.716	0.716	0.716
Motor Loss	Propel	0.316	0.557	0.346	0.323
	Brake	0.179	0.198	0.132	0.123
Accessory Load		0.064	0.076	0.076	0.076
Regen Braking		0.544	0.556	0.556	0.556
Extra DL Loss		0.000	0.300	0.300	0.300
Battery Net		1.436	2.185	1.925	1.895

*ANL date from (Lohse-Busch, 2012)

Beginning with inertia, the model mass is increased 14% from the 1498 kg found for this vehicle to match the inertia energy found in the data. Inertia energy is a simple formula and this thesis uses an inertial mass factor similar to that used by the EPA as discussed in Section 3.2.1.1. The actual test mass used to gather the data is assumed to differ from 1498 kg and be closer to 1707 kg.

Using the road load coefficients published in the Downloadable Dynamometer Database (D3) Master Summary for the 2013 Leaf, this model predicted the propel road load with an average of 0.4% error during propel and 2.8% average error during brake. Similarly, the model predicted propel tractive energy with 0.3% average error and 1.9% average error during brake. The errors in tractive energy translate to a small difference of 0.1 kWh for both propel and brake cases *(ANL, 2016b)*. The high correlation of the road load and tractive energy for both propel and brake validates the glider model of this model.

Table 4-2: HWFET 2013 Nissan Leaf Validation *(Lohse-Busch, 2012)*

HWFET		*ANL (kWh)	Standard Coefficients (kWh)	Scaled Coefficients (kWh)	Non-Scaled Coefficients (kWh)
Inertia	Propel	0.354	0.343	0.343	0.343
	Brake	0.354	0.343	0.343	0.343
Road Load	Propel	1.714	1.721	1.721	1.721
	Brake	0.138	0.133	0.133	0.133
Tractive	Propel	2.068	2.064	2.064	2.064
	Brake	0.216	0.210	0.210	0.210
Motor Loss	Propel	0.402	0.961	0.458	0.396
	Brake	0.057	0.087	0.045	0.039
Accessory Load		0.042	0.042	0.042	0.042
Regen Braking		0.159	0.169	0.169	0.169
Extra DL Loss		0.000	0.414	0.414	0.414
Battery Net		2.353	3.401	2.856	2.789

*ANL data from (Lohse-Busch, 2012).

4.3 Accessory Load Validation

While rare to find a specified accessory load value for any vehicle, ANL published the total energy attributed to the accessory load for both the UDDS and HWFET for the Leaf. Using the same 2013 Nissan Leaf energy flow data published by ANL, the accessory load, assumed constant in this model, is calibrated *(Lohse-Busch, 2012)*. Table 4-1 and Table 4-2 display a comparison. Selecting a constant accessory load of 200 W led to a difference of 0.012 kWh and 0.006 kWh respectively for the UDDS and HWFET. Due to the closeness of match, 200 W is selected as the accessory load to be used for all BEVs. This value may be overwritten if additional data is known.

4.4 Regenerative Brake Fraction Validation

The regenerative brake fraction for a FWD vehicle is assumed to be 80%. Comparing with the ANL 2013 Leaf Data, this regenerative braking fraction appears to be rather accurate *(Lohse-Busch, 2012)*. Table 4-1 and Table 4-2 display a comparison. In the UDDS, this model experienced 2.2% error. In the HWFET, the model experienced 6.3% error. These errors are only a small difference of 0.01 kWh for both cycles. Due to the overall match, FWD vehicles are assumed to have an 80% regenerative braking fraction. Similarly, as RWD vehicles are expected to capture a smaller percentage, 60% is assumed.

4.5 Motor Validation

The 2013 Nissan Leaf has an exceptionally efficient motor, but as many national labs have published data on the Leaf, this vehicle is chosen to validate the BEV model. Due to the highly efficient motor, the motor coefficients that match most motors are not exceptionally accurate for the Leaf. A Leaf motor efficiency plot is publically available and used to derive an ideal set of Leaf motor loss coefficients for comparison with the standard motor coefficients. A set of ideal motor coefficients are found by scaling the Leaf with the standard reference motor and another set of ideal motor coefficients are found using the unscaled loss equation, Equation 3-31. Table 4-3

shows a summary of the motor loss coefficients and reference motor parameters used for validation.

Table 4-3: Leaf Motor Coefficients in Data Validation

Coefficients	Tref,max	Sref,base	Sref,max	Pref,peak	Corner η	Ideal			
						kc	ki	kw	C
	(Nm)	(rpm)	(rpm)	(kW)	(%)	(---)	(---)	(---)	(---)
Standard	270	2400	6750	66	86%	0.0825	6.15	$54(10^{-7})$	200
Scaled 2013 Leaf	270	2400	6750	66	89%	0.0950	2.9	$5(10^{-7})$	400
Unscaled 2013 Leaf	280	2728	10300	80	87%	0.1400	2.3	$6(10^{-7})$	500

A comparison of the Leaf experimental efficiency plot alongside the efficiency plots using all three sets of coefficients can be referenced in Appendix B. Both sets of Leaf motor coefficients produce nearly identical efficiency plots with the experimental data validating that the motor loss equation is capable of accurately capturing motor efficiency trends. In order to best capture those motor loss trends in equation form, obtaining an efficiency map from the OEM, if available, greatly increases accuracy. The 2013 Leaf serves as an example for why model approximations may be overwritten if more detailed information becomes available. Table 4-1 and Table 4-2 display experimental data from ANL and model data using the standard, scaled, and unscaled motor coefficients. As expected, the standard motor coefficients have the least accuracy, the scaled motor coefficients fall in the middle, and the unscaled motor coefficients have the highest accuracy. The standard coefficients are inefficient as expected for the Leaf motor by 0.24 kWh. The unscaled coefficients are nearly identical as a motor but less so for a generator. This method assumes that the generator efficiency uses the same equation as the motor efficiency, while in reality the generator does not. Nonetheless, the unscaled coefficients only differ by 0.06 kWh in total generator loss.

Motor losses account for around 25% of total grid energy consumption for a BEV, as can be visualized in the BEV energy balance in Figure 4-1. While this may seem significant, the purposes of this research is to accurately predict the relative energy consumption between routes. Using the standard motor coefficients, the HWFET is found to require 55% more grid electricity than the UDDS. Using the unscaled motor coefficients, the result is 47% more. This demonstrates that the specifics of the motor loss coefficients do not dramatically impact the route decision.

4.6 Battery Validation

The battery internal resistance coefficient, R0, is not a standard value as R0 is unique to this thesis in the methodology for approximating Rint. The value of R0 is found using data from batteries of known internal resistance, energy capacity, and open circuit voltage, as shown:

$$R_0 = R_{int}\frac{E_{cap}}{V_{OC}^2} \qquad \textbf{Equation 4-1}$$

A summary table of vehicle batteries properties collected by Idaho National Lab (INL) as part of the Advanced Vehicle Testing (AVT) Activity can be found in Appendix Table B-1 *(INL, 2015)*. From the data, four groupings of R0 values emerged: the small Nickle Metal Hydride (NiMH) batteries common in HEVs and then three categories of Lithium Ion (Li-Ion) batteries. Batteries with a capacity less than 10 Ah formed the small battery category roughly including mild HEV batteries,

less than 40 Ah formed the medium category roughly including PHEV batteries, and all higher formed the large battery category roughly including BEV batteries. Table 4-4 details which resistance coefficient is assigned to which battery category.

Table 4-4: Battery Internal Resistance Coefficient Categories

Type	Max Ah Capacity	R0
Li-Ion	10	0.0052
NiMH	10	0.0126
Li-Ion	40	0.0113
Li-Ion	100	0.0199

4.7 Overall BEV Validation

In conclusion of the validation comparisons with ANL's BEV energy breakdown displayed in Table 4-1 and Table 4-2, the overall battery grid electricity is compared. Using the ideal Leaf motor coefficients, the model produced a 32% error, or difference of 0.46 kWh, for the UDDS and an 18.5% error, or a difference of 0.44 kWh, for the HWFET. While this may seem to be a large error, this is error across the entire powertrain. This model is highly simplified to be able to model a range of vehicles using only publically available vehicle component data. Further, the data published by ANL is unclear exactly how measurements were taken and does not include driveline losses.

The most interesting result is how the overall energy consumption between UDDS and HWFET compare. The UDDS and the HWFET may be considered route options. The experimental data shows the HWFET utilized 64% more grid electricity than the UDDS. The model predicted that the HWFET utilized 47% more grid electricity than the UDDS. While the values are not exact, the model demonstrates that the HWFET uses significantly more energy than the UDDS, as expected. Possible reasons for the increase in energy consumption for the HWFET include that the HWFET is 38% longer in distance with almost twice the average speed of the US06.

4.8 Conventional Vehicle Validation

The engine and transmission are reliant on one another. As such, many aspects of both engine and transmission are validated together.

4.8.1 Engine Efficiency

The engine efficiency coefficients are calibrated by matching the efficiency map of a known engine. These coefficients are selected using BMEP instead of torque so that the map may be scaled to match engines of different displacement. The coefficients are varied until the sum of the absolute value for a particular region of the map is minimized. The region selected is from 1000-4000 rpm and BMEP values less than 1000 kPa, which is around the power enrichment level of most engines. Above the power enrichment limit engine efficiency decreases with increasing torque and this simplified model is unable to capture this behavior. This region is selected as this is the region in which vehicles operate during normal driving conditions. The selected coefficients are summarized in Table 4-5.

Table 4-5: Engine Constant Summary

Variable	Value	Unit
ηthermo	0.43	[---]
fmep0	127	[kPa]
fmep1	0	[kPa/(rad/s)]
fmep2	0.00024	[kPa/(rad/s)2]

Figure 3-16 shows the final engine efficiency plot for a calibrated engine. Figure 4-3 shows the relative difference in engine efficiency between the calibrated engine and the known data for that engine. The regions of the plot that are white represent regions where the difference is greater than 1.5% engine efficiency. These inaccurate regions are uncommon for normal vehicle operation.

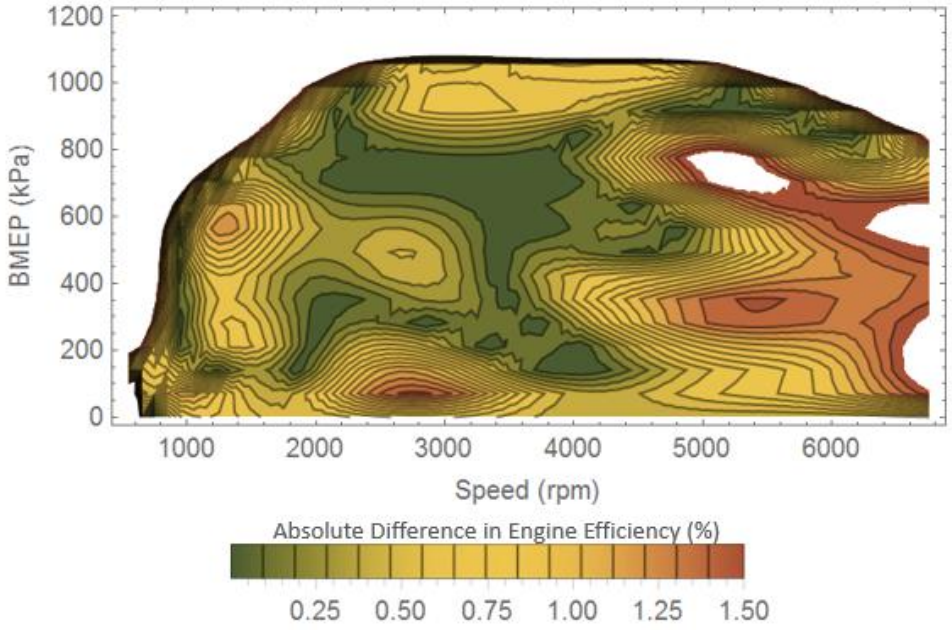

Figure 4-3: Engine Efficiency Error Plot

4.8.2 Shift Strategy Validation

ANL posted conventional vehicle data for the 2012 Ford Fusion, 2012 Chrysler 300, and the 2013 Hyundai Sonata. This data is published as "Overview Sheets" for each vehicle by ANL in the D3 *(ANL, 2016b).*The engine speed values for upshift and downshift at both 0% and 100% throttle are calibrated to produce the best fit for all nine datasets. The selected engine speed formulas can be referenced in Appendix Table D-2 and Table D-3. The formulas are functions of engine max speed, engine lug limit, and then two sizing parameters: ΔH and ΔL. Using these formulas, the final results for all nine datasets can be referenced alongside the ANL experimental data in Table 4-6. Appendix Table D-5 expands Table 4-6 to include the 8-speed Chrysler 300.

Table 4-6: Percent of Drive Cycle Spent in Each Gear

		% Time Spent in Gear											
		1		2		3		4		5		6	
		*ANL	Mod	*ANL	Mod	*ANL	Mod	*ANL	Mod	*ANL	Mod	*ANL	Mod
Fusion	UDDS	26.6	26.2	4.8	5.8	8.8	12.1	32.9	25.7	18.4	18.6	7.6	11.7
	HWFET	1.5	1.2	0.5	0.7	0.9	1.3	1.8	2.8	12.2	12.8	82.9	81.3
	US06	14.5	11.4	2.8	6.4	3.9	8.1	5.3	9.7	9.2	14.6	63.1	49.8
Sonata	UDDS	27.9	28.7	7.1	8.5	16.8	17.3	33.6	30.9	7.0	7.8	7.6	6.8
	HWFET	1.6	1.6	0.6	0.8	1.0	2.4	3.2	12.5	15.8	26.5	77.8	56.4
	US06	13.8	13.8	5.7	7.2	6.0	10.6	6.9	14.1	9.1	20.6	58.6	33.7

ANL data from “Overview Sheets” for each vehicle on the Downloadable Dynamometer Database (D3) (ANL, 2016b)*

Given the complicated nature of a transmission and the simplicity of this model, this model performs very well in comparison with the ANL experimental results. The percent of the drive cycle spent in first and second gear is almost identical for all nine datasets. The model sometimes holds gears three, four, and five too long, but other times too short. For the six gear transmissions, the Fusion and the Sonata, the model predicted excessive use of sixth gear in the UDDS and HWFET, but not enough in the US06. For the 300 eight speed transmission, a shift strategy that would frequently enter the eight gear is difficult to attain. Appendix D Table A-1 and Figure A-1 display the eight speed shift values. The shift speeds for the eighth and seventh gear are less than those of sixth to ease the transition into upper gears to match the validation data.

4.8.3 Idle and Deceleration Fuel Rates

After validating other portions of the transmission shift strategy, idle and deceleration fuel rates are calibrated. These values are also calibrated using D3 conventional vehicle data, by matching the percent of fuel attributed to propel, brake, cruise, and idle for three vehicles for UDDS, US06, and HWFET. To account for idle and deceleration losses, the engine model has a power draw in addition to the required power to the alternator to power accessory loads. Looking at the nine datasets, the values of deceleration engine additional power out and idle additional engine power out are calibrated so as to reduce the overall absolute error in comparison with the experimental data. The comparison is displayed in Table 4-7. To match the data provided by ANL, cruise is defined as acceleration rates less than ±0.2 m/s2. For continuity, acceleration and deceleration exclude acceleration rates less than ±0.2 m/s2.

In the overview sheet for each vehicle there are plots of engine speed versus vehicle speed. At a vehicle speed of 0 mph, the engine speed is roughly 600 rpm for all vehicles *(ANL, 2016b)*. As such, the model is set to force the engine to operate at 600 rpm during idle. An additional power draw of 800 W at 600 rpm is equivalent to 15.35 kW of fuel power into the engine, or 0.54 g/s of fuel during idle. This value can be overwritten if additional information in known.

Table 4-7: Percent Total Fuel Use in For Each Drive Case

		Acceleration		Cruise		Deceleration		Idle	
		ANL	Model	ANL	Model	ANL	Model	ANL	Model
Fusion	UDDS	52.7	45.2	29.7	33.3	10.0	12.3	7.6	9.1
	HWFET	28.7	20.7	62.5	75.7	7.0	3.4	1.9	0.1
	US06	59.7	50.1	30.0	43.1	8.6	5.6	1.8	1.2
Sonata	UDDS	52.4	46.6	28.7	33.5	11.2	11.4	7.7	8.5
	HWFET	28.0	21.7	64.3	75.1	5.6	3.0	2.2	0.1
	US06	62.8	51.4	27.7	42.2	7.8	5.3	1.6	1.1
300	UDDS	52.5	45.6	26.8	33.3	10.8	11.8	8.9	9.3
	HWFET	31.8	22.3	59.8	74.9	6.1	2.6	2.3	0.2
	US06	59.4	52.0	26.8	41.2	10.8	5.4	2.4	1.3

*ANL data from “Overview Sheets” for each vehicle on the Downloadable Dynamometer Database (D3)

Similarly, all engines decelerate with an additional default of 1 kW of power out of the engine. This value can be overwritten if additional information in known. The engine is assumed to decelerate with the vehicle as a function of gear ratio and final drive. Analyzing a few drive cycles for a few vehicles, the engine tends to operate around 1100 rpm during deceleration. Due to the inefficiency of the engine at such a low load, 1 kW of power out of the engine is equivalent to 19.44 kW of power into the engine via fuel. At the speed of 1100 rpm, the deceleration power out of the engine of 1 kW equates to 0.68 g/s of fuel.

4.8.4 Engine and Transmission Accuracy

Using the same D3 dataset, ANL published the Fuel Consumption (FC), Fuel Economy (FE), vehicle efficiency, average engine moving speed, and the estimate transmission shifts per cycle *(ANL, 2016b)*. Simulation results are compared with the ANL experimental data in Table 4-8. FC, FE, and vehicle efficiency are all related. FC is the inverse of FE, though the units listed for each are not the same. For all nine datasets, both FC and FE simulation results align closely with the experimental data. Vehicle efficiency is the ratio of net tractive energy to net powertrain input energy. For a conventional vehicle, the brake tractive energy is not captured and is only lost. As such, only propel tractive energy is considered for net vehicle efficiency:

$$\eta_{veh} = \frac{{E_{tr}}^{+}}{{E_{in}}^{net}} \qquad \textbf{Equation 4-2}$$

where Etr is the propel tractive energy necessary to complete the drive cycle and Ein is the energy into the powertrain. The net engine energy input is selected because the engine requires input energy during both idle and brake to power accessory loads or account for engine losses. In the case of a conventional vehicle, the energy into the powertrain is fuel energy. The tractive energy required to complete all cycles should be the same between experimental and simulated results as the glider model is verified in Section 4.2. To match the vehicle fuel consumption with that of the experimental data, the driveline torque loss is calibrated to 7% maximum engine torque. All conventional vehicles in this model have a driveline torque loss of 7% the maximum engine torque. This value matches well with all nine data sets.

The model simulated fuel consumption with an average error of 10% from the experimental values. The model is very close for all US06 results, over-efficient for UDDS results, and under-

efficient for HWFET results. For ecorouting purposes, the conventional vehicle model is sufficiently accurate. Between the three route options of UDDS, HWFET, and US06, the model consistently predicted which route required the most energy consumption.

Table 4-8: Conventional Vehicle Energy Validation

		FC (L/100 km)		FE (mpg)		Net Vehicle Eff. (%)		Avg. Eng. Speed Moving (rpm)		Est. Shift/Cycle	
		*ANL	Model	*ANL	Model	*ANL	Model	*ANL	Model	*ANL	Model
Fusion	UDDS	9.52	8.50	24.9	27.66	15.64	16.84	1391	1229	136	292
	HWFET	6.10	6.81	38.9	34.52	22.48	19.48	1625	1582	18	138
	US06	9.26	9.29	25.7	25.31	24.54	24.10	1996	1832	74	206
Sonata	UDDS	9.33	7.80	28.5	30.14	17.7	18.17	1326	1312	152	346
	HWFET	5.07	6.16	46.8	38.21	26.2	21.11	1498	1635	28	312
	US06	8.37	8.26	28.4	28.48	24.8	24.87	1878	1914	92	280
300	UDDS	10.09	9.43	23.5	24.95	18.4	19.47	1126	1148	206	352
	HWFET	6.42	7.11	37.0	33.08	27.0	24.86	1122	1242	102	278
	US06	8.37	9.43	8.37	24.93	28.4	28.42	1497	1200	92	134

*ANL data from “Overview Sheets” for each vehicle on the Downloadable Dynamometer Database (D3)

Evaluating the transmission accuracy, the model predicts significantly more frequent gear shifting, but the average engine moving speeds are close to experimental values. This model does not include engine or transmission losses associated with transmission shifting. The number of shifts per cycle are generally related to drivability which is not considered in this thesis. As the average engine speeds and percent of time in each gear for each of the nine datasets is close to experimental values, the transmission model is assumed to be reasonable correct.

4.8.5 Clutch and Torque Converter Simplification

This model does not include a clutch or a torque converter. As a simplified explanation, a torque converter consists of fluid that spins around in an enclosed container. The fluid transmits torque from the engine to the transmission. A torque converter serves the same purpose as a clutch in a manual transmission: the torque converter allows the engine to disconnect from the transmission such that the engine may continue to run while the transmission is shifting or the vehicle is stopped. The torque converter or clutch allows slip while this model only allows discrete gear changes. As such, the modeled data on the vehicle speed versus engine speed plot are cleaner than would be true of test data. This discrepancy is best exemplified in a comparison of the 2012 Ford Fusion plot of vehicle speed versus engine speed. The experimental data is displayed in Figure 4-4 and the modeled data is displayed in Figure 4-5.

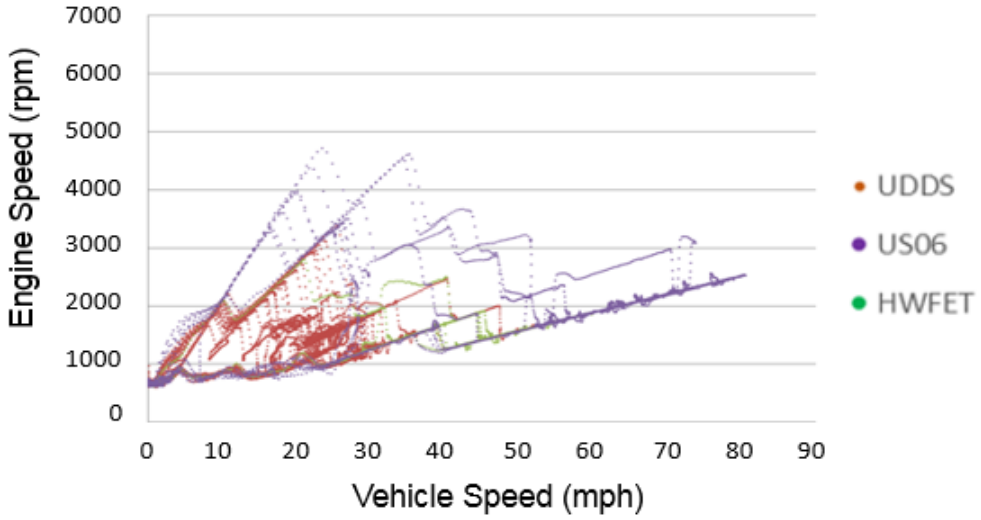

Figure 4-4: 2012 Ford Fusion Engine Speed vs Vehicle Speed *(ANL, 2016b, Public Domain)*

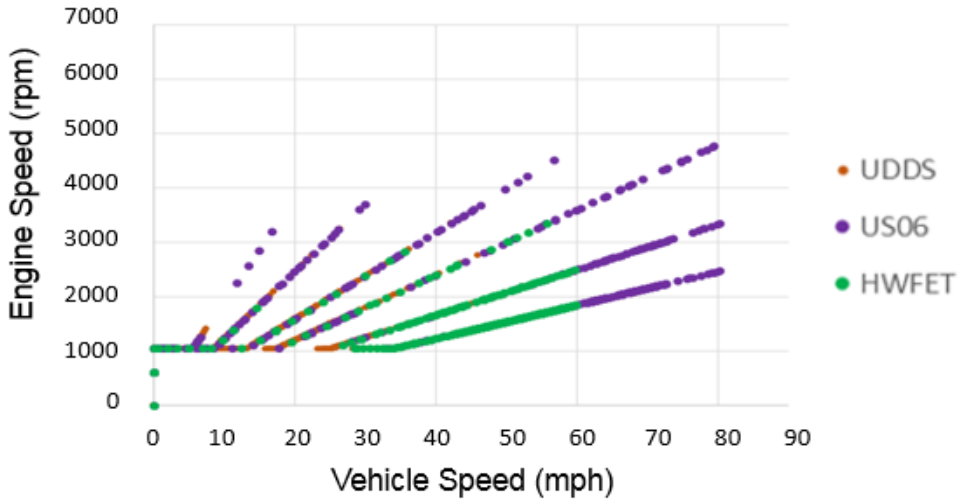

Figure 4-5: Ford Fusion Engine Speed vs Vehicle Speed Model Results

Despite the lack of torque converter or clutch slip, the slope of the lines for each gear ratio are equivalent, as expected. A point for idle operation and another point for vehicle off are displayed in the model data but not the experimental data. Other experimental data points that do not exist in the model data are the result of small variations in shift strategy.

4.9 Hybrid validation

4.9.1 Hybrid Control Strategy Validation

The HEVT Camaro is a post-transmission parallel PHEV. There are very few vehicles with this powertrain and none of which have publically available energy consumption data. The first step to validating the parallel PHEV powertrain model is to conduct an energy balance that may be referenced in Appendix A. Hybrids can be especially difficult to energy balance as energy is combined from many components, each containing the possibility of an error. The energy balance shows that all energy demanded by the driveline is met by both the motor output and the

transmission output confirming that the parallel PHEV control strategy properly accounts for all energy exchanges.

Another method for ensuring that the hybrid model is working properly is to examine when the battery and engine are each active. The HEVT Camaro engine is 5.3 L and therefore requires heavy loading to reach high efficiencies. In a hybrid, this engine should be loaded by the motor to attain more efficient operating points. Because of the high torque threshold for this engine, the engine should only need to be on for short periods of time until the battery is sufficiently recharged or the motor is capable of meeting the torque demand. Battery SOC should remain closely within the defined SOC boundaries which are 20-30% for the HEVT Camaro. Excessive engine starts are inefficient. Figure 4-6 displays the HEVT Camaro vehicle speed, engine power, and SOC on the US06 when starting with an initial SOC of 25%. This plot, as well as those for other drive cycles, are simplified but similar to how the HEVT Camaro is expected to operate.

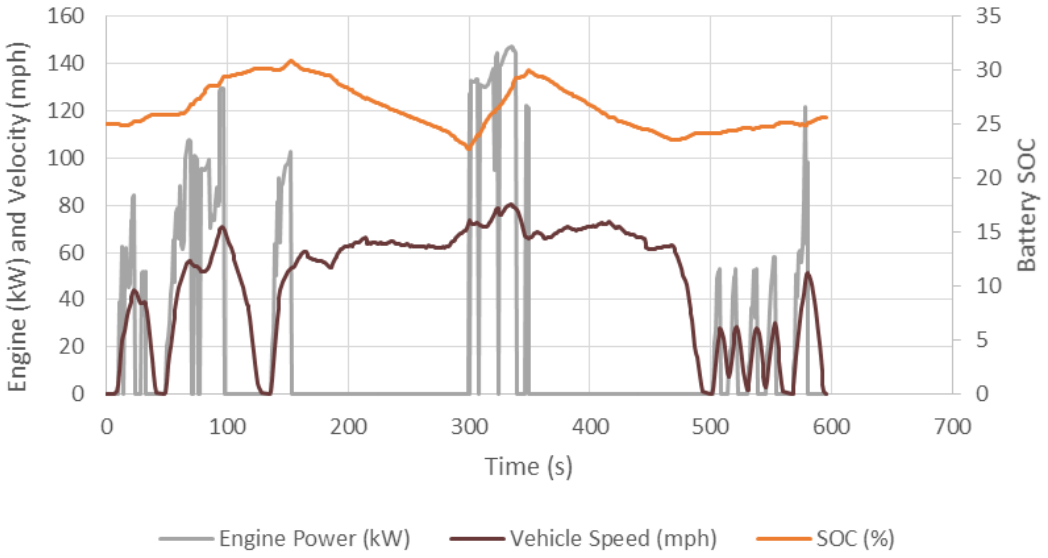

Figure 4-6: US06 HEVT Camaro Engine Power, SOC, and Vehicle Speed vs Time

4.9.2 Hybrid Experimental Data Comparison

To validate that the parallel PHEV model produces reasonable energy consumption results, other HEVs are used for validation. The 2010 Honda Insight is a parallel mild-hybrid. As the Insight is a mild hybrid, the battery and motor are substantially smaller than that of the HEVT Camaro. To look at a more electrified hybrid, the 2012 Chevrolet Volt is a series-parallel PHEV with a large motor and battery but a relatively small 1.4 L engine. For this validation, both the Honda Insight and the Chevrolet Volt are modeled as a pure parallel PHEVs. Both vehicles have CVTs, but are modeled using the Ford Fusion 6-speed transmission. Both the Insight and the Volt have small engines of 1.4 L and so the Ford Fusion transmission is selected as the Fusion transmission is designed for another small engine of 3.0 L. With these approximations the energy consumption results for either vehicle are not expected to be exact.

In order to have the ability to charge balance for all drive cycles, each vehicle required a unique combination of control strategy inputs: mode time delay, extra engine torque, and engine torque cutoff. For the UDDS, US06 City, US06 Highway, and HWFET, a set of inputs is found for each vehicle that could approximately charge balance for each drive cycle. These inputs are summarized in Table 4-9. Especially as the HEVT Camaro has a substantially larger engine than

the other vehicles, the control strategy will need to change to align with each vehicle. The Camaro is capable of loading the engine to a higher torque than the other engines. The Insight has such a small battery that very minimal engine loading is necessary to greatly increase battery SOC. To apply this model to all vehicles, matching with one or two EPA energy consumption results is necessary to calibrate the control strategy.

Table 4-9: Parallel PHEV Control Strategy Input Summary

	Mode Time Delay (s)	Extra Engine Torque (Nm)	Engine Min. Torque Cutoff (Nm)
HEVT Camaro	8	40	202
2012 Volt	7	5	126
2010 Insight	4	2	17

4.9.2.1 D3 Insight Data

D3 published experimental data for the 2010 Honda Insight. All data is close to charge balanced and is displayed in Table 4-10. The US06 runs twice to facilitate charge balancing and the results are the average of the two back-to-back runs. Rather than a perfect charge balance, the initial SOC is adjusted such that the battery net energy consumption is equivalent to that of the experimental data and no SOC correction factor is applied to the model results. A negative net battery energy consumption implies net energy is input into the battery, meaning that the battery is charged. The HWFET results are surprisingly close: 59.3 mpg to the model predicted 58.4 mpg. The US06 is also reasonably close with experimental data of 37.7 mpg and the model predicting 41.0 mpg. The UDDS is 15% more efficient than the experimental data but still considered to be reasonable validating the parallel PHEV strategy.

Table 4-10: 2010 Honda Insight D3 Energy Validation *(ANL, 2016b)*

Route	Mod. SOCi	Fuel Economy (Modal)		Battery Net Energy		Battery Net Energy Consumption	
	(%)	(mpg)		(DC Wh)		(DC Wh/mi)	
		*ANL	Model	*ANL	Model	*ANL	Model
HWFET	38.2	59.3	58.4	-5.524	-3.13	-0.538	-0.31
US06	58.0	37.7	41.0	-19.57	-17.83	-2.438	-2.23
**UDDS HS	30.9	51.9	60.0	-1.196	-2.56	-0.160	-0.34

*ANL data from the Downloadable Dynamometer Database (D3)
**UDDS Hot Start

4.9.2.2 D3 Volt Data

The 2012 PHEV Chevrolet Volt has a much larger battery than the mild HEV Honda Insight and is capable of a CD mode. D3 published data for the 2012 Volt in both CD mode and CS mode for three drive cycles. The data is shown in Table 4-11. As for the Insight, the initial SOC is adjusted such that the battery net energy consumption of the model matches that of the experimental data. No SOC correction factor is applied. Looking at the CD results, the HWFET has very close results of 242 to 236 DC Wh per mile. The UDDS is reasonable with 213 to 189 DC Wh per mile, but the US06 is largely off with 327 to 213 DC Wh per mile. The US06 CD result used the most fuel

averaging 89 mpg which likely skewed results. The control strategy forces the engine to turn on when the motor cannot meet the total demand. As such, the model results are not purely CD but use only a very small amount of fuel.

Table 4-11: 2012 Chevrolet Volt D3 Energy Validation *(ANL, 2016b)*

Route	SOCi	Fuel Economy		Fuel Consumption		Battery Net Energy		Battery Net Energy Consumption	
	(%)	(mpg)		(gal)		(DC Wh)		(DC Wh/mi)	
		*ANL	Model	*ANL	Model	*ANL	Model	*ANL	Model
UDDS	60.00	N/A	155.5	0.00	0.048	1585.9	1411.1	212.9	189.4
HS**	29.50	45.7	45.1	0.16	0.170	-4.1	-12.4	-0.6	-1.7
HWFET	60.00	N/A	3476.1	0.00	0.003	2481.5	2424.9	241.9	236.4
	26.53	48.5	53.9	0.21	0.198	-9.7	-6.9	-0.9	-0.7
US06	60.00	N/A	89.4	0.00	0.092	2621.2	1707.8	327.4	213.3
	27.59	33.0	39.1	0.24	0.213	-45.8	-57.7	-5.7	7.2

*ANL data from the Downloadable Dynamometer Database (D3)
**UDDS Hot Start

The charge sustaining fuel economies are surprisingly close to the experimental data given the number of approximations used in this model. UDDS is the closest fit with 47.7 mph to 45.1 mpg. The next closest fit is the HWFET with 48.5 to 53.9 mph followed by US06 with 33.0 mph to 39.1 mpg. Both the CD and CS modes of operation for parallel PHEV strategy are reasonably validated.

4.9.2.3 EPA Data

EPA energy consumption data is readily available for all vehicles but is not always clear on exactly how the measurements were taken or what vehicle parameters were used. Nonetheless, as EPA data is available for all production vehicles, this data can be used to tune a control strategy. Table 4-12 displays the EPA validation results. The Insight had both the HWFET and Federal Test Procedure (FTP) which was modeled as a UDDS. The model was inefficient for the HWFET and efficient for the FTP, but both validation sets were reasonably accurate. The Volt had both US06 and HWFET and the model is overly efficient for each. Charge balancing the US06 proved difficult and even ending with excessive battery draw lead to an overly efficient fuel economy. In general, the model data closely matches the EPA data with only an 8% average error in fuel economy further validating the parallel PHEV model.

Table 4-12: EPA Parallel PHEV Validation *(EPA, 2016)*

Vehicle	Route	SOCi	*EPA	Model	ΔEbatint
		(%)	(mpg)	(mpg)	(kJ)
2010 Insight	HWFET	36.00	61.2	55.9	-1.9
	FTP	31.00	55.1	57.5	0.4
2012 Volt	US06	28.57	37.5	40.1	51.5
	HWFET	26.26	53.6	57.6	-2.9

*EPA data is from the Test Car List

5 Model Application

The powertrain model is developed as a tool to be utilized within an ecorouting process. As the application of this model is to be ecorouting, this section begins by demonstrating and explaining the influence of specific vehicle parameters on energy consumption results. The model does not predict the same results for different vehicles on the same route. Next, this section progresses to demonstrate and explain which route characteristics are most influential for energy consumption results. Lastly, this section concludes by stringing a variety of route characteristics into four routes: two town routes and two bypass routes.

For all applications, the vehicle simulated is the HEVT Camaro acting as a BEV, conventional vehicle, and parallel PHEV. All vehicle parameters remain the same for all powertrain types, including vehicle mass. Vehicle parameters are only modified when that parameter is the focus of the sensitivity study and that parameter is changed for all three powertrain types.

All simulations involving the PHEV Camaro are iterated with different initial SOC values until the SOC at the start and end of the simulation are as close as possible. This process of iterating initial SOC is called charge balancing. Aggressive routes are more difficult to charge balance and some routes are impossible to even partially charge balance. A SOC correction, as discussed in Section 3.5.2.1, is applied to the fuel consumption results to account for addition energy gained or lost by the battery.

Accessory load is a constant power draw and so the total energy consumption increases with time. Many routes tested for route characteristic sensitivity vary in total time. For simplicity, the accessory load is removed from all sensitivity studies so that only the parameter of interest is evaluated. The accessory load is present for the example route selection to emulate actual ecorouting.

Only energy consumption results are discussed in this section, however, GHG and PEU results may be referenced in Appendix E, F, and G. The GHG and PEU results are based from E85 as fuel and grid electric energy. These three appendices also provided further details and results for each simulation.

5.1 Vehicle Parameter Sensitivity Study

To analyze the influence of various vehicle parameters, specific vehicle parameters are isolated and then both increased and decreased from the base value. Both the US06 City and US06 Highway are simulated to capture if the sensitivity is influenced by driving conditions. Each drive cycle is repeated twice to facilitate PHEV charge balancing. All US06 Highway results are nearly charge balanced. The US06 City results are more difficult to charge balance and often relied on the SOC correction factor.

Six vehicle parameters are selected: vehicle mass, engine displacement, battery energy capacity, and three PHEV control strategy parameters. The mass is widely recognized for a large influence on energy consumption. For the engine, the only required input is the engine displacement and so the sensitivity to variations in engine displacement is investigated. Likewise, the battery model only requires energy capacity and open circuit voltage. For most electrified vehicles, the energy capacity varies more than open circuit voltage and so energy capacity is selected.

For the parallel PHEV, the control strategy inputs are influential for each vehicle tested but difficult to obtain. All three control strategy inputs are studied. These inputs are the mode time delay, the extra engine torque, and the engine minimum torque cutoff.

5.1.1 Vehicle Mass

The HEVT Camaro has a test mass with two passengers of 2120 kg. To test the energy consumption sensitivity to mass, the mass is decreased to 80% of the mass, or 1696 kg, and increased to 120% of the mass, or 2544 kg. Full details can be referenced in Appendix Table E-1. The US06 City is more sensitive than the US06 Highway and is summarized in Table 5-1. The US06 City is more sensitive to mass as the city has higher accelerations. Heavier vehicles have more inertia and therefore require more energy to accelerate than lighter vehicles. Mass also influences rolling resistance, though to a lesser extent than vehicle inertia. As expected, all powertrains required more energy consumption for an increase in mass.

Table 5-1: Mass Sensitivity Study Summary

Vehicle	Route	Mass	Grid Electric Consumption	Grid Electric Economy
		(kg)	AC Wh/mi	(mpgge)
BEV	US06 City (x2)	1696	526	64.1
		2120	619	54.4
		2544	725	46.5
Vehicle	**Route**	**Mass**	**SOC Corr. Fuel Energy**	**SOC Corr. Fuel Econ.**
		(kg)	**Wh/mi**	**(mpgge)**
Conv.	US06 City (x2)	1696	1966	17.1
		2120	2235	15.1
		2544	2455	13.7
PHEV	US06 City (x2)	1696	1394	24.2
		2120	1582	21.3
		2544	1774	19.0

The BEV is most sensitive to mass. While the BEV energy consumption increased 38% for the same 848 kg mass increase that the conventional increased 25% and the PHEV increased 27% in energy consumption. The HEVT Camaro has a large engine. The higher load associated with more mass led to higher engine efficiency to offset some of the extra energy necessary to accelerate with more mass. Smaller engines are likely to see a more substantial influence of mass on energy consumption.

5.1.2 Engine Displacement

The HEVT Camaro has a 5.3 L engine. Increasing this engine size 50% is an 8.0 L engine and reducing to 30% the base size is 1.6 L. The vehicle mass remains constant regardless of engine displacement. The performance such as 0-60 mph time will change with engine displacement but is not modeled. Appendix Table E-2 displays the details of the study while Table 5-2 displays a summary. Increasing the engine displacement increases energy consumption because engines operate less efficiently at low torques relative to the maximum output torque of that engine. For general driving, large engines will operate at relatively low torques while small engines will operate at relatively high torques for the same demand. The conventional vehicle is more sensitive to engine displacement than the PHEV because the PHEV is not solely propelled by the engine and has an engine load-leveling control strategy. The engine displacement has no influence on a BEV.

Table 5-2: Engine Displacement Summary

Vehicle	Route	Vdisp	SOC Corr. Fuel Energy	SOC Corr. Fuel Economy
		(L)	(Wh/mi)	(mpgge)
Conv.	US06 City (x2)	1.6	1931	17.4
		5.3	2235	15.1
		8.0	2383	14.1
PHEV	US06 City (x2)	1.6	1563	21.5
		5.3	1582	21.3
		8.0	1619	20.8

5.1.3 Battery Energy Capacity

Mild hybrids have very small batteries while PHEVs may have relatively large batteries. The HEVT PHEV Camaro has a battery of 12.6 kWh. To study the impact of battery energy capacity on vehicle energy consumption three battery sizes are selected: 3.8 kWh, 12.6 kWh, and 18.9 kWh. The values are 30%, 100%, and 150% of the base value respectively. Appendix Table E-3 displays full results and Table 5-3 provides a summary. The open-circuit voltage of 340 V remains constant and the vehicle mass also remains constant regardless of battery energy capacity. The conventional vehicle is unaffected by battery energy capacity and omitted.

Table 5-3: Battery Energy Capacity Study Summary

Vehicle	Route	Ecap	Grid Electric Consumption	Grid Electric Economy	Rint
		(kWh)	(Wh/mi)	(mpgge)	(Ω)
*BEV	US06 City (x2)	3.8	805	41.9	0.35
		12.6	619	54.4	0.10
		18.9	628	53.6	0.12
Vehicle	**Route**	**Ecap**	**SOC Corr. Fuel Energy**	**SOC Corr. Fuel Econ.**	**Rint**
		(kWh)	**(Wh/mi)**	**(mpgge)**	**(Ω)**
PHEV	US06 City (x2)	3.8	1808	18.6	0.35
		12.6	1587	21.2	0.10
		18.9	1595	21.1	0.12

Internal resistance is calculated as a function of open circuit voltage, energy capacity, and resistance coefficient as shown in Equation 3-49. In this thesis, Li-Ion batteries have only three categories and these categories roughly align with those of mild hybrids, PHEVs, and BEVs. The 3.8 kWh battery is similar to that of a mild hybrid. As the battery internal resistance coefficient is assigned as a category, reducing the battery size to 3.8 kWh changes the category to align similar to mild hybrids. Likewise, the 18.9 kWh battery is similar to that very large batteries found in BEVs and is assigned to the upper internal resistance coefficient category.

The base battery has an internal resistance of 0.10 Ω, the small battery has a resistance of 0.35 Ω, and the largest battery has a resistance of 0.12 Ω. The energy consumption results align with the trend in battery resistance. Typically, the greater the energy capacity of a battery, the less internal resistance and therefore less losses. The 3.8 kWh and 18.9 kWh batteries are exceptions in relation to the base 12.6 kWh battery in that each battery is a different battery class and is therefore assigned a different battery resistance coefficient. If known, the battery internal resistance may be overwritten instead of calculated.

5.1.4 Hybrid Strategy

The parallel PHEV control strategy inputs are selected by calibrating the vehicle such that the vehicle has the greatest potential to charge balance on standard drive cycles. Every vehicle has a different set of control strategy inputs.

5.1.4.1 Mode Time Delay

The time delay in the hybrid control strategy prevents the engine from stopping and starting excessively. A short time delay allows for the control strategy to quickly adjust to the current demand. A long time delay reduces engine start fuel penalties. For the HEVT Camaro, a time delay of eight seconds is the standard. To test the energy consumption sensitivity to time delay, both six and ten seconds are also tested. Neither the US06 City nor US06 Highway produces a large impact on fuel economy. Nonetheless, the mode selection is largely dependent upon time delay. Full results can be referenced in Appendix Table E-4 and Table 5-4.

Table 5-4: PHEV Mode Time Delay Study Summary

Route	tdelay	SOC Corr. Fuel Energy	SOC Corr. Fuel Econ.	CD Mode Time	Eng. Load Mode Time	Eng. Eff. Mode Time
	(s)	(Wh/mi)	(mpgge)	(s)	(s)	(s)
US06 City (x2)	6	1542	21.8	311	69	82
	8	1582	21.3	288	70	104
	10	1658	20.3	260	70	132

The amount of time spent in the Engine Loading Mode remains mostly constant regardless of time delay. The longer the time delay, the less time is spent in CD mode and more time is spent in Engine Efficiency Mode. This result is route specific. The US06 City is very aggressive and commonly requires both the motor and the engine to work together in Engine Efficiency Mode to meet the drive cycle demand. Due to a long time delay, the vehicle must remain in this mode even as the demand decreases. As the vehicle attains similar energy consumption results regardless of time spent in each mode, the simple control strategy is considered sufficient at operating in an efficient manner.

5.1.4.2 Extra Engine Torque

The HEVT Camaro uses a base engine extra torque of 40 Nm during Engine Loading Mode. Testing both 20 Nm and 60 Nm, the total energy consumption of the vehicle is insensitive to the engine extra torque. For each the US06 City and the US06 Highway, the vehicle spent the same amount of time in each mode regardless of extra engine torque value. The HEVT Camaro has a large engine and so values around 40 Nm are likely insignificant compared to the 500 Nm maximum torque of the engine. The full study may be referenced in Appendix Table E-5 and Table 5-5 provides a summary.

Table 5-5: PHEV Engine Extra Torque Study Summary

Route	Teng,extra	SOC Corr. Fuel Energy	SOC Corr. Fuel Econ.
	(Nm)	(Wh/mi)	(mpgge)
US06 City (x2)	20	1588	21.2
	40	1582	21.3
	60	1579	21.3

5.1.4.3 Engine Torque Minimum Cut-off

Engines operate inefficiently at relatively low torques. Hybrid vehicles have the ability to load an engine to higher torques for higher operating efficiency and send the extra torque to the generator to charge the battery. With this simplified control strategy, the engine will operate just below the PE limit if the torque demand is below a specified minimum cutoff torque. The baseline for this torque is 40% maximum engine torque or around 202 Nm. 20% and 60% maximum engine torque are also tested at 101 Nm and 304 Nm, respectively. The full study may be referenced in Appendix Table E-6 and Table 5-6 provides a summary for the US06 City.

Table 5-6: PHEV Engine Minimum Cutoff Torque Study Summary

Route	Teng,min	SOC Corr. Fuel Cons.	SOC Corr. Fuel Econ.	CD Mode Time	Eng. Load Mode Time	Eng. Eff. Mode Time
	(Nm)	(Wh/mi)	(mpgge)	(s)	(s)	(s)
US06 City (x2)	101	1541	21.8	290	82	90
	202	1582	21.3	288	70	104
	304	1549	21.7	314	44	104

Similar to the time delay study, the energy consumption results are largely insensitive to the minimum engine torque cutoff. The time spent in each mode, however, is dependent. The vehicle only enters Engine Efficiency Mode when the torque demand drops below the engine cutoff or if neither the motor nor the engine can meet the torque demand independently. For the torque of 101 Nm, the cutoff reduced time spent in Engine Efficiency Mode. Conversely, for the torque of 304 Nm, the time in Engine Efficiency Mode is the same as that spent for the base torque of 202 Nm as the US06 City is an aggressive drive cycle and both the motor and engine must act together to supply the demand.

5.1.5 Powertrain Sensitivity Conclusions

A few key results are useful for ecorouting purposes. From the mass study, heavier vehicles are more sensitive to acceleration than lighter vehicles, confirming that ecorouting must make vehicle-specific decisions. Similarly, the smaller an engine, the more sensitive the engine will be to engine loads. As the torque threshold is smaller for a smaller engine, small variations in torque demand require a larger change in engine efficiency than would occur in a larger engine. The model is capable of capturing how each vehicle is influenced by different factors.

The battery energy capacity study highlights the model limitation of categorizing internal resistance coefficients. If a battery falls on the edge of two categories, the energy capacity results will vary depending on which category is selected. This study created three batteries, each that fell into a different internal resistance coefficient category. Fortunately most vehicle batteries falls distinctly into each battery category, but if the internal resistance of a battery is known, the resistance calculation should be overwritten for increased accuracy.

The parallel PHEV control strategy inputs of mode time delay, engine extra torque, and engine minimum torque cutoff each made little impact on vehicle energy consumption. These values are difficult to obtain as vehicle control strategies are often proprietary and far more complex than this model. In this research, the values have been tuned to better charge balance major drive cycles. Since the inputs have a small influence on energy consumption, any values that permit charge sustaining are considered sufficient.

5.2 Route Sensitivity Study

The objective of this research is to develop a methodology for predicting vehicle energy consumption which may be used as a tool for ecorouting. To be useful for ecorouting, the model must be capable of distinguishing energy consumption between route options. For ecorouting, the exact values of energy consumption are less important than the relative values between routes. This section investigates the impact of six route characteristics on energy consumption. The characteristics include the cruise velocity, distance between stops, acceleration rate, deceleration rate, grade, and driver aggressiveness. Appendix F Table 1 provides a summary of each route. The rest of Appendix F shows plots detailing each route.

5.2.1 Cruise Velocity

Cruise velocity is often imposed by speed limits. Highways have higher cruise velocities than local roads. To analyze the impact of cruise velocity, three speeds are selected: 30 mph, 50 mph, and 70 mph. All routes are evaluated for 100 seconds of pure constant velocity with no acceleration. In order for the model to attain eighth gear, each route began at stop and then accelerated to the respective cruise velocity. All data reported for the velocity study neglects the time spent accelerating. The energy consumption results only reflect energy consumed during cruise. Full details of each route can be found in Appendix Table F-2 and Table F-3 and the routes are demonstrated in Appendix Figure F-1. All other data such as travel distance and travel time also only include cruising. The higher velocity routes traveled more distance in the 100 seconds and so energy results are compared on a unit distance basis. Table 5-7 summarizes the study.

Table 5-7: Velocity Sensitivity Study Summary

Vehicle	Route	Cruise Velocity (mph)	Grid Electric Consumption (AC Wh/mi)	Grid Electric Economy (mpgge)
BEV	A	30	228	147.4
	B	50	312	107.8
	C	70	437	77.1
Vehicle	**Route**	**Cruise Velocity (mph)**	**SOC Corr. Fuel Cons. (Wh/mi)**	**SOC Corr. Fuel Econ. (mpgge)**
Conv.	A	30	1249	27.0
	B	50	1265	26.6
	C	70	1497	22.5
PHEV	A	30	614	54.8
	B	50	792	42.5
	C	70	1278	26.4

As expected, the higher the cruise velocity, the higher the fuel consumption for each powertrain type. Also, an increase in 20 mph from 30 mph made less of an impact on energy consumption than an increase in 20 mph from 50 mph. At higher speeds, road load is greater. Aerodynamic drag is proportional to the square of speed causing drag to increase quadratically with vehicle speed.

The velocity made the least impact on the conventional vehicle. As the HEVT Camaro has a large engine, the engine became significantly more efficient with each higher load. The drive cycle average engine net efficiency is 27% for the 30 mph case and 33% for the 70 mph case. A vehicle with a smaller engine would be expected to experience different trends. Despite an increased

component efficiency, a higher load requires more energy and typically greater losses. The engine lost 4509 kJ at 30 mph and 9775 kJ at 70 mph.

The motor efficiency is also sensitive to the cruise velocity. For the BEV, the drive cycle average motor efficiency is 73% at 30 mph and 85% at 70 mph. While an engine accounts for more than half of 60% of energy losses, a motor only accounts for around 25% of losses. Hence, an increase in motor efficiency does not decrease total energy consumption the same as an increase in engine efficiency.

5.2.2 Distance Between Stops

The distance between stops varies by road type. In a city, a vehicle may stop every few blocks. On a more suburban road, a vehicle may stop every mile or two. Similarly on a highway, a vehicle may go for many miles without stopping. Launching a vehicle into motion can be energy intensive and should typically be avoided in energy efficient driving. To test the energy consumption sensitivity to the distance between stops, three distances are selected: 0.5 miles, 1.5 miles, and 3 miles. For each route, the vehicle accelerates at a constant 1.5 m/s2 to cruise velocity and then decelerates at a constant 1.5 m/s2 to complete the route by the specified stop distance. All three cases are evaluated at 30 mph, 50 mph, and 70 mph for comparison. Table 5-8 shows a summary for the 50 mph case, but the details of all routes may be referenced in Appendix Table F-4 and Table F-5 and the routes are demonstrated in Appendix Figure F-2.

Table 5-8: Distance Sensitivity Study Summary at 50 mph

Vehicle	Route	Distance	Total Time	Average Speed	Grid Electric Consumption	Grid Electric Economy
		(mi)	(s)	(mph)	(AC Wh/mi)	(mpgge)
BEV	E	0.5	52	35.6	523	64.3
	H	1.5	123	43.9	384	87.6
	K	3	231	46.8	348	96.7
Vehicle	**Route**	**Distance**	**Total Time**	**Average Speed**	**SOC Corr. Fuel Cons.**	**SOC Corr. Fuel Econ.**
		(mi)	**(s)**	**(mph)**	**(Wh/mi)**	**(mpgge)**
Conv.	E	0.5	52	35.6	1959	17.2
	H	1.5	123	43.9	1502	22.4
	K	3	231	46.8	1378	24.4
PHEV	E	0.5	52	35.6	1255	26.8
	H	1.5	123	43.9	944	35.7
	K	3	231	46.8	866	38.9

For all powertrains, the shorter the distance the greater the energy consumption per distance, as expected. Both the motor and the engine are inefficient at low speeds and high torque as is common launching a vehicle. To average out the inefficient vehicle launch, the vehicle needs to drive a longer distance. The longer the distance, the greater percentage of the trip is spent at the max speed rather accelerating to the max speed; thus, the longer the distance the higher the average speed. While the amount of energy in each stop is significant, the longer distance cases require additional energy to combat aerodynamic drag longer than short distance cases reducing some of the difference in fuel economy.

The conventional vehicle is least sensitive to the distance between stops likely because the engine runs inefficiently at all times, in the range of 10-35% efficient during Route G. A motor has

the ability to run highly efficiently. The BEV motor efficiency ranges from 32-88% efficient during Route G. As the motor has a larger spread in efficiency, poor loading makes a larger impact on the motor.

The PHEV experienced less sensitivity to the velocity than the BEV. The PHEV has a control strategy that can allow three modes of operation for improved efficiency. The BEV consists only of one mode of operation: CD mode. With more modes of operation, there are more options for adjusting to changes in the route which makes the vehicle less sensitive to such changes in a route.

5.2.3 Acceleration Rate

Unlike cruise speed which is regulated by speed limit, acceleration rate is typically dependent upon the driver. Acceleration rate in congested areas may also be limited by traffic. Within ecorouting, driver decisions such as acceleration rate are not always considered. Instead, the average driving conditions experienced by vehicles that previously completed the route segment constitute the acceleration rates to be assumed in this model. This study starts with the vehicle at rest. There are two time categories of simulation: 10 s and 14 s. For each time category, three constant acceleration rates are assigned: 1.0 m/s2, 1.5 m/s2, and 2.5 m/s2. Those cases with a higher acceleration rate travel a greater distance in the same fixed time and so energy consumption is reported on a unit distance basis. Full results are found in Appendix Table F-6 and F-7 and the routes are demonstrated in Appendix Figure F-3.Table 5-9 provides a summary of the 10 s simulation.

Table 5-9: Acceleration Sensitivity Study Summary

Vehicle	Route	Accel. Rate (m/s2)	Grid Electric Consumption (AC Wh/mi)	Grid Electric Economy (mpgge)
BEV	V	1.0	1490	22.6
	W	1.5	2213	15.2
	X	2.5	4153	8.1
Vehicle	**Route**	**Accel. Rate (m/s2)**	**SOC Corr. Fuel Cons. (Wh/mi)**	**SOC Corr. Fuel Econ. (mpgge)**
Conv.	V	1.0	4483	7.5
	W	1.5	5572	6.0
	X	2.5	8154	4.1
PHEV	V	1.0	3888	8.7
	W	1.5	5776	5.8
	X	2.5	8926	3.8

As expected, a higher acceleration rate requires more energy consumption for all cases. In the 14 s simulation, the vehicle attains a higher speed for the same acceleration rate. In general, as a vehicle accelerates at the same rate but a higher speed, the energy consumption increases further due to increased road load. In this study, the results are inconsistent in that on some occasions accelerating at the same rate at a higher speed conveniently loaded the powertrain to more efficient operation.

As part of the control strategy, the PHEV always starts in CD mode and then holds for at least eight seconds due to the mode time delay. In very aggressive driving, such as high accelerations, operating with both the motor and the engine is ideal. The results in Table 5-9 represent a 14

second acceleration. For all three acceleration rates, the PHEV spent 8 seconds in CD mode and 6 seconds in Engine Efficiency Mode. The PHEV has lower fuel economy than the conventional vehicle for the two higher acceleration rates. As the acceleration routes are all very short, charge balancing is very difficult. As a result, a large change in SOC relied heavily upon the SOC correction factor that is very much an approximation. Also, the hybrid transmission is not as efficient as that of a conventional vehicle because the transmission assume the engine meets demand to prepare a gear for when the vehicle leaves CD mode. Upon leaving CD mode, the engine exceeds the demand as part of the hybrid strategy.

5.2.4 Deceleration Rate

Similar to the acceleration study, the deceleration study isolated a defined time period of constant deceleration. The starting velocity is defined by the time decelerating and the deceleration rate. The vehicle accelerated at a constant 1.5 m/s2 to a cruise velocity from which the vehicle will decelerate. All results only consider the deceleration portion of the test. Appendix Table F-6 and F-7 provides details and the routes are demonstrated in Appendix Figure F-4. Table 5-10 provides a summary for the 14 second deceleration case.

Table 5-10: Deceleration Sensitivity Study Summary

Vehicle	Route	Decel. Rate	Total Grid Consumption	Grid Electric Consumption	Total Fuel Consumption	Fuel Economy
		(m/s2)	(kJ)	(AC Wh/mi)	(kJ)	(Wh/mi)
BEV	AH	-1.0	-71	-334	0	N/A
	AI	-1.5	-176	-549	0	
	AJ	-2.5	-462	-864	0	
Conv.	AH	-1.0	0	N/A	149	697
	AI	-1.5	0		149	465
	AJ	-2.5	0		149	279
PHEV	AH	-1.0	-71	-334	0	N/A
	AI	-1.5	-176	-549	0	
	AJ	-2.5	-462	-864	0	

Negative grid electric consumption is not physically possible. Energy cannot be placed back into the grid from a vehicle. For consistency with other data the energy captured from regenerative braking is displayed as though this energy could be returned to the grid.

The results show that both the BEV and the PHEV have the same results. In the case of a pure deceleration, tractive energy is negative as regenerative braking sends some brake energy into the powertrain to charge the battery. Due to regenerative braking limitations, not all brake energy is captured. Both the BEV and PHEV have the same regenerative braking limitations. As described at the beginning of Section 5, accessory loads have been removed for the sensitivity studies. During ordinary deceleration, the battery would be powering vehicle accessory loads detracting further from what energy is captured in regenerative braking.

Over the same amount of time, more total energy is captured for the higher deceleration rates. This trend may be misleading. The higher deceleration cases started braking at a higher velocity and continued braking for a longer distance. The energy capture on a unit distance basis also increases with deceleration rate demonstrating the braking at higher speeds allows for more regenerative braking capture.

The conventional vehicle is incapable of regenerative braking and loses energy during braking due to a set deceleration fuel rate. As the fuel rate is dependent upon time and all three deceleration rates last for the same amount of time, all three cases require the same amount of engine fuel energy. While the total amount of energy required to decelerate is the same, the energy per unit distance decreases for higher deceleration rates as these rates occurred over a greater distance.

5.2.5 Grade

As discussed in Section 1.2.3, *(Zhang et al., 2010)* demonstrated that PHEVs, in particular, could reduce fuel consumption by strategically anticipating hills. This PHEV control strategy is not sufficiently intelligent to input upcoming route data and save or expel battery energy accordingly. Such an addition should be considered for future work. Regardless, hills can either impede or assist the vehicle powertrain and ecorouting can intelligently select routes that will reduce energy consumption. For electrified vehicles, regenerative braking is able to capture energy when the vehicle descends if negative tractive energy is required at the wheels. Other times, the downhill force is not sufficient to meet route demand the vehicle must propel down a hill.

To test the sensitivity of energy consumption to grade, three grades are selected: 0%, 2%, and 4%. This test is completed for three cruise speeds: 30 mph, 50 mph, and 70 mph. In all simulations, the vehicle accelerated at 1.5 m/s2 to a cruise speed. While cruising, the vehicle ascended a hill, or no hill in the 0% grade case. The hill ascended 0.35 miles and then descended 0.35 miles. Table 5-11 summarizes the 50 mph case. The full results may be referenced in Appendix Table F-10 and F-11 and the routes are demonstrated in Appendix Figure F-5.

Table 5-11: Grade Sensitivity Study Summary at 50 mph

Vehicle	Route	Grade	PTR Up	PTR Down	PTR Regen	Grid Electric Consumption	Grid Electric Economy
		(%)	(kW)	(kW)	(kW)	(AC Wh/mi)	(mpgge)
BEV	H	0	9.15	9.15	0.00	384	88
	N	2	18.44	-0.15	-0.09	386	87
	Q	4	27.73	-9.43	-5.66	413	82
Vehicle	**Route**	**Grade**	**PTR Up**	**PTR Down**	**PTR Regen**	**SOC Corr. Fuel Cons.**	**SOC Corr. Fuel Econ.**
		(%)	**(kW)**	**(kW)**	**(kW)**	**(Wh/mi)**	**(mpgge)**
Conv.	H	0	9.15	9.15	0.00	1502	22.4
	N	2	18.44	-0.15	0.00	1354	24.9
	Q	4	27.73	-9.43	0.00	1452	23.2
PHEV	H	0	9.15	9.15	0.00	945	35.6
	N	2	18.44	-0.15	-0.09	951	35.4
	Q	4	27.73	-9.43	-5.66	1013	33.2

As expected, an increase in grade generally required an increase in energy consumption largely due to the loss of energy to friction braking down the hill. The BEV and the PHEV are relatively insensitive to the grade as much of the energy is collected on the downhill via regenerative braking. As regenerative braking does not capture all brake energy, each increase in grade did require a small increase in energy.

While descending the 2% grade at a constant velocity of 50 mph, the HEVT Camaro required almost no tractive energy at the wheels. The downhill provided the energy necessary to meet the route demand with almost no loss to friction. The conventional vehicle exemplified this unusual

case: the 2% grade is more fuel efficient than the flat road. The engine operated at a more efficient load up the hill and then the vehicle lost almost no energy down the hill. Situations such as this demonstrate how a vehicle control strategy could take advantage of rolling hills to improve fuel economy.

5.2.6 Driver Aggressiveness

In many driving scenarios, a driver is constrained by both time and distance but is otherwise free to select an acceleration rate and cruise speed. An example of this scenario is when a driver is trying to keep up with traffic. Upon taking off from a stoplight the driver may feel social pressure to reach the next light in about the same time as the rest of the vehicles. Some drivers purposefully accelerate hard and then lightly cruise. Other drivers purposefully accelerate slowly but must attain a higher cruise speed to reach the next light *at the same time*.

From a routing perspective, the choice is between a route with high acceleration but low cruise speed and then a route with low acceleration but high cruise speed. The two options present a tradeoff. High acceleration is energy intensive due to overcoming inertia while high cruise speed is energy intensive due to road load.

To test this form of driver aggressiveness, a constant distance of 1.5 miles is assigned. Two total times are assigned: 130 seconds and 105 seconds. For each case, three accelerations are set. With a set average velocity and acceleration rate, the cruise speed can be calculated. The faster the acceleration, the slower the cruise speed within each case. The 130 second case is summarized in Table 5-12. Appendix Table F-12 and F13 display the full results and the routes are demonstrated in Appendix Figure F-6.

Table 5-12: Driver Aggressiveness Sensitivity Study Summary for 130 s vavg=41.5 mph

Vehicle	Route	Accel. Rate (m/s2)	Grid Electric Consumption (AC Wh/mi)	Grid Electric Economy (mpgge)
BEV	Y	1.0	369	91
	Z	1.5	359	94
	AA	2.5	362	93
Vehicle	**Route**	**Accel. Rate (m/s2)**	**SOC Corr. Fuel Cons. (Wh/mi)**	**SOC Corr. Fuel Econ. (mpgge)**
Conv.	Y	1.0	1474	22.8
	Z	1.5	1442	23.3
	AA	2.5	1416	23.8
PHEV	Y	1.0	912	36.9
	Z	1.5	891	37.8
	AA	2.5	904	37.3

Energy consumption is relatively insensitive to the tradeoff. This tradeoff demonstrates that slower acceleration is not always more energy efficient if the route then requires a faster cruise velocity. The same is true in that a slower cruise speed is not always more energy efficient if the route then requires a higher acceleration. Energy consumption does not offer rules that can be set for all route decisions. Instead, each route must be carefully analyzed for each powertrain.

The middle acceleration of 1.5 m/s2 consistently requires the least energy consumption for the BEV and PHEV by a small margin really demonstrating the tradeoff in acceleration and cruise

speed. The conventional vehicle is most efficient with the 2.5 m/s2 case, also by a small margin, demonstrating that there is no set of rules that dictate which route is the most energy efficient for every vehicle.

5.2.7 Route Sensitivity Conclusions

For ecorouting purposes, a few key results are useful. Higher velocities produce greater road load. Specifically, aerodynamic drag increases quadratically with vehicle speed. Accelerating at a faster rate requires more energy consumption, particularly at high speeds. Further, vehicle launch often requires a lot of energy as components tend to operate inefficiently at low speeds. Vehicle stops should be avoided when possible.

Hills typically increase energy consumption as energy is often lost to friction on the downhill; however, there are cases when rolling hills may prove beneficial and may be strategically approached for increased fuel economy. As hills require a case-by-case study, all routes should be analyzed case by case. The driver aggressiveness demonstrated that the trends identified in the other studies are typically true but not under all circumstances. Slower acceleration is not always more efficient if the tradeoff if a higher cruise velocity. The same is true for the reverse. Just as routes cannot be selected based on trends associated with the route characteristics, the route results for one vehicle are not to be applied to others as every vehicle will experience different results.

5.3 Example Route Selection

In culmination of demonstrating the utility of the model in ecorouting, full routes are compared. The routes are created in two iterations and all routes are designed to emulate common driving scenarios. Within each iteration, both the town and bypass routes take the same amount of time and both have the same start and end points. Appendix G plots various features of each route for reference.

5.3.1 First Iteration

Plots demonstrating the velocity and elevation of each route versus distance are shown in Figure 5-1 and Figure 5-2. In the first iteration, the town route is 6 miles in length and simulates driving in town. The vehicle begins by casually accelerating from rest at 1.0 m/s2 to 30 mph. There is a stop sign 1.5 miles into the route and the vehicle decelerates at 1.0 m/s2 reaching an idle of 5 seconds at the stop sign. The vehicle then accelerates once more to 45 mph at 1.0 m/s2. While cruising at 45 mph, 3 miles into the route, the vehicle ascends a 0.75 mile hill of 2% grade and then descends at the same grade for the same distance. The vehicle stops at 6 miles after decelerating at 1.0 m/s2.

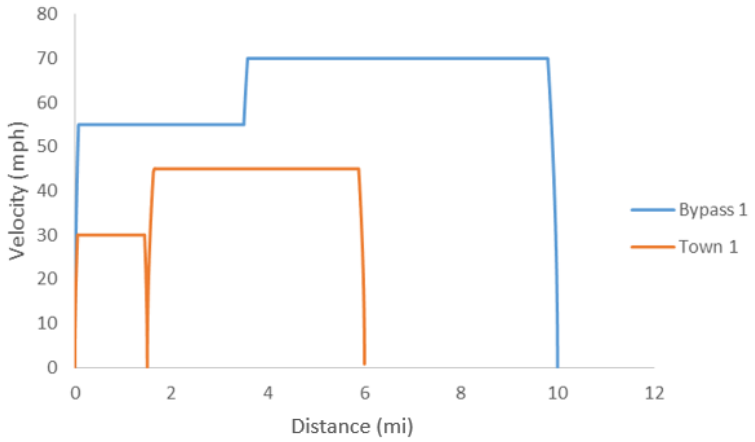

Figure 5-1: Example Route Selection First Iteration Velocity vs Distance

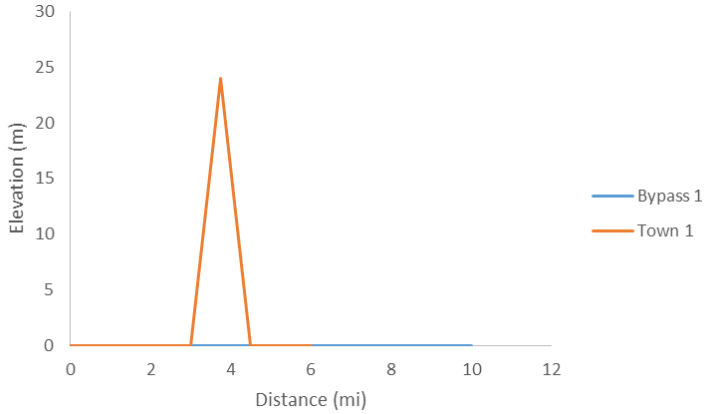

Figure 5-2: Example Route Selection First Iteration Elevation vs Distance

The first bypass route is 10 miles in length and simulates driving on a highway to avoid town. The vehicle accelerates rapidly at 2.5 m/s2 to a cruise speed of 55 mph. At 3.5 miles, the speed limit increases to 70 mph and the vehicle accelerates at 1.5 m/s2. The vehicle comes to a stop at 10 miles by decelerating at 1.5 m/s2.

In the first iteration, the bypass required more energy than the town route for all vehicles. Table 5-12 provides a summary of results for the first iteration. On average, the bypass requires 93% more energy for all vehicles. As the town route is 6 miles and the bypass is 10 miles, the distances are not the same but the fuel economy provides insight into which route is on average more efficient. Not only is the bypass a longer route, but the bypass is more energy intensive per mile for all vehicles. As the GHG emissions are directly proportional with the energy consumption, the bypass also produces more emissions. As the time duration for both routes are equivalent, the town route is expected to be selected by an ecorouting process.

Table 5-13: Example Route Selection First Iteration Summary

Route	Vehicle	Total Distance (mi)	Total Time (s)	Total Grid Consumption (kJ)	Grid Electric Consumption (AC Wh/mi)	Grid Electric Economy (mpgge)	GHG (g GHG)
Town 1	BEV	6	579	6466	299	112.5	878
ByPass 1	BEV	10	579	15436	429	78.5	2097
Route	**Vehicle**	**Total Distance (mi)**	**Total Time (s)**	**SOC Corr. Fuel Energy (kJ)**	**SOC Corr. Fuel Energy (Wh/mi)**	**SOC Corr. Fuel Econ. (mpgge)**	**GHG (g GHG)**
Town 1	Conv.	6	579	27286	1263	26.7	1849
ByPass 1	Conv.	10	579	54535	1515	22.2	3696
Town 1	Hybrid	6	579	17176	795	42.3	1340
ByPass 1	Hybrid	10	579	39517	1098	30.7	3073

5.3.2 Second Iteration

As the energy consumption results largely favored the town route, the routes are modified in a second iteration such that the town should require more energy and the bypass should require less. The second iteration routes are demonstrated in Figure 5-3 and Figure 5-4. In the second iteration, the town route is 7 miles in length. The vehicle begins by casually accelerating from rest at 1.0 m/s2 to 30 mph. There is a stop sign at 2 miles and the vehicle decelerates at 1.0 m/s2 reaching an idle of 5 seconds at the stop sign. The vehicle then accelerates at 1.0 m/s2 to a cruise speed of 45 mph before decelerating at 1.0 m/s2 to rest at another stop sign at 4 miles. The vehicle once again accelerates at 1.0 m/s2 to a cruise speed of 45 mph. While at a constant speed of 45 mph, the vehicle ascends a hill of 4% grade at 4.5 miles. At 5.75 miles, the vehicle crests the hill and then descends for another 0.75 miles at a 4% grade. The vehicle comes to a stop at 7 miles by decelerating at 1.0 m/s2.

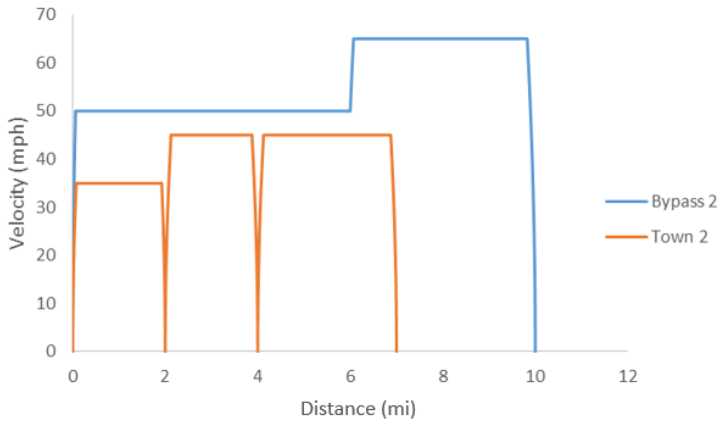

Figure 5-3: Example Route Selection Second Iteration Velocity vs Distance

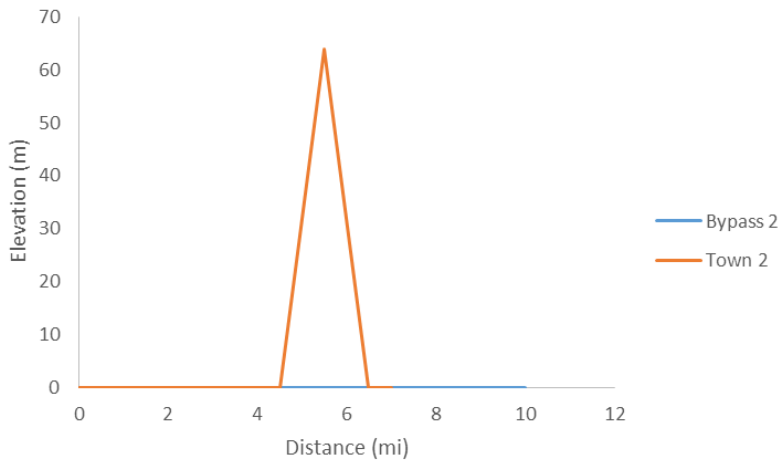

Figure 5-4: Example Route Selection Second Iteration Elevation vs Distance

The second bypass route is also 10 miles in length. The vehicle begins by accelerating from rest at 2.5 m/s2 to 50 mph. At 6 miles, the speed limit increases to 65 mph and the vehicle accelerates at 1.5 m/s2. The vehicle comes to a stop at 10 miles by decelerating at 1.5 m/s2.

As found for the first iteration, the town route required less energy consumption than the bypass. The increase in fuel consumption between the town route and bypass is less drastic: an average of 63% more energy consumption for the bypass. In terms of energy consumption magnitudes, the town route increased on average 24% while the bypass decreased an average of 10%. Adding another stop and a steeper hill to the town route succeeded in increasing energy consumption. Likewise reducing the speed on the bypass succeeding in decreasing energy consumption. As the GHG emissions are directly proportional with the energy consumption, the bypass produces more emissions. As the time duration for both routes are equivalent, the town route is expected to be selected by an ecorouting process in both iterations.

Table 5-14: Example Route Selection Second Iteration Summary

Route	Vehicle	Total Distance (mi)	Total Time (s)	Total Grid Consumption (kJ)	Grid Electric Consumption (AC Wh/mi)	Grid Electric Economy (mpgge)	GHG (g GHG)
Town 2	BEV	7	669	8277	328	102.5	1124
ByPass 2	BEV	10	668	13390	372	90.5	1819
Route	**Vehicle**	**Total Distance (mi)**	**Total Time (s)**	**SOC Corr. Fuel Energy (kJ)**	**SOC Corr. Fuel Energy (Wh/mi)**	**SOC Corr. Fuel Econ. (mpgge)**	**GHG (g GHG)**
Town 2	Conv.	7	669	33675	1336	25.2	2282
ByPass 2	Conv.	10	668	50925	1415	23.8	3452
Town 2	Hybrid	7	669	20628	819	41.1	1600
ByPass 2	Hybrid	10	668	36559	1016	33.2	2865

6 Future Work

While this research has achieved all objectives, future work for this project includes full implementation of this model on-board the HEVT Camaro, an ability to send and receive live map data, and powertrain model refinements. In future years of the EcoCAR 3 competition, students from HEVT will be implementing this model to run on-board the HEVT Camaro to demonstrate ecorouting capabilities. As such, this model will receive live updates from the vehicle controllers such as current SOC, vehicle speed, etc. Likewise, the model will send upcoming route updates to the vehicle controllers to influence the controller decisions and decrease energy consumption.

There are many areas of future research to further refine this powertrain model. Two of the main improvements are refining the hybrid control strategy and tuning the model to better match the HEVT Camaro. The hybrid control strategy is simplified to apply to all PHEVs. Multiple strategies could be implemented and further refined. Specifically, the PHEV Camaro model could be refined as this method is to operate onboard the PHEV Camaro. Not only should the control strategy be refined, but all component models could be tuned to better approximate the HEVT vehicle as experimental test data becomes available.

This model consists of a static engine fuel map at warmed up conditions. This model assumes that since all route options would either require an engine cold start or all would require hot start, the relative difference in energy consumption would remain the same between routes. However, an investigation into how to capture the effects of engine cold-start versus hot-start would further increase the validity of the energy consumption values. As engine cold versus hot start has a large impact on vehicle emissions, an improved model would also allow for criteria emission simulation. In general, further research could be conducted to better capture vehicle emission behavior such that ecorouting decisions may also be weighted by criteria emissions.

Regarding the engine, a diesel engine model would expand model application. Also, many modern engines have idle and deceleration fuel cut-off that reduce fuel consumption. Similarly, AFM modeling would be beneficial to new engines such as that of the HEVT Camaro. As HEVT gathers more experimental data from their AFM-capable engine, this model should be expanded to reflect AFM experimental results.

The proposed transmission strategy is very basic. The model shifts more frequently than regular transmissions. Further research should be conducted to capture shift delay and other rules that may be implemented into modern automatic transmissions. Many HEVs have a CVT. A lot of research already exists on this topic and could be incorporated into this model. Research should also be conducted to better understand and approximate the effect of a torque converter on engine and transmission behavior. Considering other model additions, a series-parallel HEV powertrain would provide another vehicle types.

The inclusion of Heating, Ventilation, and Air Conditioning (HVAC) into the accessory load would increase the validity of the energy consumption results. Currently the model does not include a temperature input nor any data regarding the HVAC demands inside the vehicle. Aside from cabin heating and cooling, a simulation of component thermal effects could increase model accuracy.

7 Conclusions

This research has achieved all objectives presented at the start of this thesis. The key objective is to develop and present a methodology for approximating the energy consumption of a specific vehicle such that a comparison in energy consumption between potential routes may be made. Additional objectives achieved include obtaining relatively accurate results with only publically available component parameters, approximating energy consumption for BEVs, PHEVs and conventional vehicles, validating powertrain models, demonstrating ecorouting application, and creating a user-friendly model as a tool for future HEVT team members.

For both validation and demonstration purposes, this methodology has been implemented into an excel spreadsheet. This methodology is developed as a tool for ecorouting application. The model receives distance-based route inputs to emulate receiving route information at discrete location on the roadway grid. Many other powertrain models receive inputs on a time-incremented basis.

As ecorouting would ideally be applied to all vehicles on a network, the primary objective of this research is to create a powertrain model capable of predicting the energy consumption of a variety of powertrain configurations using only minimal publically-available component specifications. The model is backwards-facing as the route is input to the model. The tractive energy required at the wheels to attain that route is computed in a vehicle glider model. Upon finding the tractive energy required at the wheels, the model backtracks through each powertrain component to find the total energy consumption from fuel or grid electricity. A key attribute to this thesis is the ability to compose different powertrain components to form different powertrain configurations. Each component model utilizes known data from a specific version of that component and scales that data to capture the behavior of different sized components. Component models rely on closed form equations instead of vehicle-specific lookup tables.

Although the methodology presented is highly simplified, experimental data has validated the glider, engine, transmission, battery, motor, accessory loads, and regenerative brake models. The total energy consumption for a BEV, conventional vehicle, and parallel PHEV have also been validated with experimental data. As is true in all modeling applications, many potential powertrain model improvements have been suggested as future work.

This model has also demonstrated an ability to differentiate energy consumption results based upon powertrain characteristics. Given a selection of a routes, a route that is most fuel efficient for one vehicle cannot be assumed to be the most fuel efficient for another. Similarly, this model has demonstrated an ability to differentiate the energy consumption between routes. For ecorouting, the relative energy consumption values between routes are necessary.

References

Ahn, K., & Rakha, H. (2008). The effects of route choice decisions on vehicle energy consumption and emissions. *Transportation Research Part D: Transport and Environment*, *13*(3), 151–167. http://doi.org/10.1016/j.trd.2008.01.005

Ahn, K., & Rakha, H. A. (2013). Network-wide impacts of eco-routing strategies: A large-scale case study. *Transportation Research Part D: Transport and Environment*, *25*, 119–130. http://doi.org/10.1016/j.trd.2013.09.006

Argonne National Laboratory. (2015). EcoCAR 3 Year 1 Rules, (Rev. E).

Argonne National Laboratory. (2016a). About Ecocar 3: An Advanced Vehicle Technology Competition. Retrieved March 19, 2016, from http://ecocar3.org/about/

Argonne National Laboratory. (2016b). Downloadable Dynamometer Database (D3). Retrieved April 5, 2016, from http://www.anl.gov/energy-systems/group/downloadable-dynamometer-database

Argonne National Laboratory. (2016c). EcoCAR 3 Non-Year Specific Rules, (Rev. G).

Bureau of Tranportation Statistics (BTS). (2014). Pocket Guide to Transportation. *RITA Bureau of Transportation Statistics*, 62. Retrieved from http://www.rita.dot.gov/bts/sites/rita.dot.gov.bts/files/pocket_guide_2013_1.pdf

Burress, T. (2013). *Benchmarking State-of-the-Art Technologies*. Retrieved from http://energy.gov/sites/prod/files/2014/03/f13/ape006_burress_2013_o.pdf

Code of Federal Regulations Title 40 86.129-94. (2000). In *Legal Information Institute*. Retrieved from https://www.law.cornell.edu/cfr/text/40/86.129-94

Code of Federal Regulations Title 40 86.529-98. (1998). In *Legal Information Institute*. Retrieved from https://www.law.cornell.edu/cfr/text/40/86.529-98

Duoba, M., Bocci, D., Bohn, T., Carlson, R., Jehlik, F., & Lohse-Busch, H. (2009). *Argonne Facilitation of PHEV Standard Testing Procedure (SAE J1711)*. Retrieved from https://www1.eere.energy.gov/vehiclesandfuels/pdfs/merit_review_2009/vehicles_and_systems_simulation/vss_05_duoba.pdf

Ehsani, Mehrdad, Gao, Y., & Ali, E. (2010). Fundamentals of Vehicle Propulsion. In *Modern Electric, Hybrid Electric, and Fuel Cell Vehicles: Fundamentals, Theory, and Design* (pp. 19–65).

Environmental Protection Agency (EPA). (2016). Test Car List Data Files. Retrieved April 17, 2016, from https://www3.epa.gov/otaq/tcldata.htm

Environmental Protection Agency (EPA), & Department of Transportation (DOT). (2012). Department of Transportation. In *Federal Register* (Vol. 77).

Federal Highway Administration (FHA). (2011). Summary of Travel Trends: 2009 National Household Travel Survey, 82. Retrieved from http://nhts.ornl.gov/download.shtml\nhttp://scholar.google.com/scholar?hl=en&btnG=Search&q=intitle:2009+National+Household+Travel+Survey#9

Franke, T., Arend, M. G., McIlroy, R. C., & Stanton, N. A. (2016). Ecodriving in hybrid electric vehicles – Exploring challenges for user-energy interaction. *Applied Ergonomics*, *55*, 33–45. http://doi.org/10.1016/j.apergo.2016.01.007

General Motors (GM). (2016). Chevrolet Camaro Performance Parts List. Retrieved March 19, 2016, from http://www.chevrolet.com/performance/camaro-parts/1le-zl1.html

Gonder, J., & Simpson, A. (2006). Measuring and Reporting Fuel Economy of Plug-In Hybrid Electric Vehicles. *22nd International Battery, Hybrid and Fuel Cell Electric Vehicle Symposium and Exhibition*. Natinal Renewable Energy Laboratory.

Idaho National Lab. (2015). Advanced Vehicle Testing Activity. Retrieved from https://avt.inl.gov/

I-Shift. (2008). In *Civinfo*. Retrieved from http://www.civinfo.com/wiki/index.php?title=I-Shift

Jaynes, N. (2013). Ford claims its regenerative braking tech has saved over 100-million gallons of gas. Retrieved April 4, 2016, from http://www.digitaltrends.com/cars/ford-uses-regenerative-braking-so-save-over-100-million-gallons-of-gas/

Larminie, J., & Lowry, J. (2003). Electric Machines and their Controllers. In *Electric Vehicle Technologies Explained* (pp. 141–181).

Lee, D., Cha, S. W., Rousseau, A., Kim, N., & Karbowski, D. (2012). Optimal Control Strategy for PHEVs using Prediction of Future Driving Schedule. In *International Battery, Hybrid and Fuel Cell Electric Vehicle Symposium*. Los Angeles, California.

Lohse-Busch, H. (2012). *Energy flow in a Battery Electric Vehicle*. Argonne National Lab. Obtained via personal communication.

Lux Research. (2015). Building the Car of 2025: How to Cost-effectively Get to 54.5 mpg Using the Right Mix of Advanced Technologies. *State of the Market Report*. Retrieved from https://portal.luxresearchinc.com/research/report_excerpt/20754

Marquez, E. D. (2016). *Model and Control Strategy Development for a Plug-In Parallel Hybrid Electric Vehicle*. Virginia Tech Thesis.

Marquez, E. D., Mackanic, D., Dennington, J., Mcclean, J., Wheeler, K., & Nelson, D. (2016). Development of a Software-In-The-Loop Model for a Parallel Plug-In Hybrid Electric Vehicle. *SAE Technical Papers*, 19. http://doi.org/10.4271/2016-01-1255

Mathworks. (2016). Modeling an Automatic Transmission Controller. Retrieved April 5, 2016, from http://www.mathworks.com/help/simulink/examples/modeling-an-automatic-transmission-controller.html

Musk, E., & Straubel, J. (2012). Model S Efficiency and Range. Retrieved April 4, 2016, from https://www.teslamotors.com/blog/model-s-efficiency-and-range

Nam, E. K., & Sorab, J. (2004). Friction Reduction Trends in Modern Engines. *SAE Technical Paper 2004-01-1456*, (724). http://doi.org/10.4271/2004-01-1456

Namdoo, K., Shidore, N., & Rousseau, A. (2015). *Advanced Transmission Selection to Provide Accurate VTO Benefits*. Retrieved from http://energy.gov/sites/prod/files/2015/07/f24/vss166_shidore_2015_p.pdf

National Academy of Sciences (NAS), America's Energy Future Panel on Alternative Liquid Transportation Fuels, National Academy of Engineering, & National Research Council. (2009). *Liquid Transportation Fuels from Coal and Biomass: Technological Status, Costs, and Environmental Impacts*. http://doi.org/ISBN-10: 0-309-13712-8

Rahman, Z., Butler, K. L., & Ehsani, M. (2000). SAE TECHNICAL A Comparison Study Between Two Parallel Hybrid Control Concepts. *SAE World Congress*, (724).

http://doi.org/10.4271/2000-01-0994

Rakha, H. a., Ahn, K., & Moran, K. (2012). INTEGRATION Framework for Modeling Eco-routing Strategies: Logic and Preliminary Results. *International Journal of Transportation Science and Technology*, *1*(3), 259–274. http://doi.org/10.1260/2046-0430.1.3.259

Rakha, H., Ahn, K., & Trani, A. (2004). Development of VT-Micro model for estimating hot stabilized light duty vehicle and truck emissions. *Transportation Research Part D: Transport and Environment*, *9*(1), 49–74. http://doi.org/10.1016/S1361-9209(03)00054-3

Rizzoni, G., Guzzella, L., & Baumann, B. M. (1999). Unified modeling of hybrid electric vehicle drivetrains. *IEEE/ASME Transactions on Mechatronics*, *4*(3), 246–257. http://doi.org/10.1109/3516.789683

Stacey, A. (2011). Energy Efficiency of Vehicles. Retrieved April 5, 2016, from http://www.azimuthproject.org/azimuth/show/Energy+efficiency+of+vehicles

Staunton, R. H., Ayers, C. W., Marlino, L. D., Chiasson, J. N., & Burress, T. a. (2006). *Evaluation of 2004 Toyota Prius Hybrid Electric Drive System*. *Energy*. http://doi.org/10.1002/1520-6793(200011)17:11<911::AID-MAR1>3.3.CO;2-W

Tesla Motors. (2016). Tesla Press Information. Retrieved April 4, 2016, from https://www.teslamotors.com/presskit

UQM Technologies. (2016). *PowerPhase 75 Specifications Sheet*. Retrieved from http://www.neweagle.net/support/wiki/docs/Datasheets/UQM/PP75.pdf

Vajedi, M., Chehrehsaz, M., & Azad, N. L. (2014). Intelligent power management of plug-in hybrid electric vehicles , part II : real-time route based power management. *International Journal of Electric and Hybrid Vehicles*, *6*(1), 68–86. http://doi.org/10.1504/IJEHV.2014.062806

White, E. H. (2014). *An Illustrative Look at Energy Flow through Hybrid Powertrains for Design and Analysis*. Virginia Tech Thesis.

White, E. H., Nelson, D. J., & Manning, C. P. (2015). An Illustrative Look at Energy Flow through Hybrid Powertrains for Design and Analysis. *SAE Technical Paper*, 14. http://doi.org/10.4271/2015-01-1231

Zhang, C., Vahidi, A., Pisu, P., Xiaopeng, L., & Tennant, K. (2010). Role of Terrain Preview in Energy Management of Hybrid Electric Vehicles. *Vehicular Technology, IEEE Transactions on*, *59*(3), 1139–1147. http://doi.org/10.1109/TVT.2009.2038707

Appendix A Energy Balance Verification

Table A-1: Example BEV Camaro UDDS Energy Balance in kJ

	Propel	Brake	Idle	Net
Road Load	2659	908	0	3567
Inertia	4517	-4517	0	0
SUBTOTAL	7176	-3609	0	3567
Tractive	7176	-3609	0	3567
Frict. Brake Loss	0	1504	0	1504
SUBTOTAL	7176	-2105	0	5071
Driveline Out	7176	-2105	0	5071
Driveline Loss	490	199	0	688
SUBTOTAL	7666	-1906	0	5759
Motor Mech.	7666	-1906	0	5759
Motor Loss	2151	548	216	2915
SUBTOTAL	9816	-1358	216	8675
Motor Electric	9816	-1358	216	8675
Accessory Load	151	75	49	274
SUBTOTAL	9967	-1283	265	8949
Battery Terminal	9967	-1283	265	8949
Battery Int. Loss	194	12	0	206
SUBTOTAL	10161	-1271	265	9156
Battery Internal	10161	-1271	265	9156
Charging Loss	1518	165	40	1764
SUBTOTAL	11680	-1106	305	10919
Grid Electric	**11680**	**-1106**	**305**	**10919**

Table A-2: Example Conventional Camaro UDDS Energy Balance in kJ

	Propel	Brake	Idle	Net
Road Load	2704.1	862.8	0.0	3567.0
Inertia	3919.8	-3919.8	0.0	0.0
SUBTOTAL	*6623.9*	*-3057.0*	*0.0*	*3567.0*
Tractive	6623.9	-3057.0	0.0	3567.0
Frict. Brake Loss	0.0	3057.0	0.0	3057.0
SUBTOTAL	*6623.9*	*0.0*	*0.0*	*6623.9*
Driveline Out	6623.9	0.0	0.0	6623.9
Driveline Loss	1005.7	0.0	0.0	1005.7
SUBTOTAL	*7629.6*	*0.0*	*0.0*	*7629.6*
Transmission Out	7629.6	0.0	0.0	7629.6
Transmission Loss	2095.2	0.0	0.0	2095.2
SUBTOTAL	*9724.8*	*0.0*	*0.0*	*9724.8*
Transmission In	9724.8	0.0	0.0	9724.8
Engine Idle Loss	0.0	0.0	195.2	195.2
Engine Decel. Loss	0.0	365.0	0.0	365.0
Accessory Load	152.6	73.0	48.8	274.4
SUBTOTAL	*9877.4*	*438.0*	*244.0*	*10559.4*
Engine Out	9877.4	438.7	244.0	10559.4
Engine Loss	25286.7	6297.4	4437.3	36024.2
Start/Stop Eng. Loss	2.0	0.0	0.0	2.0
SUBTOTAL	*35166.2*	*6736.1*	*4681.3*	*46585.6*
Engine In	**35166.2**	**6736.1**	**4681.3**	**46585.6**

Table A-3: Example Parallel PHEV Camaro UDDS Energy Balance in kJ to Torque Node

	Propel	Brake	Idle	Net
Road Load	2357.3	809.9	0.0	3167.2
Inertia	4211.7	-4211.7	0.0	0.0
SUBTOTAL	*6569.0*	*-3401.8*	*0.0*	*3167.2*
Tractive	6569.0	-3401.8	0.0	3167.2
Frict. Brake Loss	0.0	1417.5	0.0	1417.5
SUBTOTAL	*6569.0*	*-1984.3*	*0.0*	*4584.7*
Driveline Out	6569.0	-1984.3	0.0	4584.7
Driveline Loss	494.6	194.8	0.0	689.4
SUBTOTAL	*7063.6*	*-1789.5*	*0.0*	*5274.1*
Transmission Out	8010.6	1779.1	0.0	9789.8
Motor Mech.	-947.0	-3568.7	0.0	-4515.7
SUBTOTAL	*7063.6*	*-1789.5*	*0.0*	*5274.1*

Table A-4: Example Parallel PHEV Camaro UDDS Energy Balance in kJ (Conventional Side)

	Propel	Brake	Idle	Net
Transmission Out	8010.6	1779.1	0.0	9789.8
Transmission Loss	413.6	0.0	0.0	413.6
SUBTOTAL	*8424.3*	*1779.1*	*0.0*	*10203.4*
Transmission In	8424.3	1779.1	0.0	10203.4
Engine Idle Loss	0.0	0.0	0.0	0.0
Engine Decel. Loss	0.0	85.0	0.0	85.0
SUBTOTAL	*8424.3*	*1864.1*	*0.0*	*10288.4*
Engine Out	8424.3	1864.1	0.0	10288.4
Engine Eff. Loss	14733.6	3512.7	0.0	18342.3
Start/Stop Eng. Loss	96.0	0.0	0.0	96.0
SUBTOTAL	*23253.9*	*5376.8*	*0.0*	*28726.7*
Engine In	23253.9	5376.8	0.0	28726.7

Table A-5: Example Parallel PHEV Camaro UDDS Energy Balance in kJ (Electric Side)

	Propel	Brake	Idle	Net
Motor Mech.	-947.0	-3568.7	0.0	-4515.7
Motor Loss	2187.8	780.3	0.0	2968.0
SUBTOTAL	*1240.7*	*-2788.4*	*0.0*	*-1547.7*
Motor Electric	1240.7	-2788.4	0.0	-1547.7
Accessory Load	450.6	226.2	146.4	823.2
SUBTOTAL	*1691.3*	*-2562.2*	*146.4*	*-724.5*
Battery Terminal	1691.3	-2562.2	146.4	-724.5
Battery Int. Loss	402.5	51.2	0.1	453.8
SUBTOTAL	*2093.9*	*-2511.0*	*146.5*	*-270.6*
Battery Internal	2093.9	-2511.0	146.5	-270.6
Charging Loss	312.9	326.4	21.9	2226.6
SUBTOTAL	*2406.8*	*-2184.6*	*168.4*	*1955.9*
Grid Electric	2406.8	-2184.6	168.4	1955.9

Appendix B Battery Internal Resistance

Table B-1: Battery Data from INL to find Internal Resistance Coefficient *(INL, 2015)*

Model Year	Vehicle	Battery Manufact.	Type	Nom. Pack Voltage	Rated Pack Energy	Rated Pack Capacity	Rint	R0	Avg. R0	% Error From Avg
				[V]	[Wh]	[Ah]	[Ω]	[hr]	[hr]	[%]
2010	Ford Fusion	Sanyo	NiMH	275.0	1370	5.5	0.650	0.0118	0.0126	-6.8
2011	Honda CR-Z	Hitachi	NiMH	109.2	600	5.8	0.230	0.0116		-8.7
2014	Honda Insight	Panasonic	NiMH	100.8	580	5.8	0.23	0.0131		4.2
2010	Toyota Prius	Panasonic	NiMH	201.6	1340	6.5	0.420	0.0138		9.1
2013	Chevrolet Malibu Eco	Hitachi	Li-ion	115.2	500	4.4	0.130	0.0049	0.0052	-6.8
2013	Honda Civic	Blue Energy	Li-ion	144.0	680	4.7	0.210	0.0069		24.0
2015	Honda Accord	Blue Energy	Li-ion	259.2	1300	5.0	0.220	0.0043		-22.9
2013	Ford C-Max SE	Panasonic	Li-ion	281.2	1400	5.0	0.235	0.0042		-25.8
2014	Volkswagen Jetta	Sanyo	Li-ion	220.0	1100	5.0	0.198	0.0045		-16.3
2011	Hyundai Sonata	LG Chem	Li-ion	270.0	1394	5.3	0.350	0.0067		21.8
2013	Toyota Prius	Primearth EV Energy Co.	Li-ion	207.2	4400	21.5	0.110	0.0113	0.0113	-0.2
2013	Ford Fusion Energi	Panasonic	Li-ion	310.8	7600	26.0	0.135	0.0106		-6.3
2016	Camaro (HEVT)	A123 (15s2p)	Li-ion	340.0	12600	37.1	0.110	0.0120		5.8
2011	Chevrolet Volt	LG Chem	Li-ion	355.2	16000	45.0	0.160	0.0203	0.0199	1.7
2012	Mitsubishi iMiev ES	GS Yuasa	Li-ion	325.6	16300	50.0	0.14	0.0215		7.4
2013	Chevrolet Volt	LG Chem	Li-ion	355.2	16500	45.0	0.098	0.0128		-55.6
2015	Chevrolet Spark	LG Chem	Li-ion	355.2	18400	52.0	0.125	0.0182		-9.4
2014	Smart E. Coupe	Deutsche ACCUmotive/ Li-Tec	Li-ion	344.1	17600	52.0	0.185	0.0275		27.5
2014	BMW i3 BEV	Samsung SDI	Li-ion	355.2	21600	60.0	0.120	0.0205		3.0
2013	Nissan Leaf S	AESC	Li-ion	360.0	24000	66.2	0.12	0.0222		10.3
2015	Volkswagen E-Golf	Sanyo	Li-ion	320.0	24000	75.0	0.080	0.0188		-6.3
2015	Kia Soul	SK Innovation	Li-ion	355.2	27000	75.0	0.085	0.0182		-9.6
2013	Ford Focus	LG Chem	Li-ion	318.2	23000	75.0	0.085	0.0193		-3.3

Appendix C Motor Validation Data

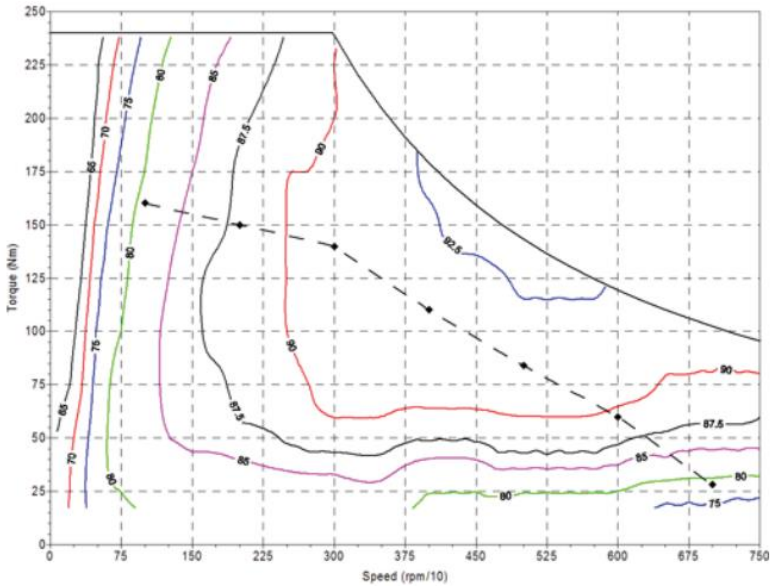

Figure C-1: UQM PP75 Motor System Efficiency Map *(UQM, 2016, Fair Use)*

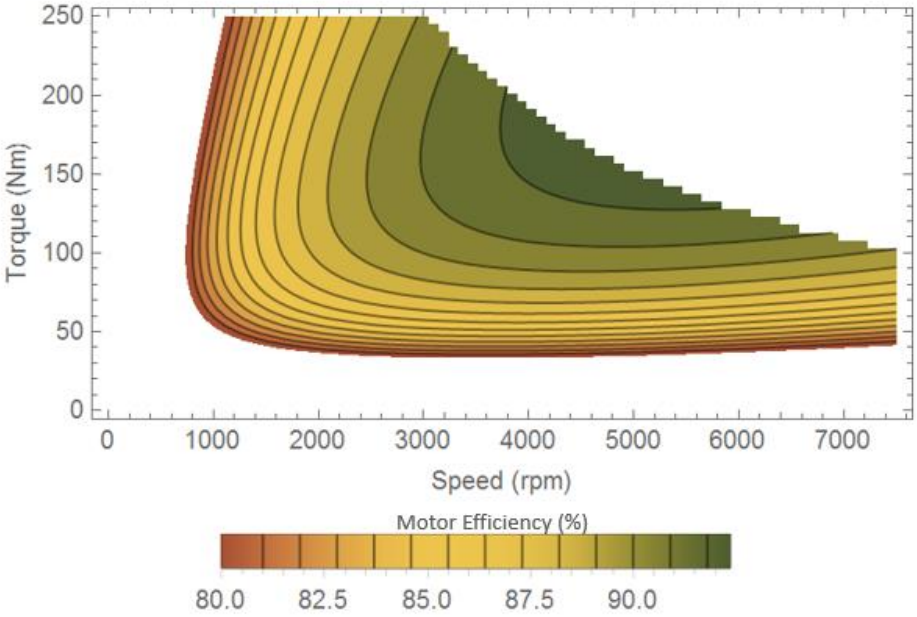

Figure C-2: UQM PP75 Motor System Efficiency Map With Ideal Loss Coefficients

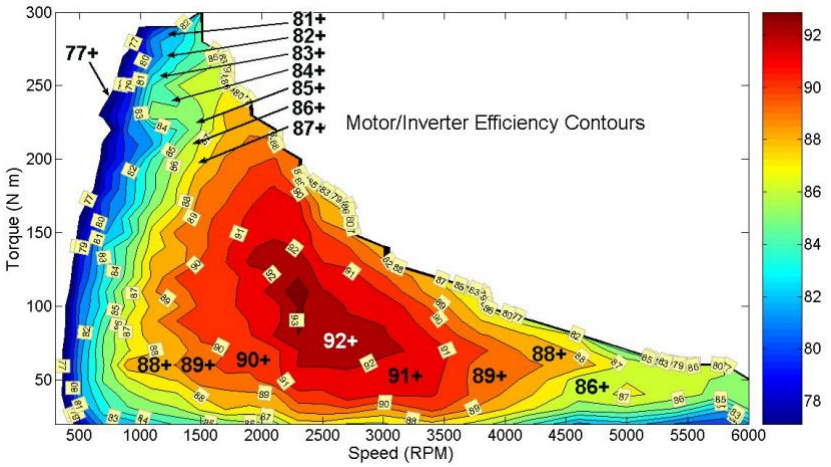

Figure C-3: 2004 Prius Motor System Efficiency Map *(Staunton et al., 2006, Public Domain)*

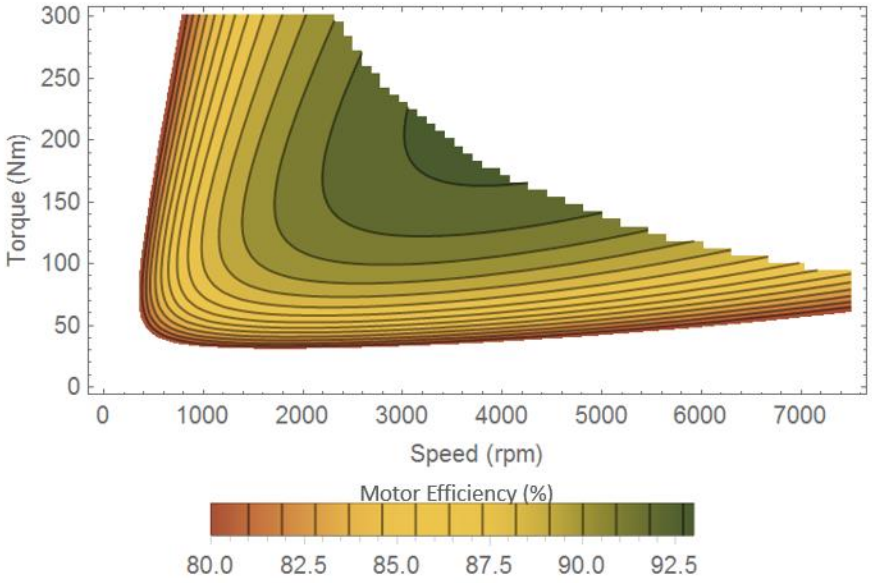

Figure C-4: 2004 Prius Motor System Efficiency Map with Ideal Loss Coefficients

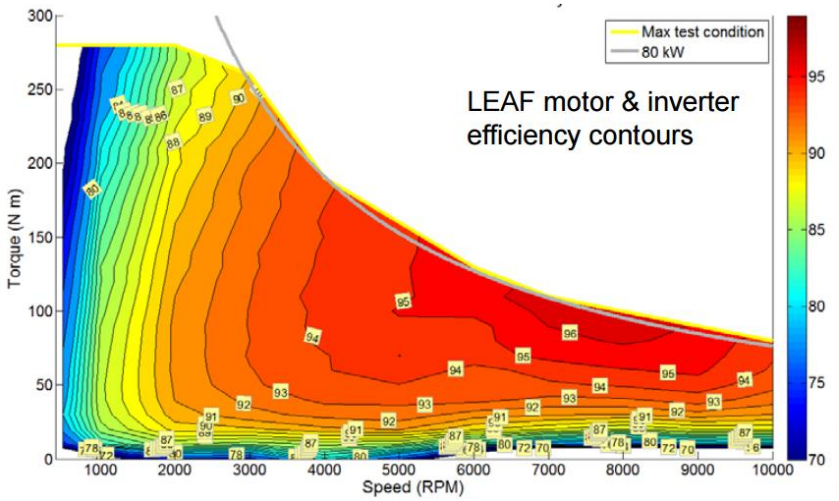

Figure C-5: 2013 Nissan Leaf Motor System Efficiency Map *(Burress, 2013, Public Domain)*

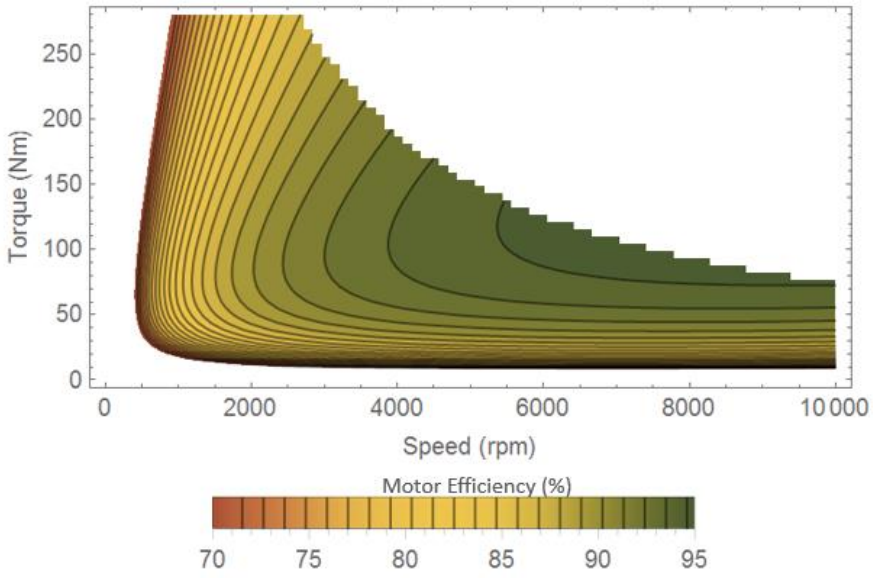

Figure C-6: 2013 Leaf Motor System Efficiency Plot with Unscaled Coefficients

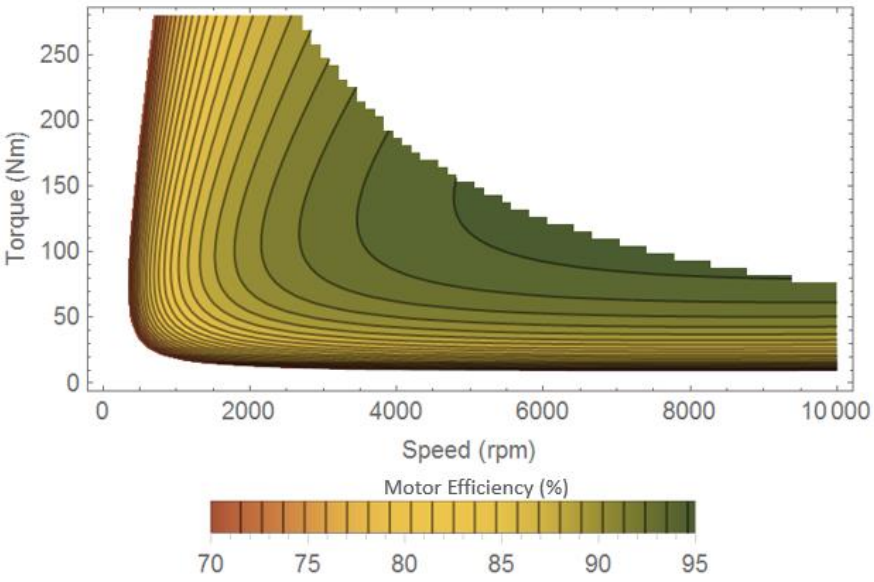

Figure C-7: 2013 Leaf Motor System Efficiency Plot with Scaled Coefficients

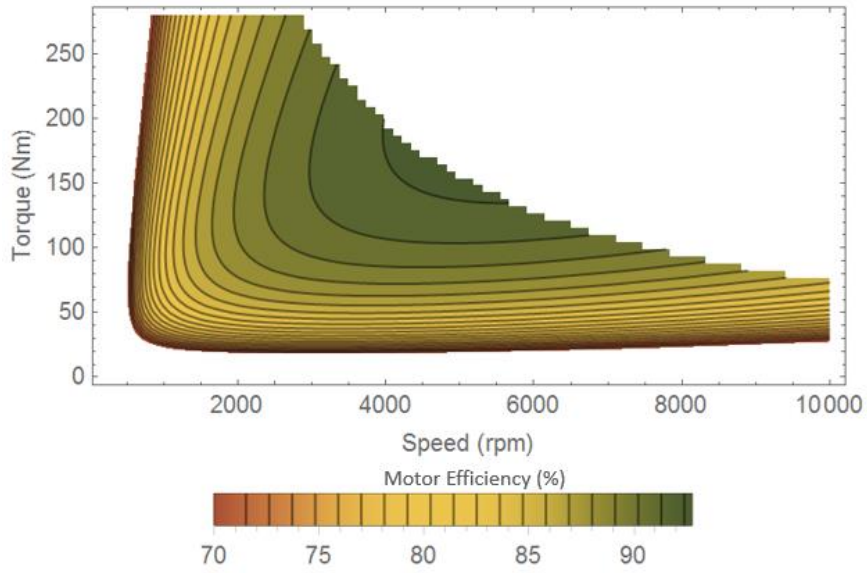

Figure C-8: 2013 Leaf Motor System Efficiency Plot with Standard Coefficients

Table C-1: UDDS Leaf Data Error Summary

UDDS		ANL*	Standard Motor Coefficients			Scaled Motor Coefficients			Unscaled Motor Coefficients		
		(kWh)	Value (kWh)	Difference (kWh)	Error (%)	Value (kWh)	Difference (kWh)	Error (%)	Value (kWh)	Difference (kWh)	Error (%)
Inertia	Propel	0.928	0.93	0.00	-0.3	0.93	0.00	-0.3	0.93	0.00	-0.3
	Brake	0.928	0.93	0.00	-0.3	0.93	0.00	-0.3	0.93	0.00	-0.3
Road Load	Propel	0.673	0.67	0.00	-0.4	0.67	0.00	-0.4	0.67	0.00	-0.4
	Brake	0.205	0.21	0.00	2.0	0.21	0.00	2.0	0.21	0.00	2.0
Tractive	Propel	1.601	1.60	-0.01	-0.4	1.60	-0.01	-0.4	1.60	-0.01	-0.4
	Brake	0.723	0.72	-0.01	-1.0	0.72	-0.01	-1.0	0.72	-0.01	-1.0
Motor Loss	Propel	0.316	0.56	0.24	76.3	0.35	0.03	9.5	0.32	0.01	2.2
	Brake	0.179	0.20	0.02	10.6	0.13	-0.05	-26.3	0.12	-0.06	-31.3
Accessory Load		0.064	0.08	0.01	18.8	0.08	0.01	18.8	0.08	0.01	18.8
Regen Braking		0.544	0.56	0.01	2.2	0.56	0.01	2.2	0.56	0.01	2.2
Extra DL Loss		0.000	0.30	0.30	N/A	0.30	0.30	N/A	0.30	0.30	N/A
Battery Net		1.436	2.19	0.75	52.2	1.93	0.49	34.1	1.90	0.46	32.0

*ANL data from (Lohse-Busch, 2012).

Table C-2: HWFET Leaf Data Error Summary

HWFET		ANL*	Standard Motor Coefficients			Scaled Motor Coefficients			Unscaled Motor Coefficients		
		(kWh)	Value (kWh)	Difference (kWh)	Error (%)	Value (kWh)	Difference (kWh)	Error (%)	Value (kWh)	Difference (kWh)	Error (%)
Inertia	Propel	0.354	0.34	-0.01	-3.1	0.34	-0.01	-3.1	0.34	-0.01	-3.1
	Brake	0.354	0.34	-0.01	-3.1	0.34	-0.01	-3.1	0.34	-0.01	-3.1
Road Load	Propel	1.714	1.72	0.01	0.4	1.72	0.01	0.4	1.72	0.01	0.4
	Brake	0.138	0.13	-0.01	-3.6	0.13	-0.01	-3.6	0.13	-0.01	-3.6
Tractive	Propel	2.068	2.06	0.00	-0.2	2.06	0.00	-0.2	2.06	0.00	-0.2
	Brake	0.216	0.21	-0.01	-2.8	0.21	-0.01	-2.8	0.21	-0.01	-2.8
Motor Loss	Propel	0.402	0.96	0.56	139.1	0.46	0.06	13.9	0.40	-0.01	-1.5
	Brake	0.057	0.09	0.03	52.6	0.05	-0.01	-21.1	0.04	-0.02	-31.6
Accessory Load		0.042	0.04	0.00	0.0	0.04	0.00	0.0	0.04	0.00	0.0
Regen Braking		0.159	0.17	0.01	6.3	0.17	0.01	6.3	0.17	0.01	6.3
Extra DL Loss		0.000	0.41	0.41	N/A	0.41	0.41	N/A	0.41	0.41	N/A
Battery Net		2.353	3.40	1.05	44.5	2.86	0.50	21.4	2.79	0.44	18.5

*ANL data from (Lohse-Busch, 2012).

Table C-3: Average Percent Error for Leaf Data between UDDS and HWFET

Average of UDDS and HWFET		Standard Motor Coefficients	Scaled Motor Coefficients	Unscaled Motor Coefficients
		Error (%)	Error (%)	Error (%)
Inertia	Propel	1.7	1.7	1.7
	Brake	1.7	1.7	1.7
Road Load	Propel	0.4	0.4	0.4
	Brake	2.8	2.8	2.8
Tractive	Propel	0.3	0.3	0.3
	Brake	1.9	1.9	1.9
Motor Loss	Propel	107.7	11.7	1.9
	Brake	31.6	23.7	31.4
Accessory Load		9.4	9.4	9.4
Regen Braking		4.2	4.2	4.2
Extra DL Loss		N/A	N/A	N/A
Battery Net		48.3	27.7	25.2

Appendix D Engine and Transmission Validation Data

Table D-1: Drive Cycle Average Transmission Efficiencies (%)

2012 Fusion				2012 300				2013 Sonata				HEVT Camaro			
UDDS	US06 City	US06 Hwy	HWFET	UDDS	US06 City	US06 Hwy	HWFET	UDDS	US06 City	US06 Hwy	HWFET	UDDS	US06 City	US06 Hwy	HWFET
87.2	92.7	91.9	89.9	90.3	94.4	95.8	93.6	86.8	92.2	91.4	89.7	81.9	90.0	90.6	84.7

Table D-2: 6-Speed Transmission 0% and 100% Shift Speeds

Current Gear	Downshift			Upshift		
	Gear Pair	0% Throttle Target Eng. Speed [rpm]	100% Throttle Target Eng. Speed [rpm]	Gear Pair	0% Throttle Post-Shift Eng. Speed [rpm]	100% Throttle Target Eng. Speed [rpm]
1	1-0	--	--	1-2	$0.85 * S_{eng,min}$	$0.71 * S_{eng,max}$
2	2-1	$S_{eng,min} - 4.5\Delta_l$	$S_{eng,max} - 2.3\Delta_h$	2-3	$0.85 * S_{eng,min}$	$0.71 * S_{eng,max}$
3	3-2	$S_{eng,min} - 4.5\Delta_l$	$S_{eng,max} - 2.2\Delta_h$	3-4	$S_{eng,min}$	$S_{eng,max}$
4	4-3	$S_{eng,min} - \Delta_l$	$S_{eng,max} - 1.35\Delta_h$	4-5	$S_{eng,min}$	$S_{eng,max}$
5	5-4	$S_{eng,min} - \Delta_l$	$S_{eng,max} - 1.35\Delta_h$	5-6	$0.9 * S_{eng,min}$	$0.98 * S_{eng,max}$
6	6-5	$S_{eng,min} - 2\Delta_l$	$S_{eng,max} - 1.35\Delta_h$	6-7	--	--

Table D-3: 8-Speed Transmission 0% and 100% Shift Speeds

Current Gear	Downshift			Upshift		
	Gear Pair	0% Throttle Target Eng. Speed [rpm]	100% Throttle Target Eng. Speed [rpm]	Gear Pair	0% Throttle Post-Shift Eng. Speed [rpm]	100% Throttle Target Eng. Speed [rpm]
1	1-0	--	--	1-2	$0.85 * S_{eng,min}$	$0.71 * S_{eng,max}$
2	2-1	$S_{eng,min} - 4.5\Delta_l$	$S_{eng,max} - 2.3\Delta_h$	2-3	$0.85 * S_{eng,min}$	$0.71 * S_{eng,max}$
3	3-2	$S_{eng,min} - 4.5\Delta_l$	$S_{eng,max} - 2.2\Delta_h$	3-4	$S_{eng,min}$	$S_{eng,max}$
4	4-3	$S_{eng,min} - \Delta_l$	$S_{eng,max} - \Delta_h$	4-5	$S_{eng,min}$	$S_{eng,max}$
5	5-4	$S_{eng,min} - \Delta_l$	$S_{eng,max} - \Delta_h$	5-6	$0.9 * S_{eng,min}$	$0.98 * S_{eng,max}$
6	6-5	$S_{eng,min} - 2\Delta_l$	$S_{eng,max} - \Delta_h$	6-7	$0.87 * S_{eng,min}$	$0.71 * S_{eng,max}$
7	7-6	$S_{eng,min} - 2\Delta_l$	$S_{eng,max} - 1.8\Delta_h$	7-8	$0.6 * S_{eng,min}$	$0.25 * S_{eng,max}$
8	8-7	$S_{eng,min} - 5\Delta_l$	$S_{eng,max} - 3.25\Delta_h$	8-9	--	--

Table D-4: Example 2012 Chrysler 300 Transmission High/Low Shift Points

Current Gear				GR1	GR2	GR3	GR4	GR5	GR6	GR7	GR8
Downshift	**Gear Pair**			**1-0**	**2-1**	**3-2**	**4-3**	**5-4**	**6-5**	**7-6**	**8-7**
	0%	Target Eng. Speed	[rpm]	--	600	600	950	950	850	850	550
		Pre-Shift Veh. Speed	[mph]	--	6.01	8.98	17.88	23.15	26.72	31.81	25.81
		Post-Shift Eng. Speed	[rpm]	--	900	897	1195	1230	1097	1012	690
	100%	Target Eng. Speed	[rpm]	--	2720	2880	4800	4800	4800	3520	1200
		Pre-Shift Veh. Speed	[mph]	--	27.23	43.12	90.36	116.98	150.90	131.74	56.31
		Post-Shift Eng. Speed	[rpm]	--	4080	4306	6036	6214	6192	4190	1504
Upshift	**Gear Pair**			**1-2**	**2-3**	**3-4**	**4-5**	**5-6**	**6-7**	**7-8**	**8-9**
	0%	Target Eng. Speed	[rpm]	1427	1335	1320	1359	1219	1088	790	--
		Pre-Shift Veh. Speed	[mph]	9.53	13.36	19.77	25.59	29.71	34.19	29.56	--
		Post-Shift Eng. Speed	[rpm]	893	893	1050	1050	945	914	630	--
	100%	Target Eng. Speed	[rpm]	4544	4544	6400	6400	6272	4544	1600	--
		Pre-Shift Veh. Speed	[mph]	30.33	45.50	95.81	120.48	152.85	142.86	59.88	--
		Post-Shift Eng. Speed	[rpm]	3029	3039	5090	4944	4862	3817	1276	--

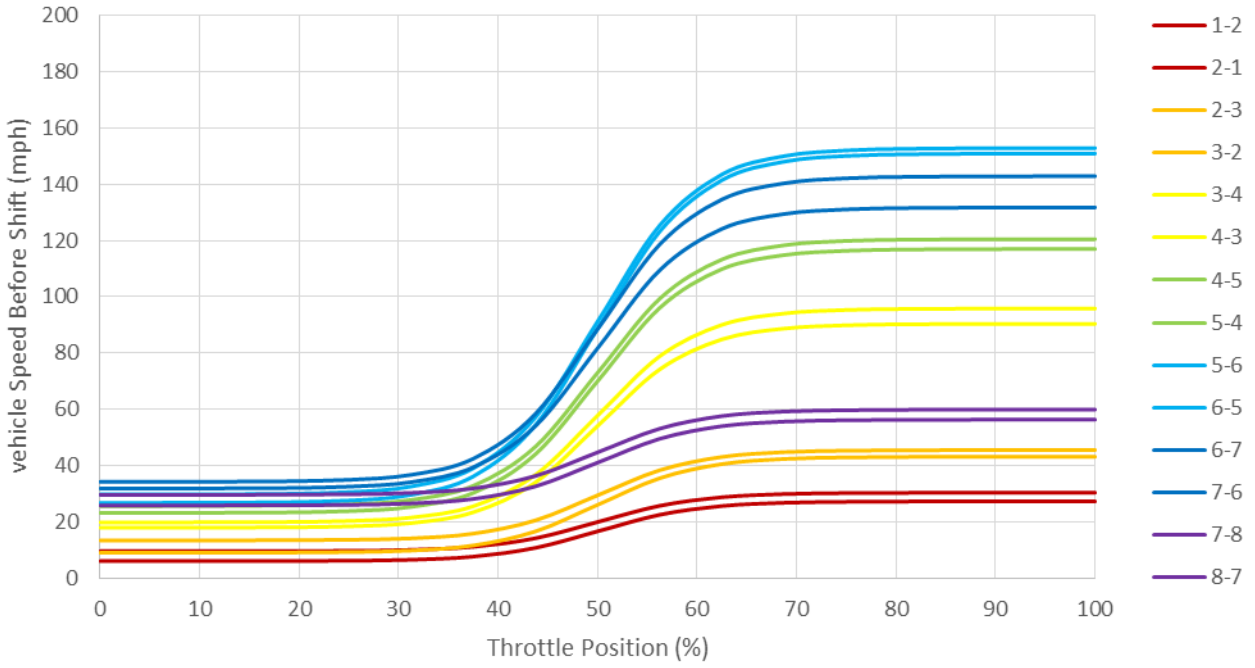

Figure D-1: Example 8-Speed Shift Strategy Map for 2012 Chrysler 30

Table D-5: Percent of Drive Cycle Spent in Each Gear

		% Time Spent in Gear															
		1		2		3		4		5		6		7		8	
		*ANL	Mod	*ANL	Mod	*ANL	Mod	*ANL	Mod	*ANL	Mod	*ANL	Mod	*ANL	Mod	*ANL	Mod
Fusion	UDDS	26.6	26.2	4.8	5.8	8.8	12.1	32.9	25.7	18.4	18.6	7.6	11.7	0.0	0.0	0.0	0.0
	HWFET	1.5	1.2	0.5	0.7	0.9	1.3	1.8	2.8	12.2	12.8	82.9	81.3	0.0	0.0	0.0	0.0
	US06	14.5	11.4	2.8	6.4	3.9	8.1	5.3	9.7	9.2	14.6	63.1	49.8	0.0	0.0	0.0	0.0
Sonata	UDDS	27.9	28.7	7.1	8.5	16.8	17.3	33.6	30.9	7.0	7.8	7.6	6.8	0.0	0.0	0.0	0.0
	HWFET	1.6	1.6	0.6	0.8	1.0	2.4	3.2	12.5	15.8	26.5	77.8	56.4	0.0	0.0	0.0	0.0
	US06	13.8	13.8	5.7	7.2	6.0	10.6	6.9	14.1	9.1	20.6	58.6	33.7	0.0	0.0	0.0	0.0
300	UDDS	26.8	27.6	6.7	7.9	16.3	13.7	14.2	22.3	20.1	13.8	6.2	4.4	2.9	1.5	6.7	8.8
	HWFET	1.5	1.4	0.6	0.5	1.3	1.3	1.0	2.4	3.0	7.7	3.9	10.2	17.9	10.5	70.8	65.9
	US06	13.1	13.1	5.4	5.5	7.4	7.2	4.1	5.2	6.0	2.3	5.0	2.3	8.8	2.0	50.3	62.2

ANL data from “Overview Sheets” for each vehicle on the Downloadable Dynamometer Database (D3) (ANL, 2016b)*

Appendix E Vehicle Sensitivity Data

Mass Study

Table E-1: Mass Sensitivity Study

Route	Parameters			Fuel Energy	*Grid Electric Energy	Grid Electric Energy	Electric Economy	Overall ΔSOC	SOC Corr Fuel Energy	SOC Corr. Fuel Energy	SOC Corr. Fuel Economy	PEU		GHG	
	Type	SOCi	kmass	(kJ)	(kJ)	(AC Wh/mi)	(mpgge)	(%)	(kJ)	(Wh/ mi)	(mpgge)	(PE Wh)	(PE Wh/mi)	(g GHG)	(g GHG/mi)
2x City	BEV	60	0.8	0	6699	526	64.1	-12.9	17483	N/A		61	17	910	257
		60	1.0	0	7886	619	54.4	-15.1	20583			72	20	1071	302
		60	1.2	0	9238	725	46.5	-17.7	24112			85	24	1255	354
2x Hwy	BEV	60	0.8	0	19645	438	76.9	-37.7	51274	N/A		180	14	2668	214
		60	1.0	0	20310	452	74.4	-39.0	53009			186	15	2759	221
		60	1.2	0	21079	470	71.7	-40.4	55016			193	15	2863	230
2x City	Conv.	60	0.8	25059	0	N/A		0.0	25059	25059	17.1	1907	538	1698	479
		60	1.0	28486	0			0.0	28486	28486	15.1	2168	612	1931	545
		60	1.2	31282	0			0.0	31282	31282	13.7	2381	672	2120	598
2x Hwy	Conv.	60	0.8	66093	0	N/A		0.0	66093	66093	22.9	5030	403	4480	359
		60	1.0	67369	0			0.0	67369	67369	22.4	5128	411	4566	366
		60	1.2	68170	0			0.0	68170	68170	22.2	5188	416	4620	370
2x City	PHEV	27.81	0.8	18211	-171	N/A		0.3	17764	17764	24.2	1352	381	1204	340
		29.8	1.0	25111	-1899			3.6	20156	20156	21.3	1534	433	1366	385
		28	1.2	28380	-2210			4.2	22612	22612	19.0	1721	486	1533	432
2x Hwy	PHEV	26.58	0.8	50980	-48	N/A		0.1	50853	50853	29.7	3870	310	3447	276
		23.82	1.0	53328	52			-0.1	53463	53463	28.3	4070	326	3631	291
		24.41	1.2	54056	-11			0.0	54025	54025	28.0	4112	330	3662	294

*A negative PHEV Grid Electric Energy is not physically possible but listed for reference.

Engine Displacement Study

Table E-2: Engine Displacement Sensitivity Study

Route	Parameters			Fuel Energy	*Grid Electric Energy	Grid Electric Energy	Electric Economy	Overall ΔSOC	SOC Corr Fuel Energy	SOC Corr. Fuel Energy	SOC Corr. Fuel Economy	PEU		GHG	
	Type	SOCi	kdisp	(kJ)	(kJ)	(AC Wh/mi)	(mpgge)	(%)	(kJ)	(Wh/mi)	(mpgge)	(PE Wh)	(PE Wh/mi)	(g GHG)	(g GHG/mi)
2x City	Conv.	60	0.3	24603	0	N/A		0.0	24603	1931	17.4	1873	528	1668	470
		60	1.0	28486	0			0.0	28486	2235	15.1	2168	612	1931	545
		60	1.5	30370	0			0.0	30370	2383	14.1	2311	652	2058	581
2x Hwy	Conv.	60	0.3	58243	0	N/A		0.0	58243	1297	26.0	4433	355	3948	317
		60	1.0	67369	0			0.0	67369	1501	22.4	5128	411	4566	366
		60	1.5	75613	0			0.0	75613	1684	20.0	5755	461	5125	411
2x City	PHEV	29.7	0.3	19002	351	N/A		-0.7	19918	1563	21.5	1519	429	1398	394
		29.8	1.0	25111	-1899			3.6	20156	1582	21.3	1534	433	1366	385
		29.2	1.5	28876	-3161			6.1	20627	1619	20.8	1570	443	1398	394
2x Hwy	PHEV	26.3	0.3	59534	-491	N/A		0.9	58252	1298	25.9	4434	356	3948	317
		23.82	1.0	53328	52			-0.1	53463	1191	28.3	4070	326	3631	291
		23.82	1.5	55396	62			-0.1	55558	1238	27.2	4229	339	3774	303
2City	BEV	60	All	0	7886	619	54.4	-15.1	20583	N/A		72	20	1071	302
2Hwy	BEV	60	All	0	20310	452	74.4	-39	53009	N/A		186	15	2759	221

*A negative PHEV Grid Electric Energy is not physically possible but listed for reference.

Battery Capacity Study

Table E-3: Battery Capacity Sensitivity Study

Route	Parameters			Fuel Energy	*Grid Electric Energy	Grid Electric Energy	Electric Economy	Overall ΔSOC	SOC Corr Fuel Energy	SOC Corr. Fuel Energy	SOC Corr. Fuel Economy	PEU		GHG	
	Type	SOCi	kEcap	(kJ)	(kJ)	(AC Wh/mi)	(mpgge)	(%)	(kJ)	(Wh/mi)	(mpgge)	(PE Wh)	(PE Wh/mi)	(g GHG)	(g GHG/mi)
2x City	BEV	60	0.3	0	10253	805	41.9	-65.6	26759	N/A		94	27	1393	393
		60	1.0	0	7886	619	54.4	-15.1	20583			72	20	1071	302
		60	1.5	0	8008	628	53.6	-10.2	20899			73	21	1088	307
2x Hwy	BEV	60	0.3	0	23738	529	63.7	-151.8	61956	N/A		218	17	3224	259
		60	1.0	0	20310	452	74.4	-39.0	53009			186	15	2759	221
		60	1.5	0	20478	456	73.8	-26.2	53447			188	15	2782	223
2x City	PHEV	31	0.3	25111	-791	N/A		5.1	23047	1808	18.6	5128	411	4566	366
		29	1.0	25659	-2080			4.0	20230	1587	21.2	1754	495	1562	441
		30	1.5	25111	-1832			2.3	20330	1595	21.1	1540	434	1371	387
2x Hwy	PHEV	24.45	0.3	60850	-153	N/A		1.0	60451	1347	25.0	1547	437	1378	389
		24.45	1.0	52311	344			-0.7	53207	1185	28.4	4601	369	4097	329
		26	1.5	53705	114			-0.2	54002	1203	28.0	4053	325	3653	293
2City	Conv.	60	All	28486	0	N/A		0	0	2235	15.1	2168	612	1931	545
2Hwy	Conv	60	All	67369	0	N/A		0	0	1501	22.4	5128	411	4566	366

*A negative PHEV Grid Electric Energy is not physically possible but listed for reference.

Mode Delay Study

Table E-4: Mode Time Delay Sensitivity Study

Route	Parameters					Time in Each Mode			Fuel Energy	*Grid Electric Energy	Overall ΔSOC	SOC Corr Fuel Energy	SOC Corr. Fuel Energy	SOC Corr. Fuel Economy	FE	PEU		GHG	
	Type	SOCi	tdelay	Teng, extra	Teng, min	#1 (s)	#2 (s)	#3 (s)	(kJ)	(AC Wh/mi)	(%)	(kJ)	(Wh/mi)	(mpgge)	(mpgge)	(PE Wh)	(PE Wh/mi)	(g GHG)	(g GHG/mi)
2x City	PHEV	31	6	40	202.4	311	69	82	19,333	120	-0.2	1624	1542	21.8	21.9	301	85	2736	772
		30	8	40	202.4	288	70	104	25,111	-1899	3.6	1686	1582	21.3	21.3	359	101	3525	995
		30	10	40	202.4	260	70	132	26,901	-2211	4.2	1790	1658	20.3	20.3	383	108	3775	1065
2x Hwy	PHEV	23.92	6	40	202.4	553	18	163	53,078	63	-0.1	1349	1186	28.4	28.4	589	47	7301	585
		23.82	8	40	202.4	553	18	163	53,328	52	-0.1	1354	1191	28.3	28.3	592	47	7335	588
		23.82	10	40	202.4	553	17	164	53,677	11	0.0	1360	1196	28.1	28.2	596	48	7383	592

*A negative PHEV Grid Electric Energy is not physically possible but listed for reference

Extra Torque Study

Table E-5: Engine Extra Torque Sensitivity Study

Route	Parameters					Time in Each Mode			Fuel Energy	*Grid Electric Energy	Overall ΔSOC	SOC Corr Fuel Energy	SOC Corr. Fuel Energy	SOC Corr. Fuel Economy	FE	PEU		GHG	
						#1	#2	#3											
	Type	SOCi	tdelay	Teng, extra	Teng, min	(s)	(s)	(s)	(kJ)	(AC Wh/mi)	(%)	(kJ)	(Wh/mi)	(mpgge)	(mpgge)	(PE Wh)	(PE Wh/mi)	(g GHG)	(g GHG/mi)
2x City	PHEV	30	8	20	202.4	288	70	104	24,671	-1700	3.3	1692	1588	21.2	21.2	305	86	3466	978
		30	8	40	202.4	288	70	104	25,111	-1899	3.6	1686	1582	21.3	21.3	359	101	3525	995
		30	8	60	202.4	288	70	104	25,592	-2094	4.0	1683	1579	21.3	21.4	336	95	3590	1013
2x Hwy	PHEV	23.92	8	20	202.4	552	18	164	53,506	-21	0.0	1355	1191	28.3	28.3	558	45	7360	590
		23.92	8	40	202.4	553	18	163	53,328	52	-0.1	1354	1191	28.3	28.3	592	47	7335	588
		23.92	8	60	202.4	553	18	163	53,483	-22	0.0	1353	1190	28.3	28.3	589	47	7356	590

*A negative PHEV Grid Electric Energy is not physically possible but listed for reference.

Minimum Engine Torque Cutoff

Table E-6: Engine Minimum Torque Cutoff Sensitivity Study

Route	Parameters					Time in Each Mode			Fuel Energy	*Grid Electric Energy	Overall ΔSOC	SOC Corr Fuel Energy	SOC Corr. Fuel Energy	SOC Corr. Fuel Economy	FE	PEU		GHG	
						#1	#2	#3											
	Type	SOCi	tdelay	Teng, extra	Teng, min	(s)	(s)	(s)	(kJ)	(AC Wh/mi)	(%)	(kJ)	(Wh/mi)	(mpgge)	(mpg)	(PE Wh)	(PE Wh/mi)	(g GHG)	(g GHG/mi)
2x City	PHEV	30.58	8	40	101.2	290	82	90	19,687	-17	0.0	1631	1541	21.8	21.9	305	86	2785	786
		30	8	40	202.4	288	70	104	25,111	-1899	3.6	1686	1582	21.3	21.3	359	101	3525	995
		30	8	40	303.6	314	44	104	22,906	-1214	2.3	1653	1549	21.7	21.8	336	95	3223	909
2x Hwy	PHEV	26.55	8	40	101.2	521	76	137	50,401	5	0.0	1260	1123	30.0	30.0	558	45	6932	556
		23.82	8	40	202.4	553	18	163	53,328	52	-0.1	1354	1191	28.3	28.3	592	47	7335	588
		23.98	8	40	303.6	557	10	167	53,049	-13	0.0	1348	1181	28.5	28.5	589	47	7297	585

*A negative PHEV Grid Electric Energy is not physically possible but listed for reference.

Appendix F Route Sensitivity Data

Table F-1: Route Study Details

Name	Total Distance	Avg Velocity	Max Velocity	Total Time	Accel. Rate	Grade	Grade Length
	(mi)	(mph)	(mph)	(s)	(m/s^2)	(%)	(mi)
A	0.8	30	30	100	1.5	0	0
B	1.4	50	50	100	1.5	0	0
C	1.9	70	70	100	1.5	0	0
D	0.5	26.2	30	70	1.5	0	0
E	0.5	35.6	50	52	1.5	0	0
F	0.5	46.8	70	47	1.5	0	0
G	1.5	28.6	30	189	1.5	0	0
H	1.5	43.9	50	123	1.5	0	0
I	1.5	46.8	70	98	1.5	0	0
J	3	39	30	369	1.5	0	0
K	3	55.1	50	231	1.5	0	0
L	3	61.7	70	175	1.5	0	0
M	1.5	28.6	30	189	1.5	2%	0.7
N	1.5	43.9	50	123	1.5	2%	0.7
O	1.5	46.8	70	98	1.5	2%	0.7
P	1.5	28.6	30	189	1.5	4%	0.7
Q	1.5	43.9	50	123	1.5	4%	0.7
R	1.5	46.8	70	98	1.5	4%	0.7
S	0.03	11.18	22.37	10	1.0	0	0
T	0.05	16.78	33.55	10	1.5	0	0
U	0.08	27.96	55.92	10	2.5	0	0
V	0.06	15.66	31.32	14	1.0	0	0
W	0.09	23.49	46.98	14	1.5	0	0
X	0.15	39.15	78.29	14	2.5	0	0
Y	1.5	41.5	50.21	130	1.0	0	0
Z	1.5	41.5	46.49	130	1.5	0	0
AA	1.5	41.5	44.23	130	2.5	0	0
AB	1.5	51.4	76.06	105	1.0	0	0
AC	1.5	51.4	62.52	105	1.5	0	0
AD	1.5	51.4	56.95	105	2.5	0	0
AE	0.03	11.04	22.37	10	-1.0	0	0
AF	0.05	16.57	33.55	10	-1.5	0	0
AG	0.08	27.61	55.92	10	-2.5	0	0
AH	0.06	15.46	31.32	14	-1.0	0	0
AI	0.09	23.19	46.98	14	-1.5	0	0
AJ	0.15	38.66	78.29	14	-2.5	0	0

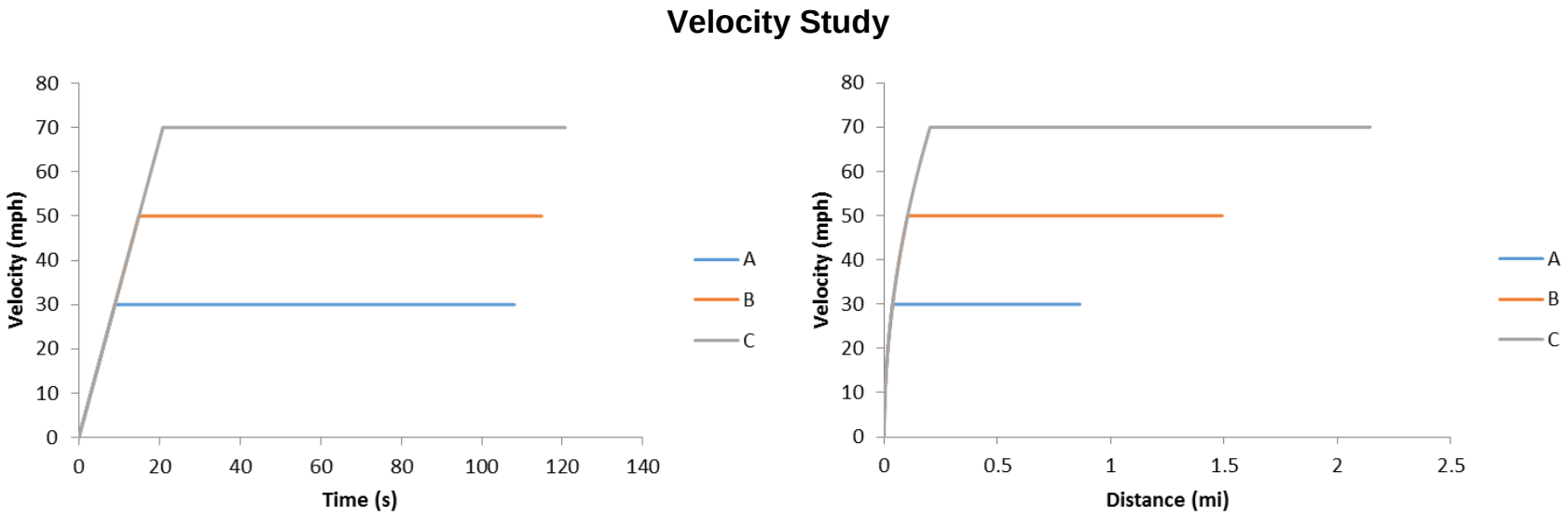

Figure F-1: Velocity Study Velocity vs both Distance and Time

Table F-2: Velocity Study Route Details

Route	Vehicle	SOCi	Total Distance	Total Time	Average Vehicle Speed	Max Vehicle Speed	Max Grade	Max Elevation	Max Accel.	Engine Time	Motor Time	Max Gear
		(%)	(mi)	(s)	(mph)	(mph)	(%)	(m)	(m/s2)	(s)	(s)	(---)
A	BEV	60	0.8	99	30.0	30.0	0	0	1.5	0	99	N/A
B		60	1.4	100	50.0	50.0	0	0	1.5	0	100	
C		60	1.9	100	70.0	70.0	0	0	1.5	0	100	
A	Conv.	60	0.8	99	30.0	30.0	0	0	1.5	99	0	8
B		60	1.4	100	50.0	50.0	0	0	1.5	100	0	8
C		60	1.9	100	70.0	70.0	0	0	1.5	100	0	8
A	PHEV	21.72	0.8	99	30.0	30.0	0	0	1.5	17	99	8
B		24.26	1.4	100	50.0	50.0	0	0	1.5	18	100	8
C		27.70	1.9	100	70.0	70.0	0	0	1.5	22	100	8

Table F-3: Velocity Study Results

Route	Vehicle	Total Fuel Energy	Total Grid Electric Energy	Total Grid Energy	Grid Electric Econ.	Overall ΔSOC	SOC Corr Fuel Energy	SOC Corr. Fuel Energy	SOC Corr. Fuel Econ.	PEU		GHG	
		(kJ)	(kJ)	(Wh/mi)	(mpgge)	(%)	(kJ)	(Wh/mi)	(mpgge)	(PE Wh)	(PE Wh/mi)	(g GHG)	(g GHG/mi)
A	BEV	0	679	228	147.4	-1.30	1773	N/A		6	8	92	112
B		0	1561	312	107.8	-2.99	4075			14	10	212	153
C		0	3052	437	77.1	-5.85	7965			28	14	415	214
A	Conv.	3714	0	N/A		0.00	3714	1249	27.0	283	342	252	305
B		6325	0			0.00	6325	1265	26.6	481	347	429	309
C		10467	0			0.00	10467	1497	22.5	797	410	709	365
A	PHEV	1909	112	N/A		-0.02	1826	614	54.8	140	169	139	168
B		4341	199			0.08	3960	792	42.5	303	218	295	213
C		9096	527			0.02	8932	1278	26.4	685	353	677	349

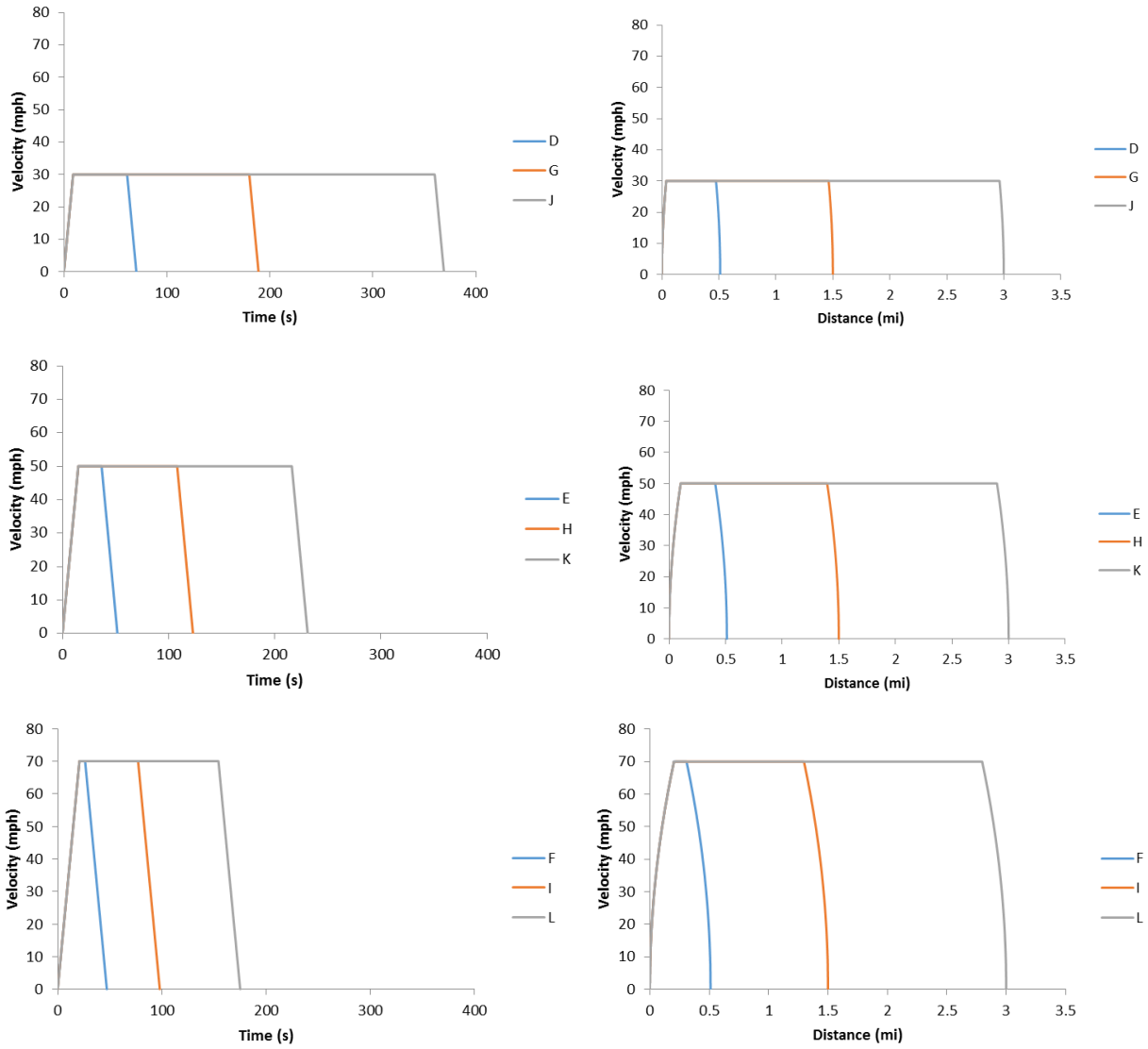

Figure F-2: Distance Study Velocity vs both Distance and Time

Table F-4: Distance Study Route Details

Route	Vehicle	SOCi	Total Distance	Total Time	Avg. Vehicle Speed	Max Vehicle Speed	Max Grade	Max Elevation	Max Accel.	Engine Time	Motor Time	Max Gear
		(%)	(mi)	(s)	(mph)	(mph)	(%)	(m)	(m/s2)	(s)	(s)	(---)
D	BEV	60	0.5	70	26.2	30	0	0	1.5	0	70	N/A
G		60	1.5	189	28.6	30	0	0	1.5	0	189	
J		60	3.0	369	29.3	30	0	0	1.5	0	369	
E	BEV	60	0.5	52	35.6	50	0	0	1.5	0	52	N/A
H		60	1.5	123	43.9	50	0	0	1.5	0	123	
K		60	3.0	231	46.8	50	0	0	1.5	0	231	
F	BEV	60	0.5	47	39.0	70	0	0	1.5	0	47	N/A
I		60	1.5	98	55.1	70	0	0	1.5	0	98	
L		60	3.0	175	61.7	70	0	0	1.5	0	175	
D	Conv.	60	0.5	70	26.2	30	0	0	1.5	70	0	8
G		60	1.5	189	28.6	30	0	0	1.5	189	0	8
J		60	3.0	369	29.3	30	0	0	1.5	369	0	8
E	Conv.	60	0.5	52	35.6	50	0	0	1.5	52	0	8
H		60	1.5	123	43.9	50	0	0	1.5	123	0	8
K		60	3.0	231	46.8	50	0	0	1.5	231	0	8
F	Conv.	60	0.5	47	39.0	70	0	0	1.5	47	0	8
I		60	1.5	98	55.1	70	0	0	1.5	98	0	8
L		60	3.0	175	61.7	70	0	0	1.5	175	0	8
D	Hybrid	21.1	0.5	70	26.2	30	0	0	1.5	13	69	8
G		22.4	1.5	189	28.6	30	0	0	1.5	32	187	8
J		24.4	3.0	369	29.3	30	0	0	1.5	59	367	8
E	Hybrid	22.0	0.5	52	35.6	50	0	0	1.5	8	50	8
H		23.7	1.5	123	43.9	50	0	0	1.5	22	121	8
K		26.4	3.0	231	46.8	50	0	0	1.5	40	229	8
F	Hybrid	23.0	0.5	47	39.0	70	0	0	1.5	9	45	8
I		28.6	1.5	98	55.1	70	0	0	1.5	21	96	8
L		25.2	3.0	175	61.7	70	0	0	1.5	37	173	8

Table F-5: Distance Study Results

Route	Vehicle	Total Fuel Energy	Total Grid Electric Energy	Total Grid Energy	Grid Electric Econ.	Overall ΔSOC	SOC Corr Fuel Energy	SOC Corr. Fuel Energy	Adj. Conv. FE	PEU		GHG	
		(kJ)	(kJ)	(AC Wh/mi)	(mpgge)	(%)	(kJ)	(Wh/mi)	(mpgge)	(PE Wh)	(PE Wh/mi)	(g GHG)	(g GHG/mi)
D	BEV	0	590	320	105.1	-1.09	1480	N/A		5	11	80	157
G		0	1403	260	129.6	-2.65	3601			13	9	191	127
J		0	2636	244	138.0	-5.01	6819			24	8	358	119
E	BEV	0	963	523	64.3	-1.72	2343	N/A		9	17	131	256
H		0	2075	384	87.6	-3.85	5245			19	13	282	188
K		0	3762	348	96.7	-7.09	9647			34	11	511	170
F	BEV	0	1451	788	42.7	-2.54	3462	N/A		13	26	197	385
I		0	3005	556	60.5	-5.52	7518			28	18	408	272
L		0	5363	497	67.8	-10.05	13671			49	16	728	243
D	Conv.	2848	0	N/A		0.00	2848	1547	21.8	217	424	193	377
G		7296	0			0.00	7296	1351	24.9	555	370	495	330
J		13973	0			0.00	13973	1294	26.0	1064	355	947	316
E	Conv.	3606	0	N/A		0.00	3606	1959	17.2	274	537	244	478
H		8112	0			0.00	8112	1502	22.4	617	412	550	367
K		14885	0			0.00	14885	1378	24.4	1133	378	1009	336
F	Conv.	4834	0	N/A		0.00	4834	2626	12.8	368	719	328	641
I		10172	0			0.00	10172	1884	17.9	774	516	689	460
L		18224	0			0.00	18224	1687	20.0	1387	462	1235	412
D	Hybrid	1397	178	N/A		-0.10	1527	830	40.6	118	230	128	250
G		3530	346			-0.10	3672	680	49.5	283	188	296	197
J		6409	709			-0.38	6923	641	52.5	533	178	566	189
E	Hybrid	1902	372	N/A		-0.30	2311	1255	26.8	179	351	207	405
H		5272	419			0.13	5098	944	35.7	392	261	402	268
K		9479	775			0.09	9356	866	38.9	719	240	739	246
F	Hybrid	3401	326	N/A		-0.10	3539	1922	17.5	272	533	284	556
I		8282	525			0.13	8111	1502	22.4	622	415	621	414
L		14920	1039			-0.03	14967	1386	24.3	1149	383	1156	385

Acceleration Study

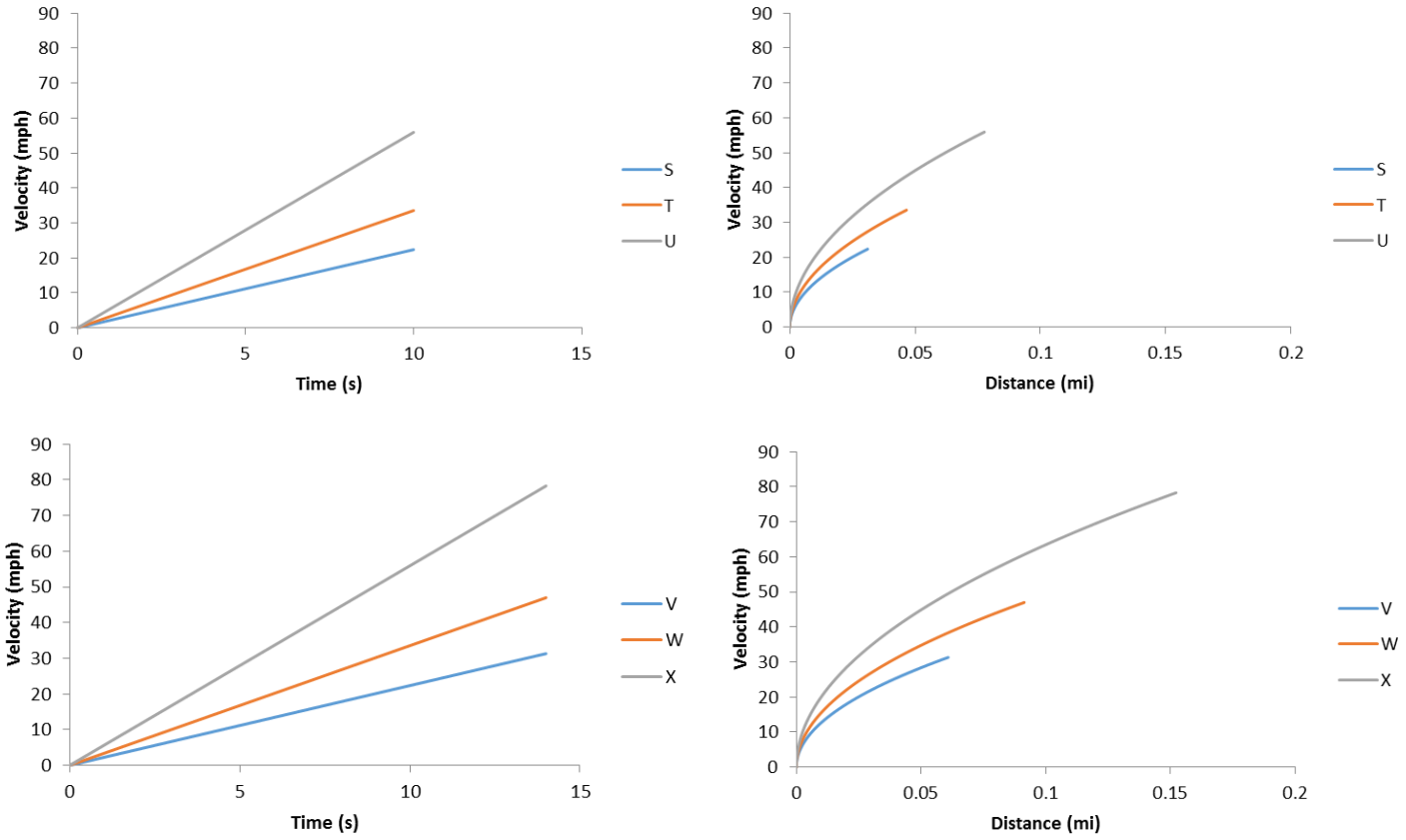

Figure F-3: Acceleration Study Velocity vs both Distance and Time

Table F-6: Acceleration Study Route Details

Route	Vehicle	SOCi	Total Distance	Total Time	Average Vehicle Speed	Max Vehicle Speed	Max Grade	Max Elevation	Max Accel.	Engine Time	Motor Time	Max Gear
		(%)	(mi)	(s)	(mph)	(mph)	(%)	(m)	(m/s2)	(s)	(s)	(---)
S	BEV	60	0.0	10	11.2	22.4	0	0	1.0	0	10	N/A
T		60	0.0	10	16.8	33.6	0	0	1.5	0	10	
U		60	0.1	10	28.0	55.9	0	0	2.5	0	10	
V	BEV	60	0.1	14	15.7	31.3	0	0	1.0	0	14	N/A
W		60	0.1	14	23.5	47.0	0	0	1.5	0	14	
X		60	0.2	14	39.1	78.3	0	0	2.5	0	14	
S	Conv.	60	0.0	10	11.2	22.4	0	0	1.0	10	0	4
T		60	0.0	10	16.8	33.6	0	0	1.5	10	0	4
U		60	0.1	10	28.0	55.9	0	0	2.5	10	0	3
V	Conv.	60	0.1	14	15.7	31.3	0	0	1.0	14	0	5
W		60	0.1	14	23.5	47.0	0	0	1.5	14	0	4
X		60	0.2	14	39.1	78.3	0	0	2.5	14	0	4
S	PHEV.	30	0.0	10	11.2	22.4	0	0	1.0	0	10	3
T		30	0.0	10	16.8	33.6	0	0	1.5	0	10	3
U		30	0.1	10	28.0	55.9	0	0	2.5	2	10	4
V	PHEV	30	0.1	14	15.7	31.3	0	0	1.0	0	14	3
W		30	0.1	14	23.5	47.0	0	0	1.5	0	14	3
X		30	0.2	14	39.1	78.3	0	0	2.5	6	14	4

Table F-7: Acceleration Study Results

Route	Vehicle	Total Fuel Energy	Total Grid Electric Energy	Grid Electric Energy	Grid Electric Econ.	Overall ΔSOC	SOC Corr Fuel Energy	SOC Corr. Fuel Energy	SOC Corr. Fuel Econ.	PEU		GHG	
		(kJ)	(kJ)	(Wh/mi)	(mpgge)	(%)	(kJ)	(Wh/mi)	(mpgge)	(PE Wh)	(PE Wh/mi)	(g GHG)	(g GHG/mi)
S	BEV	0	171	1532	22.0	-0.33	447	N/A		2	50	23	748
T		0	375	2236	15.1	-0.72	979			3	74	51	1093
U		0	1095	3914	8.6	-2.10	2857			10	129	149	1915
V	BEV	0	327	1490	22.6	-0.63	852	N/A		3	49	44	729
W		0	728	2213	15.2	-1.40	1899			7	73	99	1083
X		0	2276	4153	8.1	-4.37	5940			21	137	309	2031
S	Conv.	560	0	N/A		0.00	560	5006	6.7	43	1372	38	1222
T		973	0			0.00	973	5801	5.8	74	1589	66	1415
U		2274	0			0.00	2274	8133	4.1	173	2228	154	1984
V	Conv	983	0	N/A		0.00	983	4483	7.5	75	1229	67	1094
W		1832	0			0.00	1832	5572	6.0	139	1527	124	1359
X		4469	0			0.00	4469	8154	4.1	340	2234	303	1990
S	PHEV	0	171	N/A		-0.33	447	3997	8.4	2	50	23	748
T		0	375			-0.72	979	5835	5.8	3	74	51	1093
U		736	745			-1.43	2677	9575	3.5	211	2711	283	3639
V	PHEV	0	327	N/A		-0.63	852	3888	8.7	3	49	44	729
W		0	728			-1.40	1899	5776	5.8	7	73	99	1083
X		2612	879			-1.68	4891	8925	3.8	380	2498	451	2962

Deceleration Study

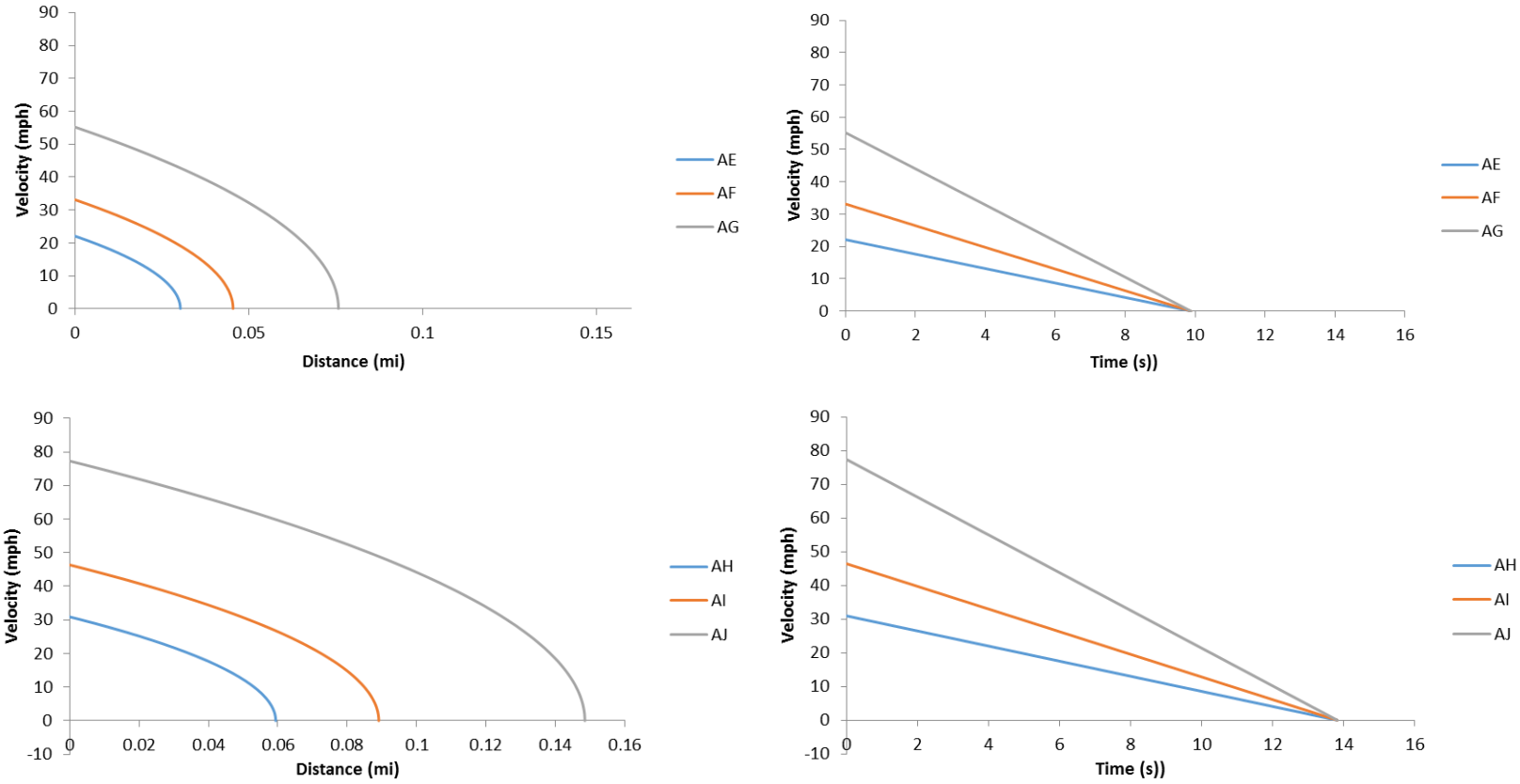

Figure F-4 Deceleration Study Velocity vs both Distance and Time

Table F-8: Deceleration Study Route Details

Route	Vehicle	SOCi	Total Distance	Total Time	Average Vehicle Speed	Max Vehicle Speed	Max Grade	Max Elevation	Max Decel	Engine Time	Motor Time	Max Gear
		(%)	(mi)	(s)	(mph)	(mph)	(%)	(m)	(m/s2)	(s)	(s)	(---)
AE	BEV	60	0.03	10	11.0	22.4	0	0	-1.0	0	10	N/A
AF		60	0.05	10	16.6	33.6	0	0	-1.5	0	10	
AG		60	0.08	10	27.6	55.9	0	0	-2.5	0	10	
AH	BEV	60	0.06	14	15.5	31.3	0	0	-1.0	0	14	N/A
AI		60	0.09	14	23.2	47.0	0	0	-1.5	0	14	
AJ		60	0.15	14	38.7	78.3	0	0	-2.5	0	14	
AE	Conv.	60	0.03	10	11.0	22.4	0	0	-1.0	10	0	5
AF		60	0.05	10	16.6	33.6	0	0	-1.5	10	0	8
AG		60	0.08	10	27.6	55.9	0	0	-2.5	10	0	8
AH	Conv.	60	0.06	14	15.5	31.3	0	0	-1.0	14	0	8
AI		60	0.09	14	23.2	47.0	0	0	-1.5	14	0	8
AJ		60	0.15	14	38.7	78.3	0	0	-2.5	14	0	8
AE	PHEV	30	0.03	10	11.0	22.4	0	0	-1.0	0	8	5
AF		30	0.05	10	16.6	33.6	0	0	-1.5	0	8	8
AG		30	0.08	10	27.6	55.9	0	0	-2.5	0	9	8
AH	PHEV	30	0.06	14	15.5	31.3	0	0	-1.0	0	12	8
AI		30	0.09	14	23.2	47.0	0	0	-1.5	0	12	8
AJ		30	0.15	14	38.7	78.3	0	0	-2.5	0	13	8

Table F-9: Deceleration Study Results

Route	Vehicle	Total Fuel Energy	Total Grid Electric Energy	Grid Electric Energy	Grid Electric Econ	Overall ΔSOC	SOC Corr Fuel Energy	Fuel Energy	SOC Corr. Fuel Econ.	*PEU		*GHG	
		(kJ)	(kJ)	(AC Wh/mi)	(mpgge)	(%)	(kJ)	(Wh/mi)	(mpgge)	(PE Wh)	(PE Wh/mi)	(g GHG)	(g GHG/mi)
AE	BEV	0	-35	-321	-105	0.1	-121	N/A		0	-11	-5	-157
AF		0	-89	-542	-62	0.2	-306			-1	-18	-12	-266
AG		0	-259	-948	-36	0.7	-892			-2	-31	-35	-464
AH	BEV	0	-71	-334	-101	0.2	-246	N/A		-1	-11	-10	-162
AI		0	-176	-549	-61	0.4	-607			-2	-18	-24	-268
AJ		0	-462	-864	-39	1.2	-1593			-4	-29	-63	-423
AE	Conv.	106	0	N/A		0.0	106	976	34.5	8	266	7	237
AF		106	0			0.0	106	650	51.8	8	178	7	158
AG		106	0			0.0	106	390	86.3	8	107	7	95
AH	Conv.	149	0	N/A		0.0	149	697	48.3	11	191	10	170
AI		149	0			0.0	149	465	72.5	11	127	10	113
AJ		149	0			0.0	149	279	120.8	11	76	10	68
AE	PHEV	0	-35	N/A		-0.3	357	3274	10.3	0	-11	-5	-157
AF		0	-89			-0.5	707	4322	7.8	-1	-18	-12	-266
AG		0	-259			-1.4	1899	6965	4.8	-2	-31	-35	-464
AH	PHEV	0	-71	N/A		-0.5	643	3007	11.2	-1	-11	-10	-162
AI		0	-176			-1.0	1349	4208	8.0	-2	-18	-24	-268
AJ		0	-462			-0.6	784	1466	23.0	-4	-29	-63	-423

*Note that negative GHG and PEU are not physically possible, but demonstrates regenerative braking stores energy that may be used to reduce later emissions.

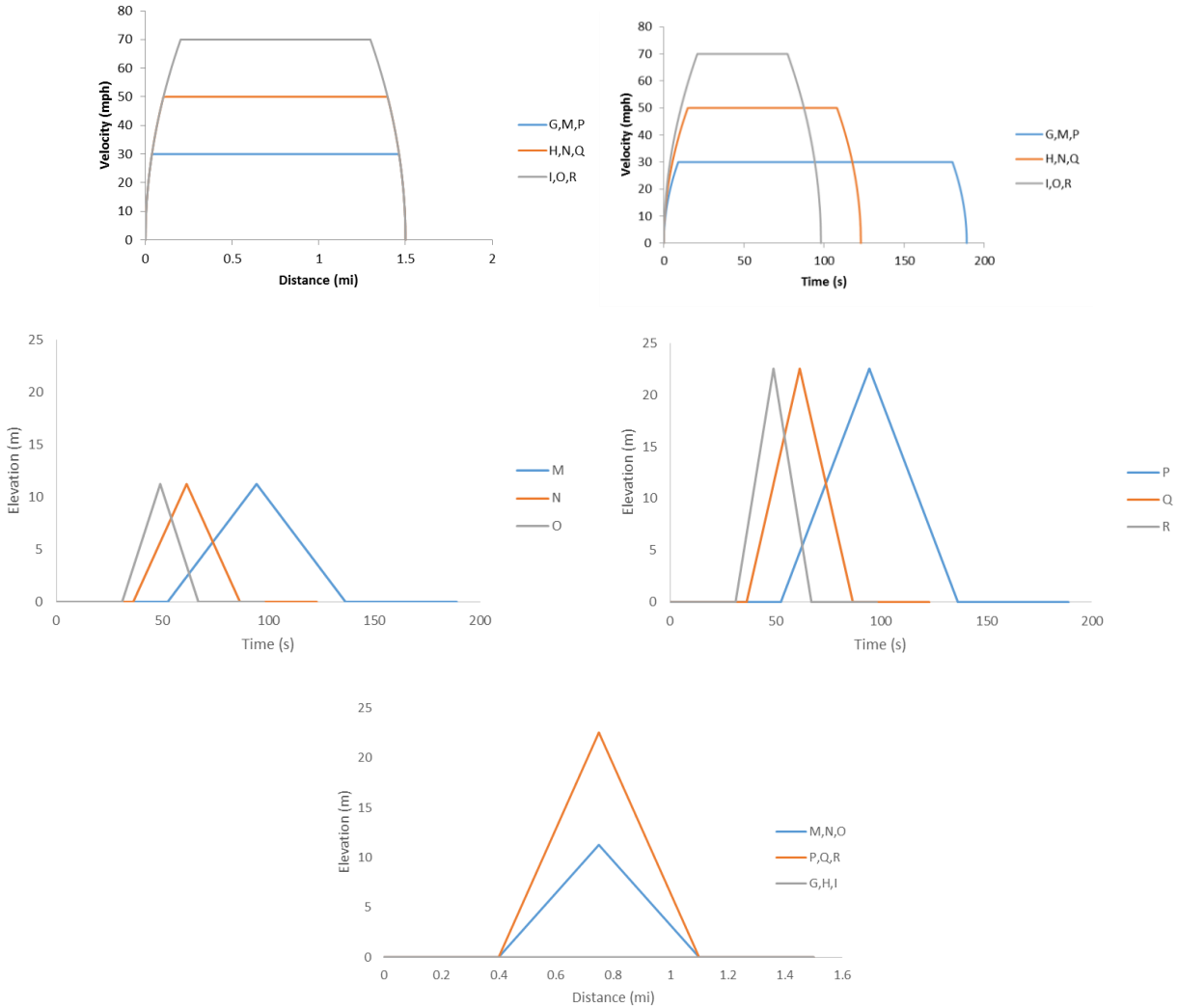

Figure F-5: Grade Study Velocity and Elevation vs both Distance and Time

Table F-10: Grade Study Route Details

Route	Vehicle	SOCi	Total Distance	Total Time	Average Vehicle Speed	Max Vehicle Speed	Max Grade	Max Elevation	Max Accel.	Engine Time	Motor Time	Max Gear
		(%)	(mi)	(s)	(mph)	(mph)	(%)	(m)	(m/s2)	(s)	(s)	(---)
G	BEV	60	1.5	189	28.6	30	0	0.0	1.5	0	189	N/A
M		60	1.5	189	28.6	30	2	11.3	1.5	0	189	
P		60	1.5	189	28.6	30	4	22.5	1.5	0	189	
H	BEV	60	1.5	123	43.9	50	0	0.0	1.5	0	123	N/A
N		60	1.5	123	43.9	50	2	11.3	1.5	0	123	
Q		60	1.5	123	43.9	50	4	22.5	1.5	0	123	
I	BEV	60	1.5	98	55.1	70	0	0.0	1.5	0	98	N/A
O		60	1.5	98	55.1	70	2	11.3	1.5	0	98	
R		60	1.5	98	55.1	70	4	22.5	1.5	0	98	
G	Conv.	60	1.5	189	28.6	30	0	0.0	1.5	189	0	8
M		60	1.5	189	28.6	30	2	11.3	1.5	189	0	8
P		60	1.5	189	28.6	30	4	22.5	1.5	189	0	8
H	Conv.	60	1.5	123	43.9	50	0	0.0	1.5	123	0	8
N		60	1.5	123	43.9	50	2	11.3	1.5	123	0	8
Q		60	1.5	123	43.9	50	4	22.5	1.5	123	0	8
I	Conv.	60	1.5	98	55.1	70	0	0.0	1.5	98	0	8
O		60	1.5	98	55.1	70	2	11.3	1.5	98	0	8
R		60	1.5	98	55.1	70	4	22.5	1.5	98	0	8
G	Hybrid	22.38	1.5	189	28.6	30	0	0.0	1.5	102	187	8
M		22.47	1.5	189	28.6	30	2	11.3	1.5	118	187	8
P		22.80	1.5	189	28.6	30	4	22.5	1.5	121	187	8
H	Hybrid	23.72	1.5	123	43.9	50	0	0.0	1.5	96	121	8
N		23.74	1.5	123	43.9	50	2	11.3	1.5	113	121	5
Q		23.95	1.5	123	43.9	50	4	22.5	1.5	113	121	5
I	Hybrid	28.71	1.5	98	55.1	70	0	0.0	1.5	88	96	5
O		28.88	1.5	98	55.1	70	2	11.3	1.5	88	96	5
R		28.98	1.5	98	55.1	70	4	22.5	1.5	88	96	5

Table F-11: Grade Study Results

Route	Vehicle	Total Fuel Energy	Total Grid Electric Energy	Total Grid Energy	Grid Electric Econ.	Overall ΔSOC	SOC Corr Fuel Energy	SOC Corr. Fuel Energy	SOC Corr. Fuel Econ.	PEU		GHG	
		(kJ)	(kJ)	(Wh/mi)	(mpgge)	(%)	(kJ)	(Wh/mi)	(mpgge)	(PE Wh)	(PE Wh/mi)	(g GHG)	(g GHG/mi)
G	BEV	0	1403	260	130	-2.6	3601	N/A		13	9	191	127
M		0	1455	270	125	-2.7	3739			13	9	198	132
P		0	1611	298	113	-3.0	4081			15	10	219	146
H	BEV	0	2075	384	88	-3.9	5245	N/A		19	13	282	188
N		0	2086	386	87	-3.9	5272			19	13	283	189
Q		0	2229	413	82	-4.1	5618			20	14	303	202
I	BEV	0	3005	556	61	-5.5	7518	N/A		28	18	408	272
O		0	3015	558	60	-5.5	7545			28	18	410	273
R		0	3098	574	59	-5.7	7760			28	19	421	281
G	Conv.	7296	0	N/A		0.0	7296	1351	24.9	555	370	495	330
M		6693	0			0.0	6693	1239	27.2	509	340	454	302
P		7226	0			0.0	7226	1338	25.2	550	367	490	327
H	Conv.	8112	0	N/A		0.0	8112	1502	22.4	617	412	550	367
N		7309	0			0.0	7309	1354	24.9	556	371	495	330
Q		7842	0			0.0	7842	1452	23.2	597	398	532	354
I	Conv.	10172	0	N/A		0.0	10172	1884	17.9	774	516	689	460
O		10157	0			0.0	10157	1881	17.9	773	515	688	459
R		9536	0			0.0	9536	1766	19.1	726	484	646	431
G	Hybrid	3685	299	N/A		0.0	3674	680	49.5	282	188	290	193
M		3782	322			0.0	3814	706	47.7	293	195	302	201
P		4719	195			0.4	4166	772	43.6	319	213	309	206
H	Hybrid	5103	472	N/A		0.0	5103	945	35.6	393	262	410	273
N		5187	460			0.0	5137	951	35.4	395	263	411	274
Q		5481	499			0.0	5471	1013	33.2	421	281	439	292
I	Hybrid	8152	560	N/A		0.0	8095	1499	22.5	621	414	625	416
O		8068	545			0.0	8036	1488	22.6	617	411	619	412
R		8145	552			0.0	8174	1514	22.2	627	418	629	419

Driver Aggressiveness Study

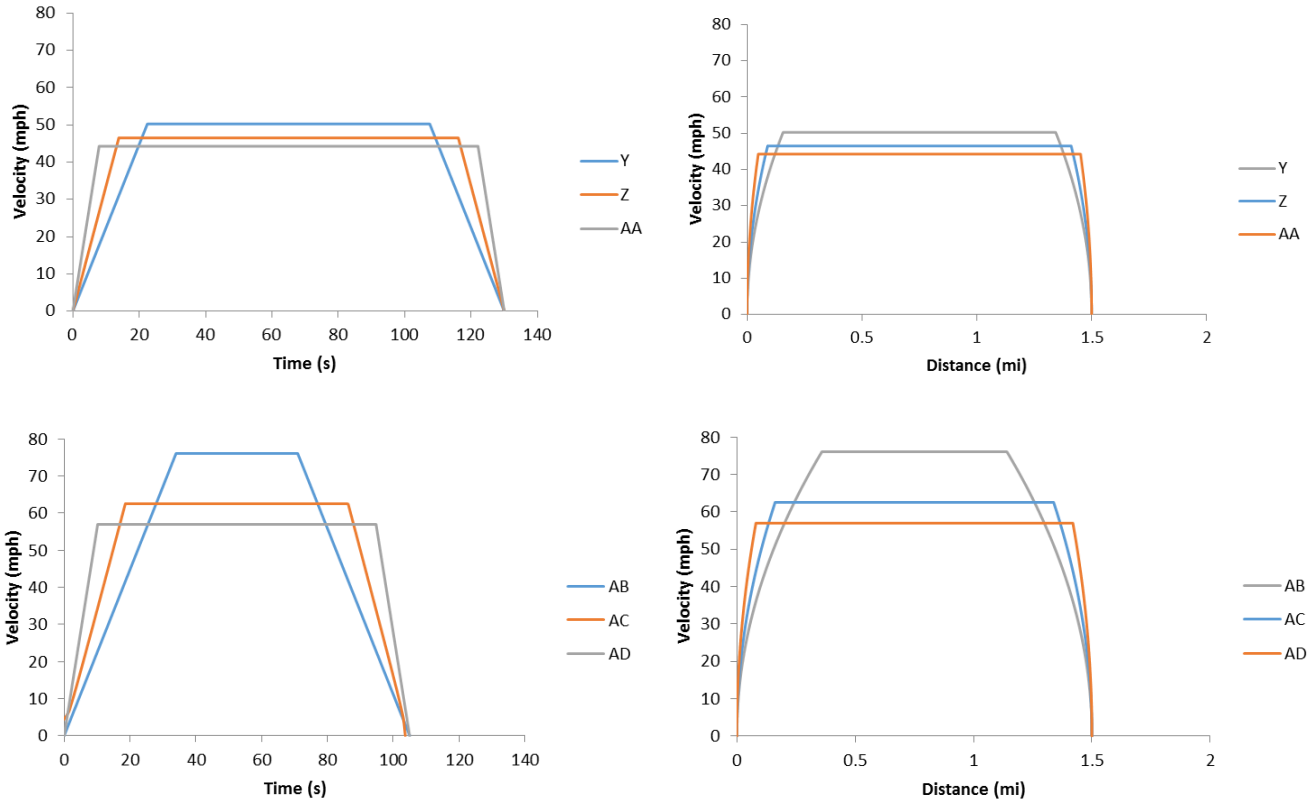

Figure F-6: Driver Aggressiveness Study Velocity vs both Distance and Time

Table F-12: Driver Aggressiveness Study Route Details

Route	Vehicle	SOCi	Total Distance	Total Time	Average Vehicle Speed	Max Vehicle Speed	Max Grade	Max Elevation	Max Accel.	Engine Time	Motor Time	Max Gear
		(%)	(mi)	(s)	(mph)	(mph)	(%)	(m)	(m/s2)	(s)	(s)	(---)
Y	BEV	60	1.5	130	41.54	50.21	0	0	1.0	0	130	N/A
Z		60	1.5	130	41.54	46.49	0	0	1.5	0	130	
AA		60	1.5	130	41.54	44.23	0	0	2.5	0	130	
AB	BEV	60	1.5	105	51.43	76.06	0	0	1.0	0	105	N/A
AC		60	1.5	105	51.43	62.52	0	0	1.5	0	105	
AD		60	1.5	105	51.43	56.95	0	0	2.5	0	105	
Y	Conv.	60	1.5	130	41.54	50.21	0	0	1.0	130	0	8
Z		60	1.5	130	41.54	46.49	0	0	1.5	130	0	8
AA		60	1.5	130	41.54	44.23	0	0	2.5	130	0	8
AB	Conv.	60	1.5	105	51.43	76.06	0	0	1.0	105	0	8
AC		60	1.5	105	51.43	62.52	0	0	1.5	105	0	8
AD		60	1.5	105	51.43	56.95	0	0	2.5	105	0	8
Y	Hybrid	28.92	1.5	130	41.54	50.21	0	0	1.0	68	128	8
Z		28.3	1.5	130	41.54	46.49	0	0	1.5	76	129	8
AA		27.52	1.5	130	41.54	44.23	0	0	2.5	73	129	8
AB	Hybrid	25	1.5	105	51.43	76.06	0	0	1.0	94	103	6
AC		30.37	1.5	105	51.43	62.52	0	0	1.5	69	104	8
AD		29.78	1.5	105	51.43	56.95	0	0	2.5	62	104	8

Table F-13: Driver Aggressiveness Study Results

Route	Vehicle	Total Fuel Energy	Total Grid Electric Energy	Total Grid Energy	Grid Electric Econ.	Overall ΔSOC	SOC Corr Fuel Energy	SOC Corr. Fuel Energy	SOC Corr. Fuel Econ.	PEU		GHG	
		(kJ)	(kJ)	(Wh/mi)	(mpgge)	(%)	(kJ)	(Wh/mi)	(mpgge)	(PE Wh)	(PE Wh/mi)	(g GHG)	(g GHG/mi)
Y	BEV	0	1995	369	91	-3.7	5050	N/A		18	12	271	181
Z		0	1937	359	94	-3.6	4907			18	12	263	175
AA		0	1953	362	93	-3.6	4959			18	12	265	177
AB	BEV	0	3026	560	60	-5.6	7571	N/A		28	18	411	274
AC		0	2629	487	69	-4.8	6598			24	16	357	238
AD		0	2554	473	71	-4.7	6436			23	16	347	231
Y	Conv.	7962	0	N/A		0.0	7962	1474	22.8	606	404	540	360
Z		7788	0			0.0	7788	1442	23.3	593	395	528	352
AA		7644	0			0.0	7644	1416	23.8	582	388	518	345
AB	Conv.	10231	0	N/A		0.0	10231	1895	17.8	779	519	693	462
AC		9383	0			0.0	9383	1738	19.4	714	476	636	424
AD		8963	0			0.0	8963	1660	20.3	682	455	607	405
Y	Hybrid	4539	570	N/A		-0.3	4927	912	36.9	380	253	411	274
Z		4604	493			-0.2	4813	891	37.8	371	247	393	262
AA		4713	479			-0.1	4880	904	37.3	376	251	396	264
AB	Hybrid	7386	604	N/A		0.1	7234	1340	25.1	556	371	572	382
AC		7551	501			0.2	7345	1360	24.8	564	376	566	377
AD		7412	395			0.3	7069	1309	25.7	542	361	533	355

Appendix G Example Route Selection Data

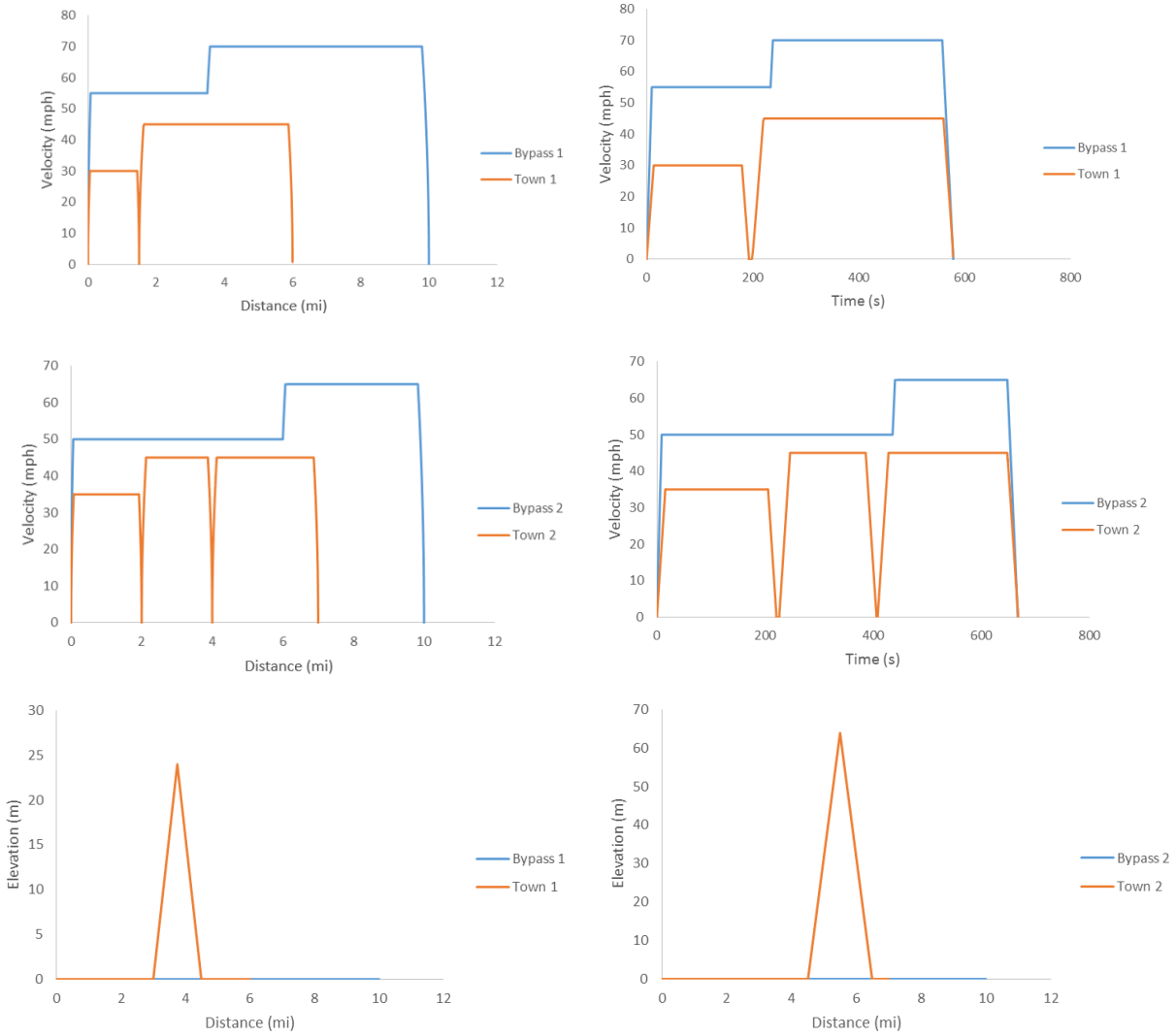

Figure G-1: Example Route Demonstration Plots

Table G-1: Example Route Selection Data

Route	Vehicle	SOCi	Total Distance	Total Time	Idle Time	Average Vehicle Speed	Max Vehicle Speed	Max Grade	Max Elevation	Max Accel.	Engine Time	Motor Time	Max Gear
		(%)	(mi)	(s)	(s)	(mph)	(mph)	(%)	(m)	(m/s2)	(s)	(s)	(---)
Town1	BEV	60	6	579	5	37.3	45.0	2	24	1.2	0	579	N/A
ByPass1	BEV	60	10	579	0	62.2	70.0	0	0	2.5	0	579	
Town2	BEV	60	7	669	7	37.7	45.0	4	64	1.0	0	669	N/A
ByPass2	BEV	60	10	668	0	53.9	65.0	0	0	2.5	0	668	
Town1	Conv.	60	6	579	5	37.3	45.0	2	24	1.2	579	0	8
ByPass1	Conv.	60	10	579	0	62.2	70.0	0	0	2.5	579	0	8
Town2	Conv.	60	7	669	7	37.7	45.0	4	64	1.0	669	0	8
ByPass2	Conv.	60	10	668	0	53.9	65.0	0	0	2.5	668	0	8
Town1	Hybrid	28.2	6	579	5	37.3	45.0	2	24	1.2	122	570	8
ByPass1	Hybrid	28.5	10	579	0	62.2	70.0	0	0	2.5	121	578	8
Town2	Hybrid	30.3	7	669	7	37.7	45.0	4	64	1.0	115	655	8
ByPass2	Hybrid	22.1	10	668	0	53.9	65.0	0	0	2.5	132	666	8

Table G-2: Example Route Selection Results

Route	Vehicle	Total Fuel Energy	Total Grid Energy	Grid Energy	Electric Economy	Overall ΔSOC	SOC Corr Fuel Energy	SOC Corr. Fuel Energy	SOC Corr. Fuel Econ.	PEU		GHG	
		(kJ)	(kJ)	(AC Wh/mi)	(mpgge)	(%)	(kJ)	(Wh/mi)	(mpgge)	(PE Wh)	(PE Wh/mi)	(g GHG)	(g GHG/mi)
Town1	BEV	0	6466	299	112.5	-12.3	16697	N/A		59	10	878	146
ByPass1	BEV	0	15436	429	78.5	-29.4	39964			141	14	2097	210
Town2	BEV	0	8277	328	102.5	-15.6	21183	N/A		76	11	1124	161
ByPass2	BEV	0	13390	372	90.5	-25.5	34666			123	12	1819	182
Town1	Conv.	27286	0	N/A		0.0	27286	1263	26.7	2077	346	1849	308
ByPass1	Conv.	54535	0			0.0	54535	1515	22.2	4151	415	3696	370
Town2	Conv.	33675	0	N/A		0.0	33675	1336	25.2	2563	366	2282	326
ByPass2	Conv.	50925	0			0.0	50925	1415	23.8	3876	388	3452	345
Town1	Hybrid	17320	1294	N/A		0.1	17176	795	42.3	1319	220	1340	223
ByPass1	Hybrid	39468	2908			0.0	39517	1098	30.7	3034	303	3073	307
Town2	Hybrid	20378	1485	N/A		-0.2	20628	819	41.1	1584	226	1600	229
ByPass2	Hybrid	35908	2850			-0.5	36559	1016	33.2	2809	281	2865	287

Appendix H Consolidated Model Parameters

Table H-1: Required Model Inputs

Component	Parameter	*Value	Unit
Glider	Mass	2120	[kg]
	ETW	3750	[lb]
	EPA A	30.1	[lbf]
	EPA B	0.4825	[lbf/mph]
	EPA C	0.01823	[lbf/mph2]
Driveline	Driven Axle	RWD	[---]
	rwheel	0.34	[m]
	Final Drive	3.27	[---]
Motor	Tmax	500	[Nm]
	Sbase	1900	[rpm]
Battery	Type	Li-Ion	[---]
	Ecap	12.6	[kWh]
	Voc	340	[V]
	SOCi	40	[%]
Transmission	# Gears	8	[---]
	GR1	4.56	[---]
	GR2	2.97	[---]
	GR3	2.08	[---]
	GR4	1.69	[---]
	GR5	1.27	[---]
	GR6	1.00	[---]
	GR7	0.85	[---]
	GR8	0.65	[---]
Engine	Vdispl	5.3	[L]
	Fuel Type	E85	[---]
Control Strategy	Type	Parallel PHEV	[---]
	Motor Pos.	Post-Trans	[---]
	tdelay	8	[s]
	Tengextra	40	[Nm]
	Tengmin	202	[Nm]

*Values represent the HEVT Camaro, as an example

Table H-2: Calculated Vehicle Parameters

Component	*Parameter	Value	Unit	Explanation
Glider	Gravity	9.81	[m/s2]	Constant
	ρair	1.2	[kg/m3]	Constant
	kinertia	1.04	[---]	Constant; Section 3.2.1.1
Driveline	Tdl,loss	6	[Nm]	Equation 3-26
Motor	Ppeak	99.5	[kW]	Equation 3-40
	Smax	4500	[rpm]	May be entered to limit motor
	kc	0.0825	[s/kg*m2]	Constant; Section 3.3.4.2
	ki	6.15	[J]	Constant; Section 3.3.4.2
	kw	54(10-7)	[kgm2]	Constant; Section 3.3.4.2
	C	200	[W]	Constant; Section 3.3.4.2
	Tref (Max)	270	[Nm]	Constant; Section 3.3.4.2
	Sref (Base)	2400	[rpm]	Constant; Section 3.3.4.2
Battery	R0	0.01129	[hr]	Discussed in Section 3.3.5.2
	Rint	0.10	[Ω]	Equation 3-49
	SOCmin	20	[%]	May be changed to match vehicle
	SOCmax	30	[%]	May be changed to match vehicle
	ηcharger	87	[%]	Discussed in Section 3.3.5.4
Transmission	Ttrans,loss	16.2	[Nm]	Equation 3-54
	ΔH	1600	[rpm]	Discussed in Section 3.3.6.2
	ΔL	100	[rpm]	Discussed in Section 3.3.6.2
Engine	Smax	5800	[rpm]	May be entered to limit engine
	ηthermal	0.43	[---]	Constant; Discussed in Section 3.3.7.1
	fmep0	127	[kPa]	Constant; Discussed in Section 3.3.7.1
	fmep1	0	[kPa/(rad/s)]	Constant; Discussed in Section 3.3.7.1
	fmep2	0.00024	[kPa/(rad/s)2]	Constant; Discussed in Section 3.3.7.1
	Max T	506	[Nm]	May be entered to limit engine
	Sidle	600	[rpm]	Constant; Discussed in Section 3.3.7.4
	PIdle	0.80	[kW]	Constant; Discussed in Section 3.3.7.4
	Pdecel	1.00	[kW]	Constant; Discussed in Section 3.3.7.4
	Smin	1050	[rpm]	May be entered to limit engine
	Start Eeng,in	16	[kJ]	Constant; Discussed in Section 3.3.7.4
Fuel	ρfuel	2.98	[kg/gal]	Discussed in Section 3.3.7.6
	LHV	8.0	[kWh/kg]	Discussed in Section 3.3.7.6
	E Density	23.7	[kWh/gal]	Discussed in Section 3.3.7.6
	GHGWTW	244	[g GHG/kWh]	Discussed in Section 3.3.7.6
	PEUWTW	0.274	[kWh PE/kWh]	Discussed in Section 3.3.7.6
Regenerative Braking	Fraction	0.6	[---]	Discussed in Section 3.4.2
	Speedmin	5	[mph]	Constant; Discussed in Section 3.4.2
	Ptr,min	-70	[kW]	Discussed in Section 3.4.2
	Tw,min	-2000	[Nm]	Discussed in Section 3.4.2
	Ftr,min	-5.88	[kN]	Discussed in Section 3.4.2
Control Strategy	Paccy	600	[W]	Discussed in Section 3.3.3